

NATIONAL AERONAUTICS AND SPACE ADMINISTRATION

*Technical Report 32-1550*

*Volume V*

*Mariner Mars 1971 Project Final Report*

*Science Experiment Reports*

*Prepared by  
Mariner Mars 1971 Science Experimenter Teams  
and Science Evaluation Team Working Groups*

JET PROPULSION LABORATORY  
CALIFORNIA INSTITUTE OF TECHNOLOGY  
PASADENA, CALIFORNIA

August 20, 1973

NATIONAL AERONAUTICS AND SPACE ADMINISTRATION

*Technical Report 32-1550*

*Volume V*

*Mariner Mars 1971 Project Final Report*

*Science Experiment Reports*

*Prepared by*

*Mariner Mars 1971 Science Experimenter Teams  
and Science Evaluation Team Working Groups*

**JET PROPULSION LABORATORY  
CALIFORNIA INSTITUTE OF TECHNOLOGY  
PASADENA, CALIFORNIA**

August 20, 1973

## Preface

The work described in this Report was performed under the cognizance of the Mariner Mars 1971 Project.

This five-volume document constitutes the Mariner Mars 1971 Project Final Report. Volume I consists of Project development through launch and trajectory-correction maneuver. Volume II presents the preliminary science results derived from data evaluation to December 14, 1971. (The information contained in Volume II has appeared in *Science*, Vol. 175, January 1972.) Volume III describes the Mission Operations System and covers flight operations after trajectory-correction maneuver through the standard orbital mission up to the onset of solar occultations in April 1972. Volume IV consists of the science results derived from the standard orbital mission and some preliminary interpretations of the data obtained from the extended mission. Volume V is an evaluation of mission success based upon comparisons of science results with the experiment objectives.

Detailed information on Project organization, Project policies and requirements, subsystem development, and other technical subjects has been excluded from the Project Final Report volumes. Where appropriate, reference is made to the JPL informal documentation containing this information. The development of most *Mariner 9* subsystems is documented in JPL Technical Memorandums.

# Contents

<b>I. Project Objectives and Mission Profile</b> . . . . .	<b>1</b>
R. H. Steinbacher and A. B. Whitehead	
References . . . . .	11
<b>II. Celestial Mechanics Experiment</b> . . . . .	<b>13</b>
J. Lorell, J. D. Anderson, J. F. Jordan, R. D. Reasenberg, and I. I. Shapiro	
A. Introduction . . . . .	13
1. Organization of Experiment Team . . . . .	13
2. Objectives and Experiment Status . . . . .	13
B. Gravity Field of Mars . . . . .	15
1. Scope and Methods of Analysis of the Gravity Field Investigation . . . . .	15
2. Current Results on the Gravity Field of Mars . . . . .	16
3. Interpretation of the Gravity Results . . . . .	21
C. Test of General Relativity . . . . .	22
1. Generation of Normal Points . . . . .	23
2. Status of the Normal-Point Analysis . . . . .	23
3. Conclusions . . . . .	30
References . . . . .	30
<b>III. S-Band Occultation Experiment: A Summary</b> . . . . .	<b>33</b>
A. J. Kliore, D. L. Cain, G. Fjeldbo, B. L. Seidel, M. J. Sykes, P. M. Woiceshyn, and S. I. Rasool	
A. Objectives and Achievements . . . . .	34
B. Atmosphere and Ionosphere . . . . .	34
C. Radius and Shape . . . . .	35
D. Work in Progress . . . . .	36
References . . . . .	36
<b>IV. Infrared Radiometry Experiment</b> . . . . .	<b>37</b>
S. C. Chase, H. H. Kieffer, E. Miner, G. Münch, and G. Neugebauer	
A. Objectives . . . . .	37
1. Global Thermophysical Structure . . . . .	37
2. Large-Scale Irregularities . . . . .	37
3. Small-Scale Hot or Cold Spots . . . . .	38

## Contents (contd)

B. Significant Additional Results . . . . .	38
C. Problem Areas . . . . .	38
Reference . . . . .	40
<b>V. Infrared Spectroscopy Experiment: An Overview . . . . .</b>	<b>41</b>
R. Hanel, B. Conrath, R. Curran, W. Hovis, V. Kunde, P. Lowman, W. Maguire, J. Pearl, J. Pirraglia, C. Prabhakara, B. Schlachman, G. Levin, and T. Burke	
A. Instrumentation . . . . .	41
B. Scientific Objectives and Results . . . . .	42
1. General Atmospheric Composition . . . . .	43
2. Atmospheric Water Vapor . . . . .	43
3. Surface Pressure . . . . .	45
4. Atmospheric Temperature Fields . . . . .	45
5. Atmospheric Circulation . . . . .	46
6. Particulate Matter . . . . .	48
7. Surface Properties . . . . .	48
C. Summary . . . . .	51
References . . . . .	52
<b>VI. Ultraviolet Spectrometer Experiment . . . . .</b>	<b>53</b>
C. A. Barth, C. W. Hord, A. I. Stewart, and A. L. Lane	
A. Scientific Objectives . . . . .	53
B. Scientific Results . . . . .	54
1. Original Objectives . . . . .	54
2. Additional Scientific Objectives . . . . .	59
References . . . . .	60
<b>VII. Television Experiment . . . . .</b>	<b>63</b>
G. A. Briggs, J. A. Cutts, R. H. Steinbacher, T. E. Thorpe, A. B. Whitehead, G. de Vaucouleurs, M. E. Davies, H. Masursky, and J. B. Pollack	
A. Experiment Background . . . . .	63
B. Atmospheric Phenomena . . . . .	64
C. Geodesy/Cartography . . . . .	66
D. Geology . . . . .	71
E. Variable Surface Features . . . . .	72

## Contents (contd)

F. Satellite Astronomy . . . . .	73
G. Polar Phenomena . . . . .	76
References . . . . .	77
<b>VIII. Surface Properties Working Group . . . . .</b>	<b>81</b>
A. B. Whitehead and D. L. Cain	
A. Shape of the Planet . . . . .	82
B. Topography . . . . .	82
1. Nix Olympica . . . . .	83
C. Isobaric Surface . . . . .	83
D. Gravity Field . . . . .	83
E. Crustal Density Model . . . . .	84
F. Conclusions . . . . .	84
G. Participants in the Working Group . . . . .	84
References . . . . .	85
<b>IX. Volatiles Working Group . . . . .</b>	<b>87</b>
J. A. Cutts	
A. Physics of Polar Frosts . . . . .	88
B. Carbon Dioxide Budget . . . . .	89
C. Atmospheric Minor Constituents . . . . .	90
D. Chemical and Physical Properties of Surface Materials . . . . .	92
E. Layered Deposits and Climatic Cycles . . . . .	93
F. Role of Volatiles in Martian Landscape Formation . . . . .	94
G. Planetology . . . . .	94
H. Conclusions . . . . .	94
I. Participants in the Working Group . . . . .	95
References . . . . .	95
<b>X. Atmospheric Phenomena Working Group . . . . .</b>	<b>99</b>
C. B. Leovy	
A. Atmospheric Temperature and Wind . . . . .	99
B. Cloud Processes . . . . .	100
C. Limb and Terminator Profiles . . . . .	101
D. Minor Constituents . . . . .	101
E. Global Dust Storm . . . . .	101

## Contents (contd)

F. Special Problems . . . . .	101
G. Conclusions . . . . .	102
H. Participants in the Working Group . . . . .	102
Bibliography . . . . .	103

## **Abstract**

On November 14, 1971, *Mariner 9* became the first spacecraft to orbit another planet. Its objectives were to map photographically a significant part of the planet Mars and to observe from orbit, for a minimum of 90 days, the dynamic characteristics of the surface and atmosphere.

The scientific objective of each experiment, as originally stated; the results derived from 18 months of data analysis; and the degrees to which these objectives were met are presented in this report.

# I. Project Objectives and Mission Profile

R. H. Steinbacher and A. B. Whitehead

Jet Propulsion Laboratory/California Institute of Technology, Pasadena, California 91103

In 1968, the Mariner Mars 1971 Project was authorized by the National Aeronautics and Space Administration as a dual-spacecraft mission to Mars (*Mariners 8 and 9*; see Fig. I-1); the objectives were to map the surface of the planet and to observe the dynamic characteristics of its surface and atmosphere from orbit for a period of 90 days.

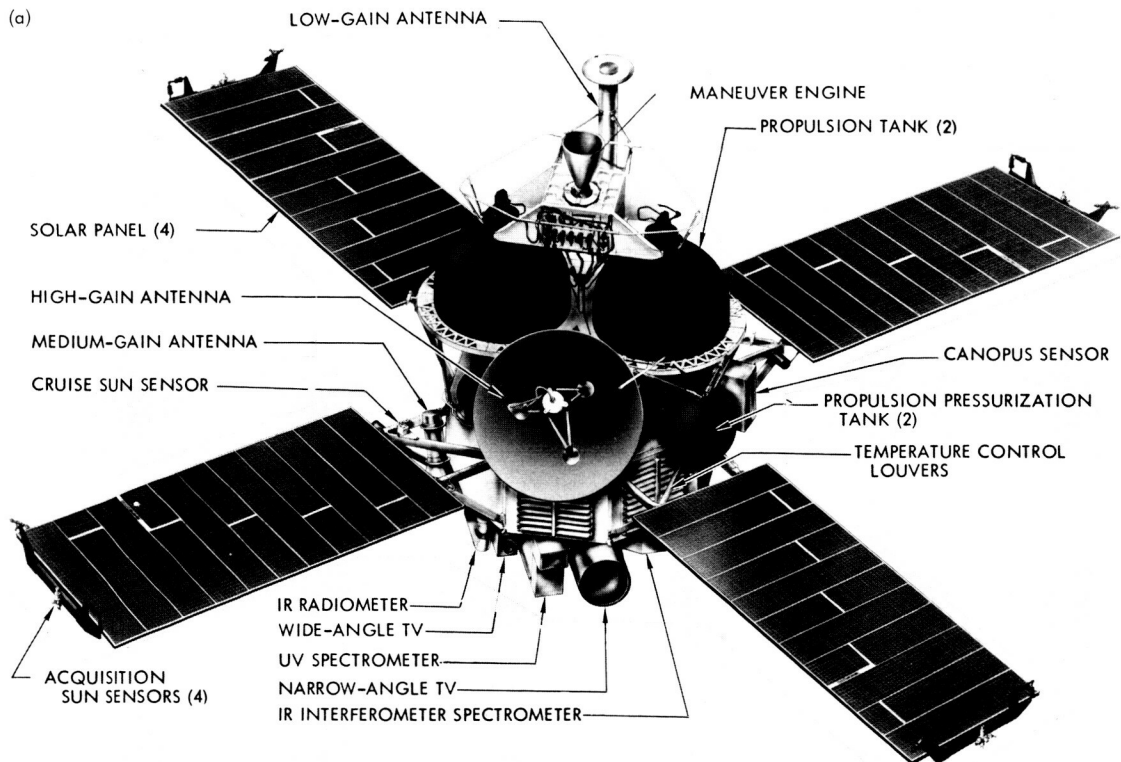
To achieve these objectives, six experiments were carried as part of the science payload: television, ultraviolet spectrometer, infrared spectroscopy, infrared radiometry, S-band occultation, and celestial mechanics (see Table I-1). Two experiments (S-band occultation and celestial mechanics) utilized the radio telemetry subsystem to derive data; the others required specially developed instruments (infrared radiometer, infrared and ultraviolet spectrometers, and wide- and narrow-angle television cameras) mounted, and boresighted to each other, on the spacecraft's scan platform, an articulating instrument mount providing a pointing selection capability of 215° in azimuth and 69° in elevation (see Fig. I-2). The fields of view, relative coverages, and boresight relationships of each instrument are shown in Fig. I-3. Figure I-4 shows the spectral ranges.

Pre-launch mission planning encompassed two separate, but complementary, missions. The orbit of each spacecraft was optimized to match the corresponding objective (Ref. I-1). The mapping mission was designed with an Earth-synchronous orbit (about a 12-hr period) to maximize antenna utilization, or communications efficiency.

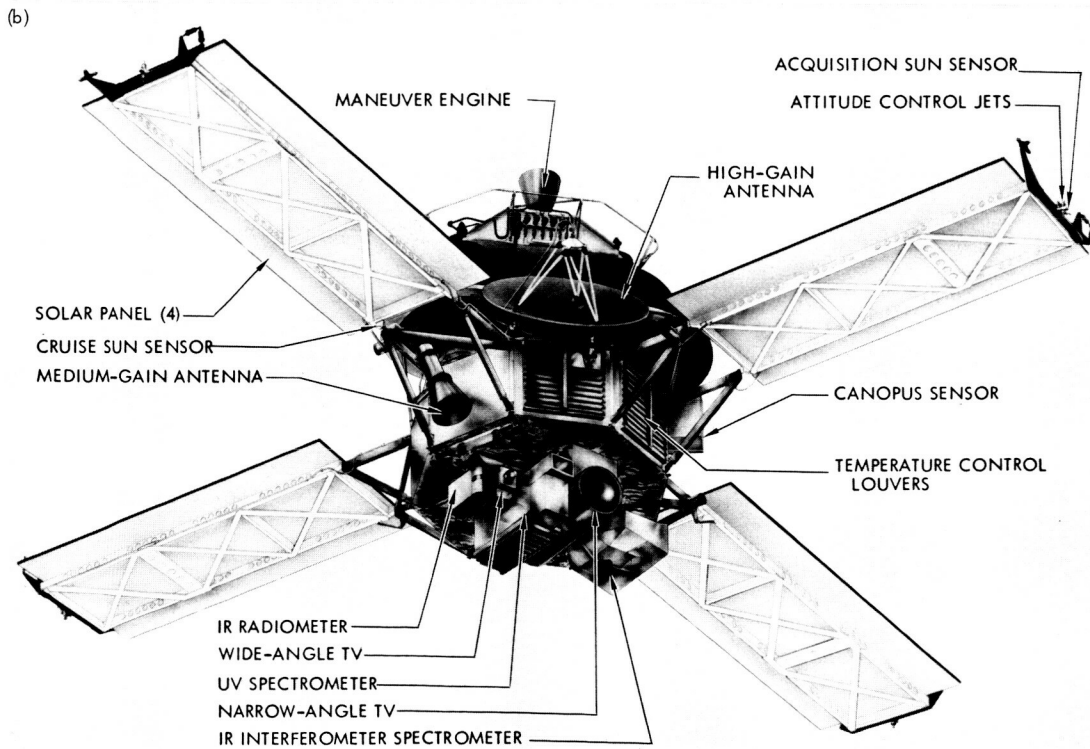
**Table I-1. Mariner 9 science experiments and Principal Investigators**

Experiment	Instrument	Instrument weight, kg	Principal Investigator
Television	Television cameras	26.3	Mr. H. Masursky, <sup>a</sup> U.S. Geological Survey, Flagstaff Dr. G. Briggs, JPL Dr. G. de Vaucouleurs, University of Texas Dr. J. Lederberg, Stanford University Dr. B. Smith, New Mexico State University
Ultraviolet spectrometer	Ultraviolet spectrometer	15.6	Dr. C. Barth, University of Colorado
Infrared spectroscopy	Infrared interferometer spectrometer	24.1	Dr. R. Hanel, Goddard Space Flight Center
Infrared radiometry	Infrared radiometer	3.6	Dr. G. Neugebauer, California Institute of Technology
S-band occultation	None	—	Dr. A. Kliore, JPL
Celestial mechanics	None	—	Mr. J. Lorell, <sup>a</sup> JPL Dr. I. Shapiro, Massachusetts Institute of Technology
		Total	69.6

<sup>a</sup>Team Leader.



PROPULSION MODULE AND SCAN PLATFORM INSULATION BLANKETS NOT SHOWN



PROPULSION MODULE AND SCAN PLATFORM INSULATION BLANKETS NOT SHOWN

Fig. I-1. Spacecraft configuration. (a) Top view. (b) Bottom view.

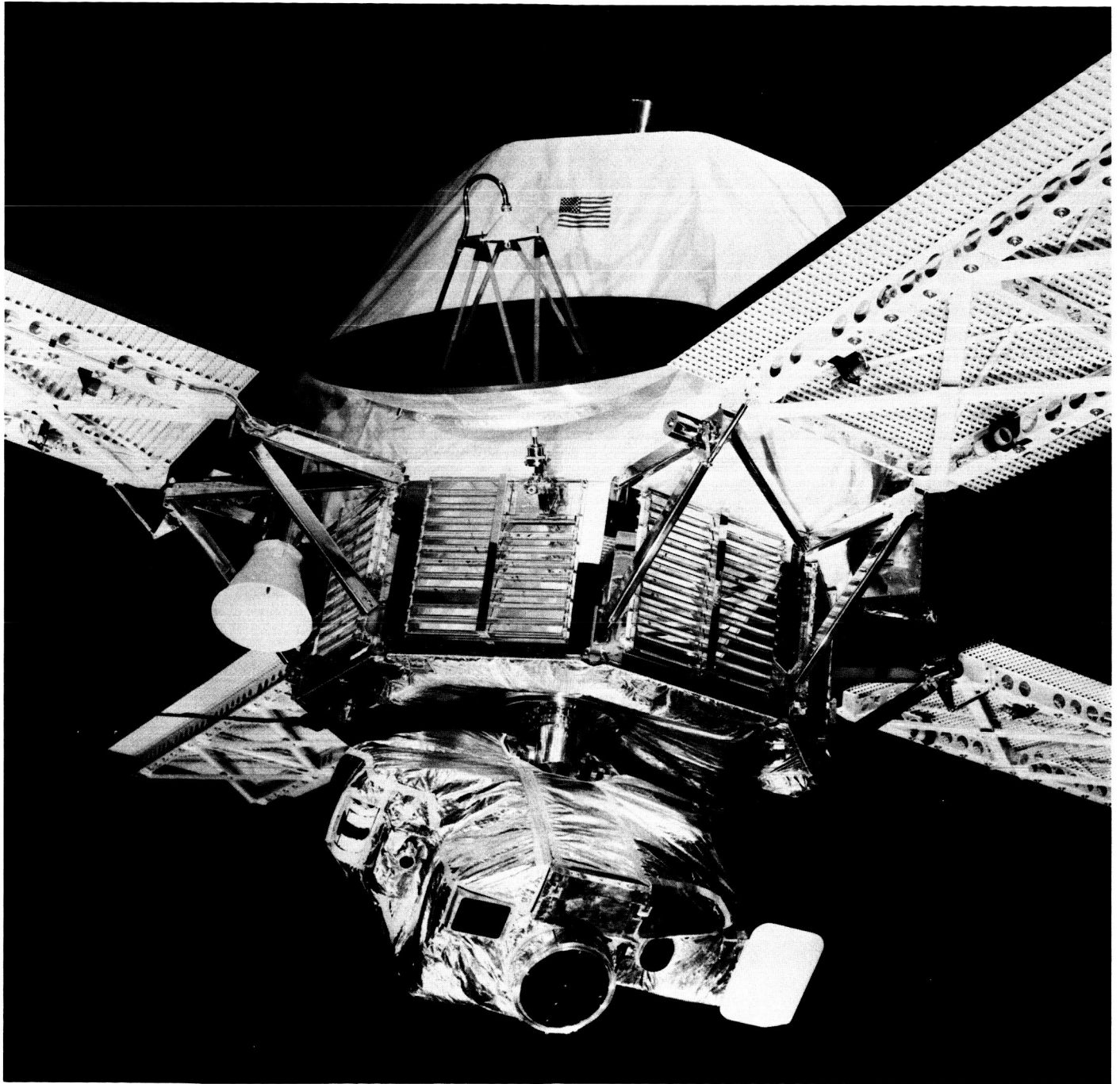


Fig. I-2. Science instruments mounted on scan platform.

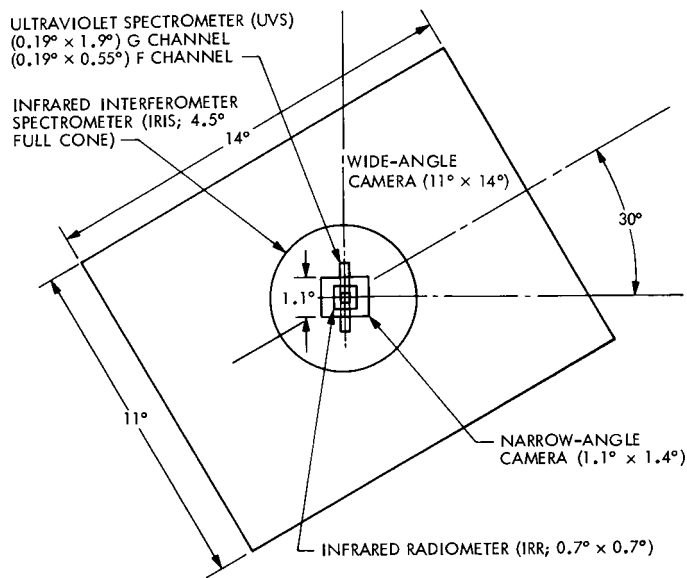


Fig. I-3. Nesting field-of-view configuration of the boresighted scan platform instruments.

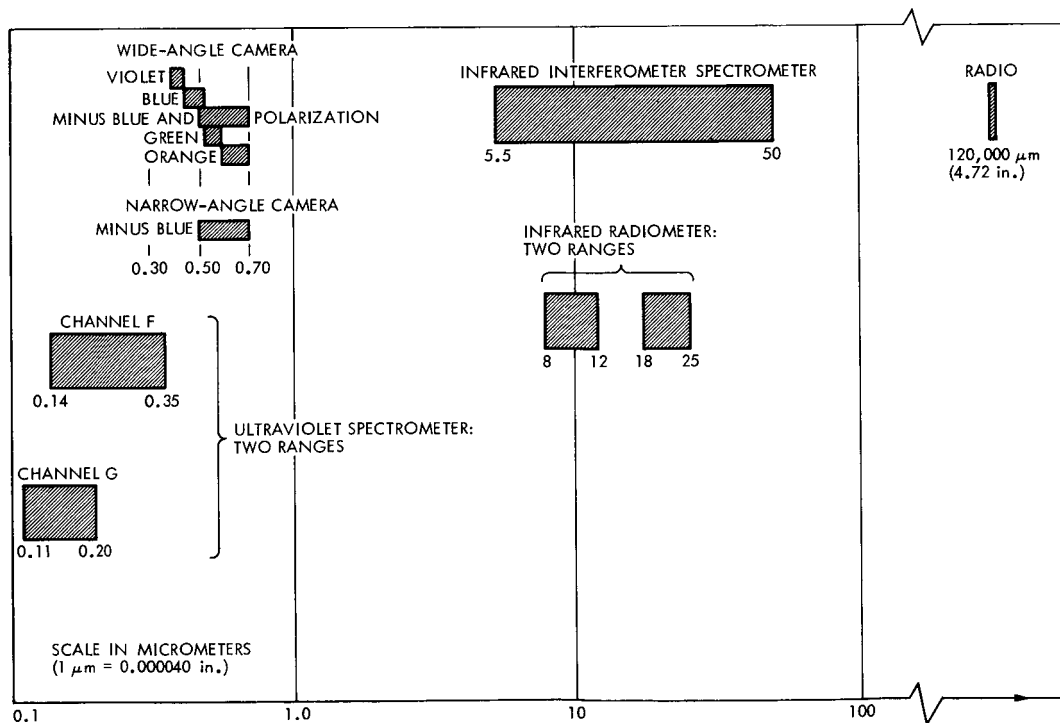


Fig. I-4. Spectral ranges of instruments.

For maximum surveillance of an area, it was designed with a steep inclination ( $80^\circ$ ) to the equatorial plane of Mars. The dynamic objective dictated a Mars-synchronous (or sub-synchronous) orbit and a lower ( $50^\circ$ ) inclination for closer observation of specific areas. The plans for the two missions were in detailed stages of development on May 9, 1971, when *Mariner 8* was lost because of guidance difficulties in the second stage of the launch vehicle.

It was determined that an orbit for a single-spacecraft mission could be developed to meet all basic mission and specific science objectives (see Ref. I-2). However, compromises were necessary, and much of the optimization developed with the two-spacecraft capability was lost (Fig. I-5). A single-spacecraft plan, involving an inclination of  $65^\circ$ , a period of about 12 hr, a periapsis altitude of 1350 km, and an arrival date of November 14, 1971, was evaluated and formalized in 2 weeks.

*Mariner 9* was successfully launched from Cape Kennedy, Florida, on May 30, and 6 days later, on June 5, a planned trajectory correction was made. Martian ephemeris data and spacecraft tracking calculations were determined with such accuracy that no other midcourse corrections were necessary for the entire 167-day flight to Mars. Details of the orbital operation sequences (Ref. I-3) were designed and studied during the Earth-to-Mars transfer trajectory flight (see Fig. I-6).

The insertion into planetary orbit, on November 14, gave *Mariner 9* the distinction of being the first man-made object to orbit another planet. The 1398-km periapsis altitude of the insertion orbit was accurate to within 50 km from the aiming point (Fig. I-7), and the initial period of 12 hr and 34 min was within seconds of the time desired for the insertion orbit. The non-synchronization with Earth provided the timing slip until coincidence of the Goldstone 64-m antenna zenith position and orbit periapsis was obtained and a trim maneuver "locked" the two into synchronization.

It had been planned that, upon arrival at Mars, *Mariner* would start systematically to photograph the surface and to record the associated spectral and radiometric data for analysis, but the Martian dust storm, first observed through telescopes in late September, was still in full development, obscuring the entire surface of the planet with the exception of the bright south polar cap and four dark spots in the equatorial regions. The well laid plans had to be abandoned. The hope of some science investigators to glimpse a Martian dust storm were fully realized.

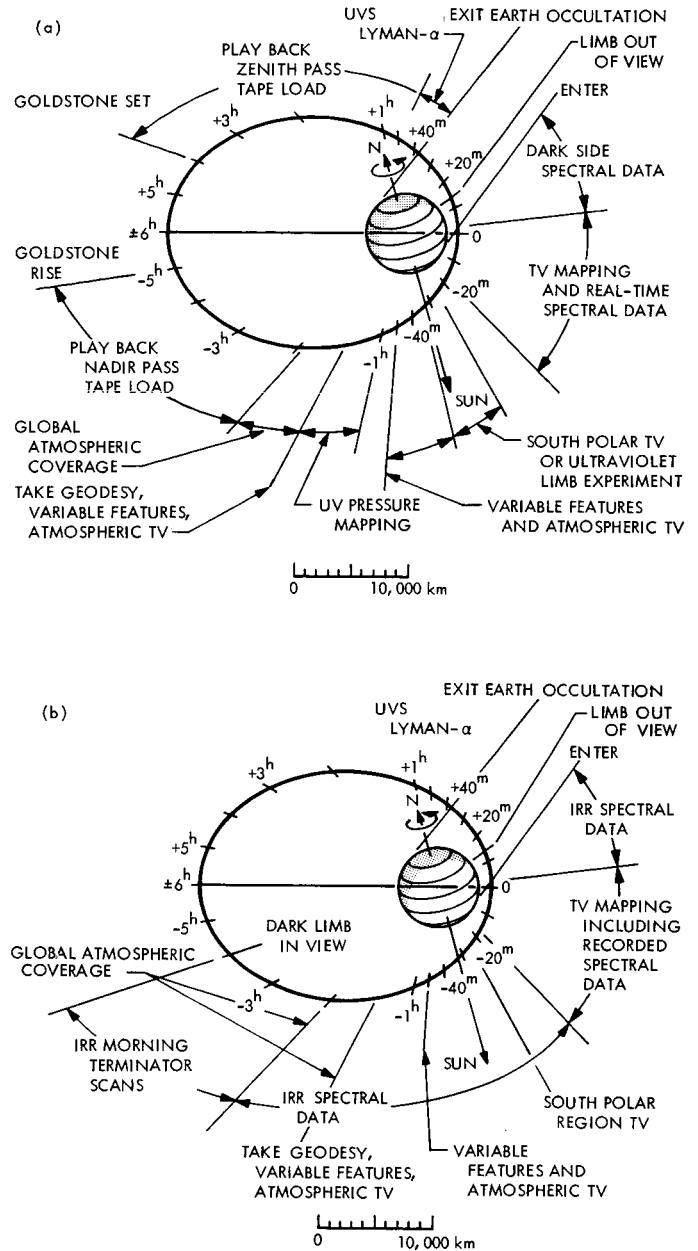


Fig. I-5. Single spacecraft orbital plan. (a) Goldstone zenith pass. (b) Goldstone nadir pass.

On November 16, the spacecraft's orbital period was changed by more than 30 min by a 6-sec firing of the rocket engines (see Table I-2). However, because of the previously unknown gravity-field variation of the planet the average orbital period was found to be slightly shorter than the 11:58:52 planned (Fig. I-8), gradually changing the time relationship of periapsis to the view period of the 64-m antenna at Goldstone, California (Fig. I-9), which would eventually affect data playbacks.

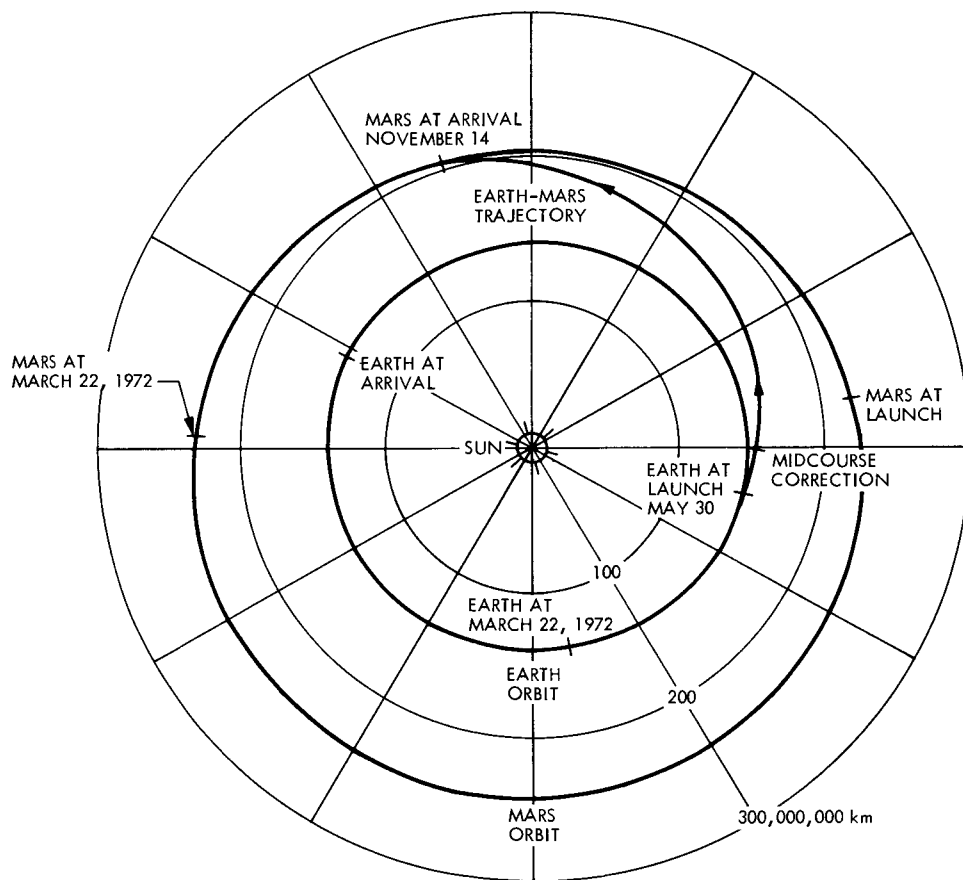


Fig. I-6. Earth-Mars heliocentric view with spacecraft trajectory.

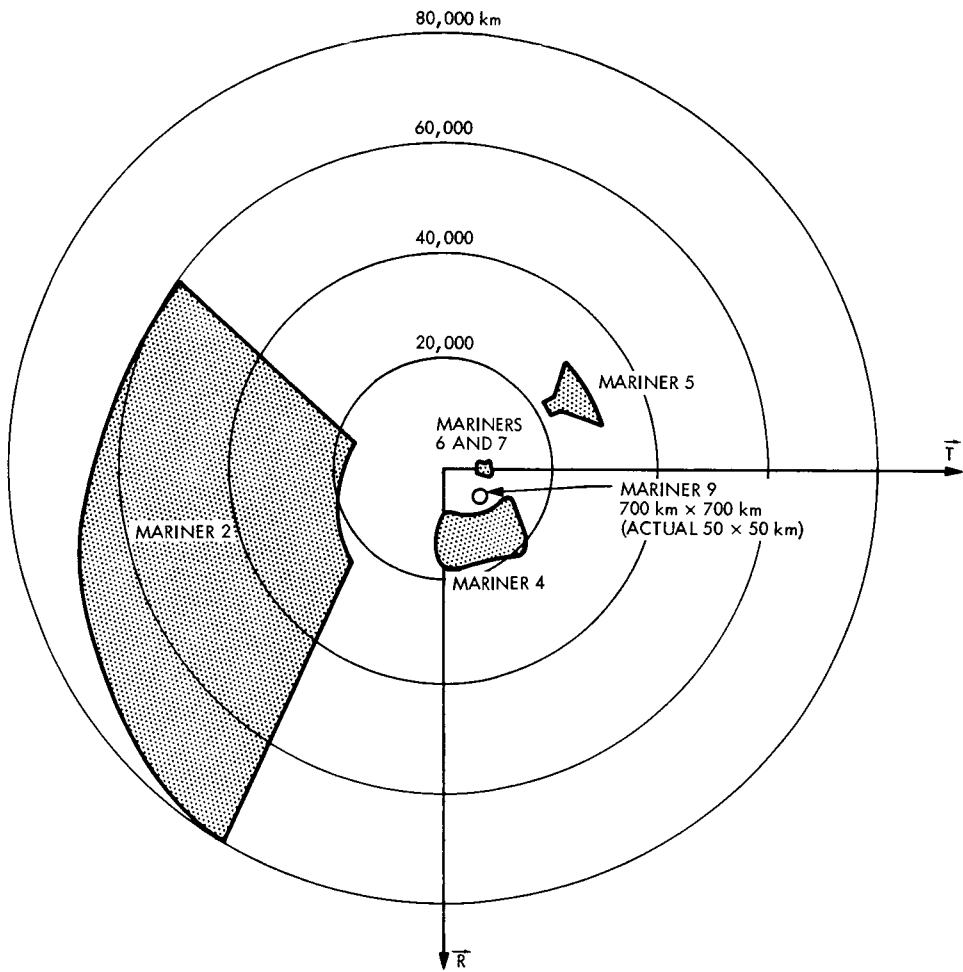


Fig. I-7. Relative size of interplanetary mission aiming zones.

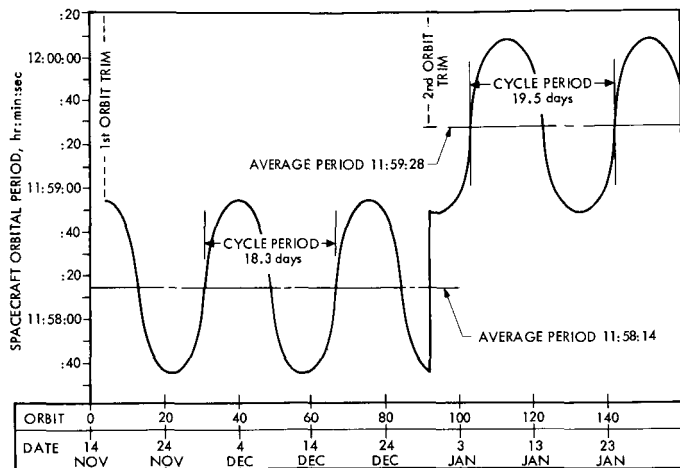


Fig. I-8. Orbital period variation.

Table I-2. Mariner 9 orbit parameters

Event	Period of orbit, hr:min:sec	Periapsis, km	Inclination, deg
After orbit insertion	12:34:01	1398	64.4
After first orbit trim (revolution 4)	11:58:14 (mean period)	1387	64.4
After second orbit trim (revolution 94)	11:59:28 (mean period)	1650	64.4

New sequences were designed (Fig. I-10) to accommodate the raging atmospheric storm. Mission parameters such as new orbital periods, optimum orbital height, communications performance values, etc., were analyzed thoroughly to determine the best method of acquiring data to maximize objectives (Ref. I-3). Finally, on December 22, 38 days after insertion into orbit, the decision was made to establish new orbit parameters and to proceed with the surface mapping.

On December 30 (revolution 94), a second trim maneuver adjusted the orbital period, correcting periapsis-passage timing with the view period of the 64-m antenna (Fig. I-9). This new orbit established a higher periapsis altitude, which provided a broader area coverage for each television picture, thus requiring fewer pictures to complete the desired mapping of 70% of the surface during the standard 90-day mission. The broader area coverage for each picture resulted in a corresponding loss of surface resolution. This picture coverage allowed the mapping to be conducted before communications capability deteriorated, but required stretching the standard mission 20 days longer.

In three 20-day cycles, the surface was recorded from  $-65^\circ$  latitude to about  $+45^\circ$  latitude. The south polar regions ( $-65^\circ$  to  $-90^\circ$  latitude) were covered as frequent targets for the scan platform instruments. The northern hemisphere from about  $45^\circ$  to the pole was obscured by a seasonal polar hood, an ever-present crown of clouds. This area was photographed during the extended mission, when the clouds had dissipated, allowing a clearer view of the surface and permitting additional surface coverage that provided 100% mapping of the planet.

About 122 days after orbit insertion, the pointing direction of the spacecraft's high-gain antenna drifted off of Earth, and communications became more difficult. The Sun-oriented stabilized spacecraft and the geometry of the Sun, Mars, and Earth had been used to optimize the positioning of the fixed high-gain antenna for best communication during the final approach to the planet and

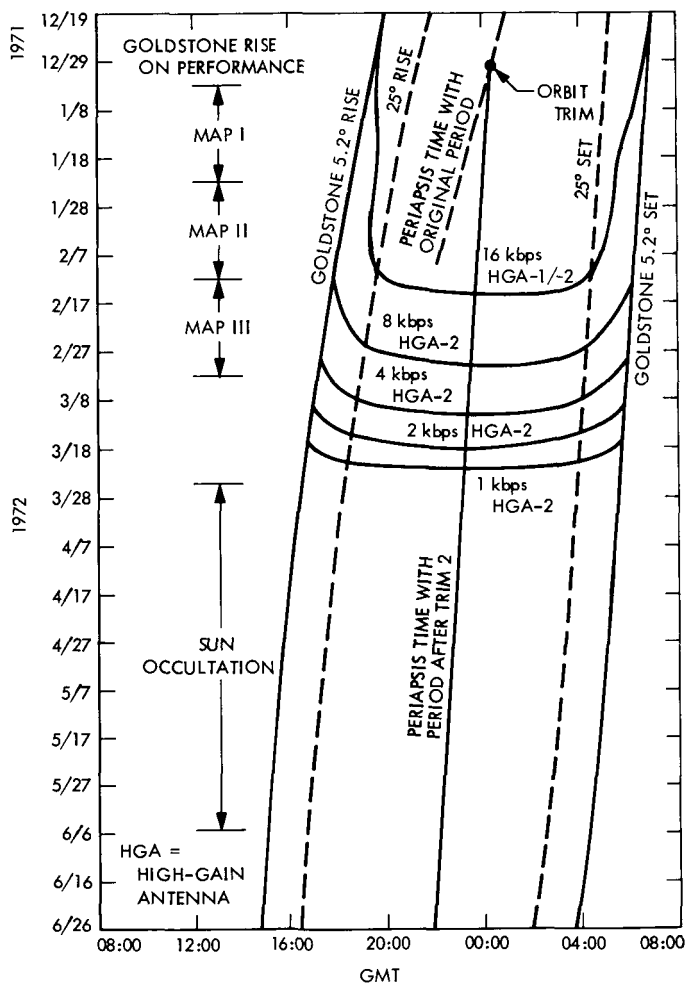


Fig. I-9. Goldstone rise and set times on performance for various data rates vs days.

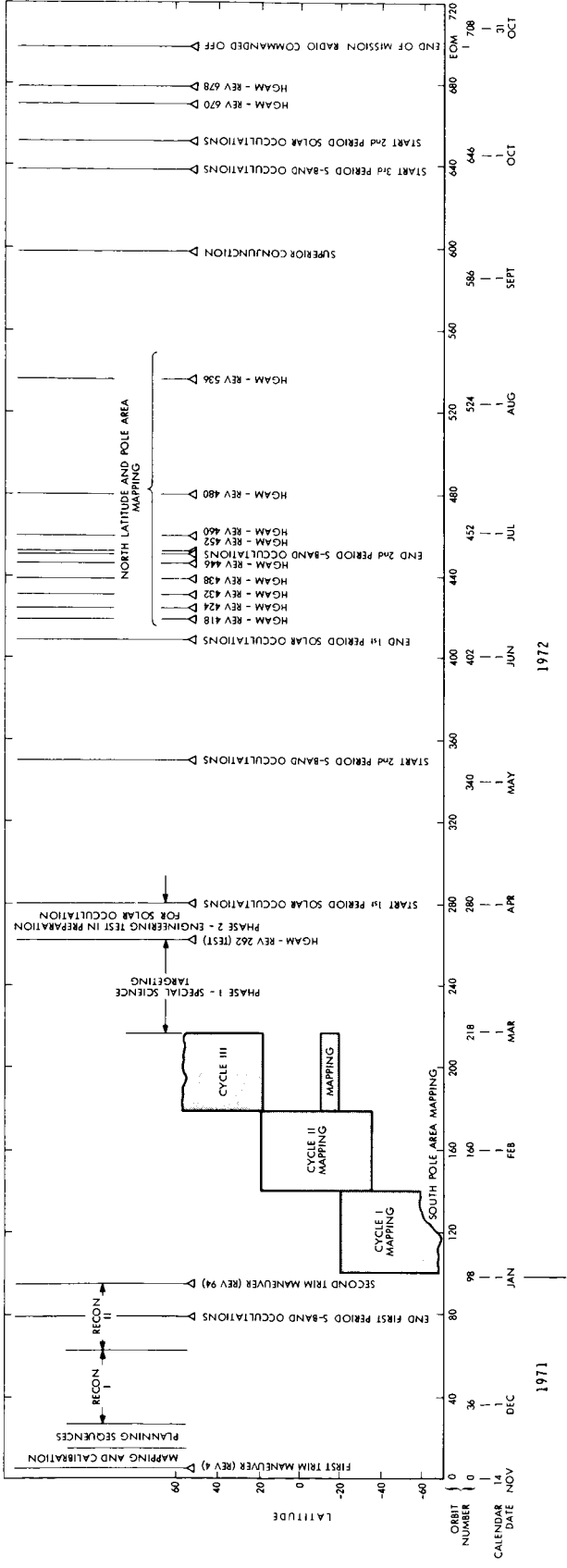


Fig. I-10. Mission sequences and planet coverage as a function of time in orbit.

for the first 90 to 100 days in orbit. Because of the excellent performance of Earth and spacecraft telemetry equipment, high-rate data communications had been extended 10 to 20 days more than originally planned, until the Earth had moved out of the antenna beam. A high-gain antenna maneuver (HGAM) of the spacecraft became necessary to point the antenna at Earth.

The first test of a HGAM was made on March 21, 1972, for relay to Earth of the last scan platform science data recording before the spacecraft began a series of solar occultations (Fig. I-11); the spacecraft's trajectory cut through the shadow of the planet each orbit, requiring the use of the battery to maintain vital systems functions. The spacecraft was battery-operated each orbit during solar occultation for a period of 60 days, requiring a battery-recharging sequence in readiness for the next occultation.

Communications with the spacecraft were maintained during the solar occultation period, enabling the continuation of celestial mechanics data acquisition. The changing relationship of the orbital plane and the Mars-Earth positions provided a second series of spacecraft radio occultations. The first series occurred at insertion and each orbit through revolution 79, and the second series from revolutions 350 to 451 (May through June).

On June 5, 1972, the last solar occultation occurred, and a new set of operational plans was instigated. A tape load of data was recorded on one or two revolutions, and the HGAM was executed for science data playback. Nine sequences were successfully completed during June, July, and August.

Throughout the extended mission period, sequence designers were concerned that the limited supply of attitude-control compressed gas would be expended too quickly. HGAM sequences were particularly extravagant on gas usage, although any scan platform motion also increased its use. Thus, fewer HGAM sequences than operationally possible were performed during the summer months.

The Earth-Mars-Sun relationship continued to change until the positions of Earth and Mars were diametrically opposite each other from the Sun (superior conjunction), which occurred on September 7. With the path of the radio signal approaching the Sun, difficulties in communi-

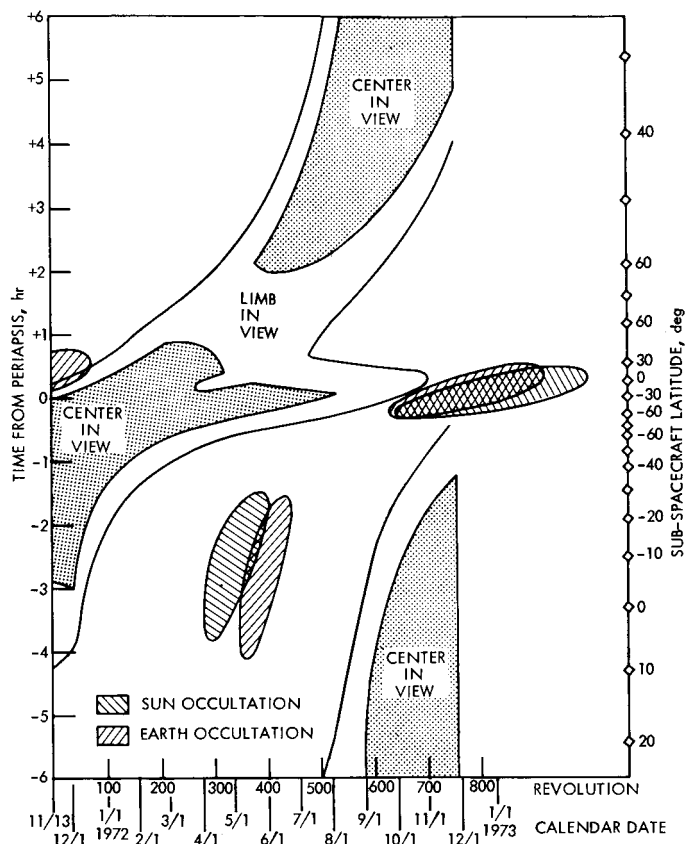


Fig. I-11. Mars limb and center viewing times and solar and Earth occultation times: revolutions 0 to 760.

cations arose from solar corona noise interference. Scan platform science acquisition was postponed until the line of sight to the spacecraft had moved sufficiently away from the Sun for clear telemetry signal reception.

High-gain antenna maneuvers for science data playbacks were conducted on October 13 and 17. However, the attitude-control subsystem had almost depleted the compressed gas supply, causing the spacecraft to lose the Sun acquisition and source of electrical power from the solar panels. On October 27, 1972, telemetry data indicated that the spacecraft was no longer capable of holding the fixed attitude and, as the last battery power was being used, a final command was sent to stop transmitting. The slowly tumbling *Mariner 9* will remain in orbit for a minimum of 50 years before it enters the atmosphere of Mars, disintegrates, and falls to the surface.

## References

- I-1. Steinbacher, R. H., and Haynes, N. R., "Mariner 9 Mission Profile and History," *Icarus*, Vol. 18, p. 64, 1973.
- I-2. Steinbacher, R. H., and Gunter, S. Z., "The Mariner Mars 1971 Experiments: Introduction," *Icarus*, Vol. 12, p. 3, 1970.
- I-3. Haynes, N. R., Bollman, W. E., Neilson, R. A., Nock, K. T., and Travers, E. S., *Mariner Mars 1971 Adaptive Mission Planning*, AIAA Paper 72-944, presented at AIAA/AAS Astrodynamics Conference, Palo Alto, Calif., Sept. 11-12, 1972.

## II. Celestial Mechanics Experiment

J. Lorell, J. D. Anderson, and J. F. Jordan

Jet Propulsion Laboratory/California Institute of Technology, Pasadena, California 91103

R. D. Reasenberg and I. I. Shapiro

Massachusetts Institute of Technology, Cambridge, Massachusetts 02139

### A. Introduction

#### 1. Organization of Experiment Team

In this final report for the celestial mechanics experiment (CME), the accomplishments and current status are reviewed in comparison with the objectives stated in the original proposal (Ref. II-1).

The CME was organized as a team effort, consisting of two groups: one at the Jet Propulsion Laboratory (JPL) and one at the Massachusetts Institute of Technology (MIT).<sup>1</sup> Because the data acquisition was to be through the NASA-operated Deep Space Network with the base of operations at JPL, the data validation and preliminary processing were to be performed at JPL. Analysis and interpretation were to be accomplished cooperatively,

<sup>1</sup>The CME Team consists of:

Team Leader and Principal Investigator for JPL: J. Lorell

Principal Investigator at MIT: I. I. Shapiro

Co-Investigator at MIT: R. Reasenberg

Co-Investigators at JPL: J. D. Anderson, G. H. Born, P. B. Esposito, J. F. Jordan, P. A. Laing, W. L. Martin, W. L. Sjogren

Additional Team Members:

MIT: M. E. Ash, R. Cappallo, A. W. Forni, G. L. Slater, S. Synnott, and R. D. White

JPL: P. S. Callahan, E. J. Christensen, A. J. Ferrari, R. K. Hylkema, M. S. Keesey, J. H. Lieske, E. K. Lau, S. J. Reinbold, G. L. Sievers, S. K. Wong, and A. I. Zygielbaum

with complementary efforts at JPL and MIT. These plans were implemented; the data were acquired and are being analyzed as a joint effort at the two institutions.

In the following paragraphs the efforts and accomplishments of the CME Team are summarized; no attempt has been made to identify individual contributions.

#### 2. Objectives and Experiment Status

The original purpose of the CME was to use the metric information in the *Mariner 9* radio tracking data to investigate the dynamical and physical properties of the solar system in general and of the planet Mars in particular. An itemized list of specific objectives as originally proposed (Ref. II-1) and the present experiment status of each are given in the following paragraphs.

- (a) *Objective.* Obtain a more accurate description of the gravity field of Mars than that provided by the natural satellites; determine the orientation of the spin axis. *Present status.* Gravity field has been determined to approximately two-digit precision through the third degree except for  $J_3$ . Higher-degree models currently are being developed, as is a mascon model. The value for the pole direction of Mars has been improved, and corrected by about  $\frac{1}{2}^\circ$  from the previously accepted value (Ref. II-2),

and is in excellent agreement with Sinclair's value (see Ref. II-3).

- (b) *Objective.* Obtain a highly accurate determination of the astronomical unit good to a fraction of 1 km. *Present status.* The *Mariner 9* data have proved of marginal use in improving the determination of the astronomical unit.
- (c) *Objective.* Obtain corrections to the ephemeris of Mars, a two-order-of-magnitude improvement during the time interval of the *Mariner 9* mission. *Present status.* About a ten-fold improvement has been obtained for the Earth-Mars distance component in the ephemerides.
- (d) *Objective.* Determine the magnitude of general relativistic effects on the orbital motions and signal propagation; estimate the parameters  $\beta$  and  $\gamma$ . *Present status.* Measurements of the round-trip delay time for ranging signals sent to *Mariner 9*, after conversion to equivalent Earth-Mars delays, have been analyzed to test general relativity and to attempt to improve the Earth-Mars ephemeris and other astronomical constants. The converted time delays ("normal points") are at present dominated by systematic errors probably induced by improper modeling. As a result, the accuracy of the test of general relativity is not yet superior to previous results. Similarly no improvements can be made in the determination of any astronomical constants or planetary masses. Only the orbit of Mars can be improved significantly. Several techniques will be applied over the next few months to better model the solar corona, which should then allow a substantial improvement to be made in the accuracy of the time-delay test of general relativity. It is hoped that the resulting accuracy will enable a reliable choice to be made between the theory of general relativity and the scalar-tensor theory of Brans and Dicke with the scalar admixture set at 6%.
- (e) *Objective.* Use the relativistic effects to distinguish between competing gravitational theories (e.g., Einstein vs Brans-Dicke). *Present status.* Same as (d).
- (f) *Objective.* Combine the measurements of the geocentric distance to the center of Mars with Earth-based radar time-delay measurements to yield topographic data. *Present status.* Radar delay measurements that had been obtained during the 1971 opposition have been processed. It has been possible in this manner to remove a residual ephemeris

error in a particular fit to the *Mariner 9* data, a fit which included all radar data, and to use the corrected spacecraft-determined ephemeris to investigate the radar-determined topography. Heights above a reference sphere were obtained to an accuracy of 100 m.

- (g) *Objective.* Coordinate the result with other determinations of constants and ephemerides from optical, radar, and previous space probe observations. *Present status.* Work is just starting in this area; several efforts are underway: (1) topography work mentioned in (f) above, (2) use of combined occultation and radio tracking data to improve accuracy of gravity model, and (3) use of television pictures of natural satellites to improve both the gravity model and the determination of the spin direction.

Additional objectives that were added later include:

- (h) *Objective.* Determine an upper limit to the atmospheric density at spacecraft altitude by observing the drag retardation. *Present status.* Doppler data indicate absence of measurable drag retardation (see Ref. II-4).
- (i) *Objective.* Analyze the superior conjunction Doppler and range data and obtain an improved model of the solar corona. *Present status.* Solar corona parameters  $B$  and  $\epsilon$  are being determined along with the relativistic time-delay parameter, as it is important to separate these two distinctly different effects. Correlations between the corona and relativistic parameters are high, and the corona parameters are being influenced by an inadequate modeling of the spacecraft's trajectory. Although several different models exist for  $B$  and  $\epsilon$ , the analysis is not complete enough to specify their values for the time covered by the experiment.
- (j) *Objective.* Study the changes of electron columnar content between Earth and *Mariner 9* by using the comparison between ranging and Doppler signals, referred to as differenced range vs integrated Doppler (DRVID). *Present status.* Columnar content changes up to  $10^{19}$  electrons  $\text{m}^{-2} \text{hr}^{-1}$  were observed. Power spectra of the DRVID data records yield power-law spectral indices in good agreement with those from in situ spacecraft measurements of proton density fluctuations. Analysis now underway may allow an approximate determination of  $\epsilon$  (see item i) from careful comparison among the spectra and measurements near 1 AU. An attempt will be made to relate the widely differing levels of

columnar content activity to solar latitude and surface features.

Of these objectives, the determination of the Mars gravity field and the estimation of the relativity parameters, particularly  $\gamma$ , have received the most attention, as they are basic to the achievement of most of the others. The gravity work is discussed first.

## B. Gravity Field of Mars

### 1. Scope and Methods of Analysis of the Gravity Field Investigation

The *Mariner 9* mission, like any other exploration of virgin territory, provided surprises. For example, the intensity of the dust storm that covered Mars during the early part of the mission was not anticipated, and forced major changes in the television experiment data acquisition. The dust storm itself did not have a direct effect on the CME work, although it did have its impact in that the spacecraft orbit was never lowered as had been hoped. In fact, the limited maneuver capability was used to raise rather than lower the orbit to obtain more effective picture coverage after the dust cleared.

The CME was directly affected by the unexpected roughness of the gravity field. As the description of a rough field requires more terms in the harmonic expansion, the effect on the analysis was to require the estimation of many more parameters than originally planned. The gravity results became more sensitive to the modeling procedure, the data processing more costly.

The gravity field analysis was limited primarily by two conditions: (1) There was only one spacecraft, and therefore only one type of orbit. (2) The actual orbit was not designed for gravity analysis: e.g., the inclination was  $63^\circ$  to  $64^\circ$ , close to the critical inclination at which the periapsis point always stays at the same latitude. On the favorable side, we note that the orbital period is 12 hr, just enough to allow the periapsis point to progress in longitude about  $9^\circ$ /day, and thus to move around the planet in slightly less than 20 days (accounting for the two revolutions per day).

Modeling the non-gravitational forces on the spacecraft does not seem to be a problem. The most difficult non-gravitational effects to model, in terms of engineering and computer program complexity, are those due to reflected radiation pressure and to attitude-control gas leaks. Analysis has shown that these effects are small enough to be neglected at the level of analysis currently contemplated.

The major complicating factor in the analysis seems to be the effects of the unmodeled portion of the gravity field. When expressed in spherical harmonics, the gravity field is represented as a series expansion which must be truncated at some practical value. Most of our analysis has been limited to eighth-degree expansions, though some work has been performed with tenth degree. The higher-degree terms that are not modeled because of practical considerations tend to bias the results.

In an effort to understand the quantitative nature of these biases and to circumvent difficulties imposed on the experiment by the complexity of the gravity field itself, several alternate approaches of analysis other than the directed least-squares reduction of the radio data (Ref. II-5) have been undertaken. These approaches involve the use of alternate analytical descriptions of the field, alternate data processing methods, and additional independent data. The following paragraphs list these activities.

a. **Batch sequential processing.** Direct analysis of data from 19 revolution arcs and from 38 revolution (one resonance cycle) arcs have been statistically combined to produce composite fields over several such cycles. The statistical synthesis of the models has been carried out in the traditional weighted least-squares sense, with the exception that respective spacecraft state vectors were not combined, but left independent from data batch to data batch. It is felt that the independence of the state vectors will allow the computation of a composite gravity model that is less adversely sensitive to unmodeled forces.

b. **Mean motion reduction.** The mean orbital motion of *Mariner 9* is being analyzed in an effort to improve the values of resonant tesseral coefficients. The method makes use of compressed data spanning the whole mission. Compressed points based on one-orbit fits to the apoapsis data (apoapsis  $\pm 4$  hr), and represented by five of the Kepler orbit parameters time-tagged at apoapsis have already been generated for most of the mission. We are currently in the process of fitting spherical harmonic models to these data.

c. **Mascons and mascon disk analysis and short-arc reduction.** This activity involves the direct reduction of many short arcs (each arc only a fraction of a revolution) to obtain the gravity field represented in terms of a distribution of surface mass points or disks. The work is similar to that performed with the *Lunar Orbiter* and *Apollo* data for the Moon (Ref. II-6). In addition to the

short-arc analysis, a more ambitious effort is currently underway to map the entire planet by simultaneously estimating some 50 to 60 mass disks. This work is being done under contract with Aerospace Corporation, and is scheduled for completion by June 20, 1973. This model should be effective for quantitative geophysical interpretation.

**d. Use of occultation data.** The radio tracking data for revolutions 102 to 141 (one resonant cycle) and the occultation pressure/elevation data have been merged to obtain a spherical harmonic representation of the gravity field with more precise determination of the northern hemisphere than the radio data alone have yielded.

More than 200 measurements of the near-surface pressures have been obtained from analysis of the radio signal as it passed through the atmosphere of Mars. These measurements have been reduced by S-band occultation experimenters to produce radius lengths to the 6.1-mb pressure surface over a broad region of the Martian surface from a latitude of  $+85^\circ$  to  $-80^\circ$ . Although effects due to the Martian atmospheric dynamics on the height of a constant pressure surface limit the accuracy of the results, it is felt that this method will yield the most precise zonal coefficients.

**e. Use of television pictures of the natural satellites.** The natural satellites Phobos and Deimos have been photographed from *Mariner 9*. The metric information from the pictures taken during revolutions 25 to 220 plus one picture during revolution 647 is being used to extract information regarding the orbits of the natural satellites and the gravity field of Mars. These optical data will be processed simultaneously with the radio tracking data. The long time span covered by the pictures makes it necessary to use a trajectory calculation scheme which can predict the long arcs of the three orbiting bodies accurately. To this end, an analytic theory has been developed involving series expansions in powers of eccentricity,  $e$ . The motions of the natural satellites whose orbits are nearly circular can be calculated using terms through  $e^2$ . However, the highly eccentric spacecraft orbit requires the use of terms through  $e^{20}$ .

The prospect of success in obtaining a more precise model of the gravity field from the activities listed depends in the last analysis on the quality of the data, or rather the information content. The quality of the data cannot be faulted, particularly the radio-tracking data. In general, the Doppler measurements are about two orders of magnitude more precise than we have so far been able to use effectively. Our current efforts are aimed

in part at taking better advantage of this unused precision. But, as mentioned, the biasing due to the unmodeled part of the force field is difficult to bypass, and masks the results at this higher level of precision. The auxiliary data types, if they are precise enough, can serve to decouple the biases, and thus permit a better result. We are cautiously optimistic about the success of these approaches.

## 2. Current Results on the Gravity Field of Mars

**a. General gravity structure.** The general gravitational properties of Mars have been verified by all of the methods of analysis itemized in Section II-B-1, and have been presented in Refs. II-4 and II-5. The gravity field of Mars has been found to be much rougher than anticipated, with the same global oblateness as that observed by *Mariners 4* and *6*, and with a large bulge in the equatorial region at about  $105^\circ$  longitude, in the area known as Tharsis.

If the general gravity shape is characterized by the values of coefficients in a spherical harmonic expansion, then the value of the second-degree harmonic coefficient  $J_{22}$  can be said to be very large in comparison with Earth or the Moon. The harmonic coefficients  $J_{31}$  and  $J_{33}$  are also large. Table II-1 gives available best estimates for the coefficients through the third degree, omitting only  $J_3$  as it is not yet well enough determined.

**b. Specific gravity description.** Specific gravity models are perhaps better exhibited by contour plots of a geoidal (equipotential) surface or of an equivalent surface mass distribution than by extended harmonic coefficient lists. References II-4 and II-5 contain such plots generated from early incomplete data sets and give promise for a reasonably reliable eighth-degree harmonic model. This section presents interim results, obtained from the direct analysis and short-arc analysis of the data, which we feel are the most representative of the expected final definitive results.

Figures II-1 and II-2 show, respectively, the geoid and the equivalent surface mass distribution for the current best field from the direct analysis as listed in Table II-2. A similar plot is shown in Fig. II-3 for a field obtained from short-arc analyses based on independent least-squares reductions to determine six to seven point masses along each orbital track. This rather qualitative map yields essentially the same results in that the Tharsis anomaly is the predominant positive gravity feature surrounded by a broad negative region and that the Hellas basin does not display any mascon type anomaly.

**Table II-1. Second- and third-degree harmonic coefficients**

		Not normalized		Normalized		Maximum radius change
		Value	$\sigma$	Value	$\sigma$	$\Delta R$ , km
$10^2$	$J_2$	0.1960	$\pm 0.0009$			
$10^4$	$C_{22}$	-0.546	$\pm 0.004$	-0.846	$\pm 0.007$	
	$S_{22}$	0.316	$\pm 0.011$	0.490	$\pm 0.016$	
	$J_{22}$	0.631	$\pm 0.007$	0.978	$\pm 0.010$	1.07
	$\lambda_{22}$	75.0° E	$\pm 0.4^\circ$			
	$C_{31}$	0.04	$\pm 0.01$	0.04	$\pm 0.01$	
	$S_{31}$	0.28	$\pm 0.01$	0.26	$\pm 0.01$	
	$J_{31}$	0.28	$\pm 0.01$	0.26	$\pm 0.01$	.046
	$\lambda_{31}$	80.8° E	$2.4^\circ$			
	$C_{32}$	-0.06	$\pm 0.02$	-0.17	$\pm 0.05$	
	$S_{32}$	0.03	$\pm 0.02$	0.08	$\pm 0.05$	
	$J_{32}$	0.06	$\pm 0.02$	0.18	$\pm 0.05$	0.286
	$\lambda_{32}$	77° E	$\pm 8^\circ$			
	$C_{33}$	0.050	$\pm 0.002$	0.36	$\pm 0.01$	0.737
	$S_{33}$	0.036	$\pm 0.002$	0.26	$\pm 0.02$	
	$J_{33}$	0.062	$\pm 0.002$	0.44	$\pm 0.01$	
	$\lambda_{33}$	11.8° E	$\pm 0.6^\circ$			

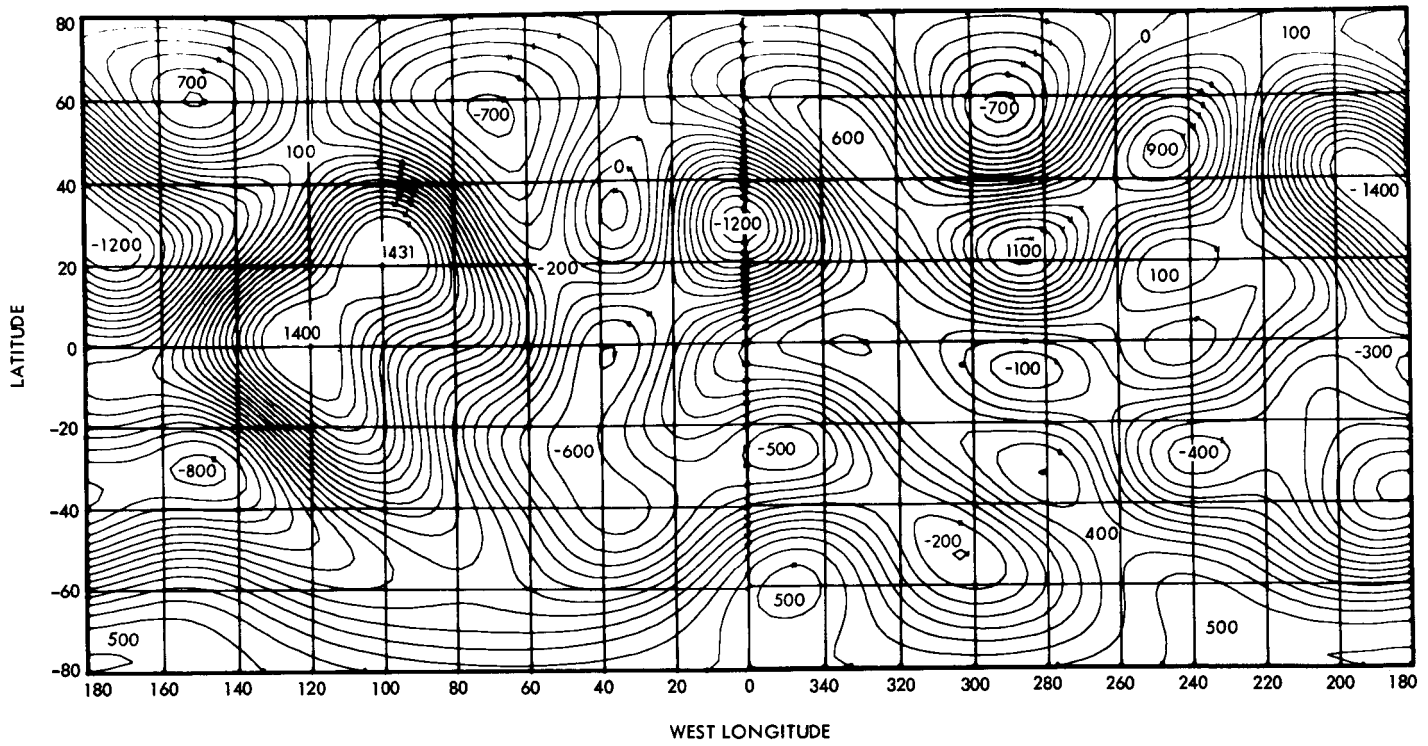


Fig. II-1. Geoid, based on interim eighth-degree model (see Table II-2). Contours at 100-m intervals.

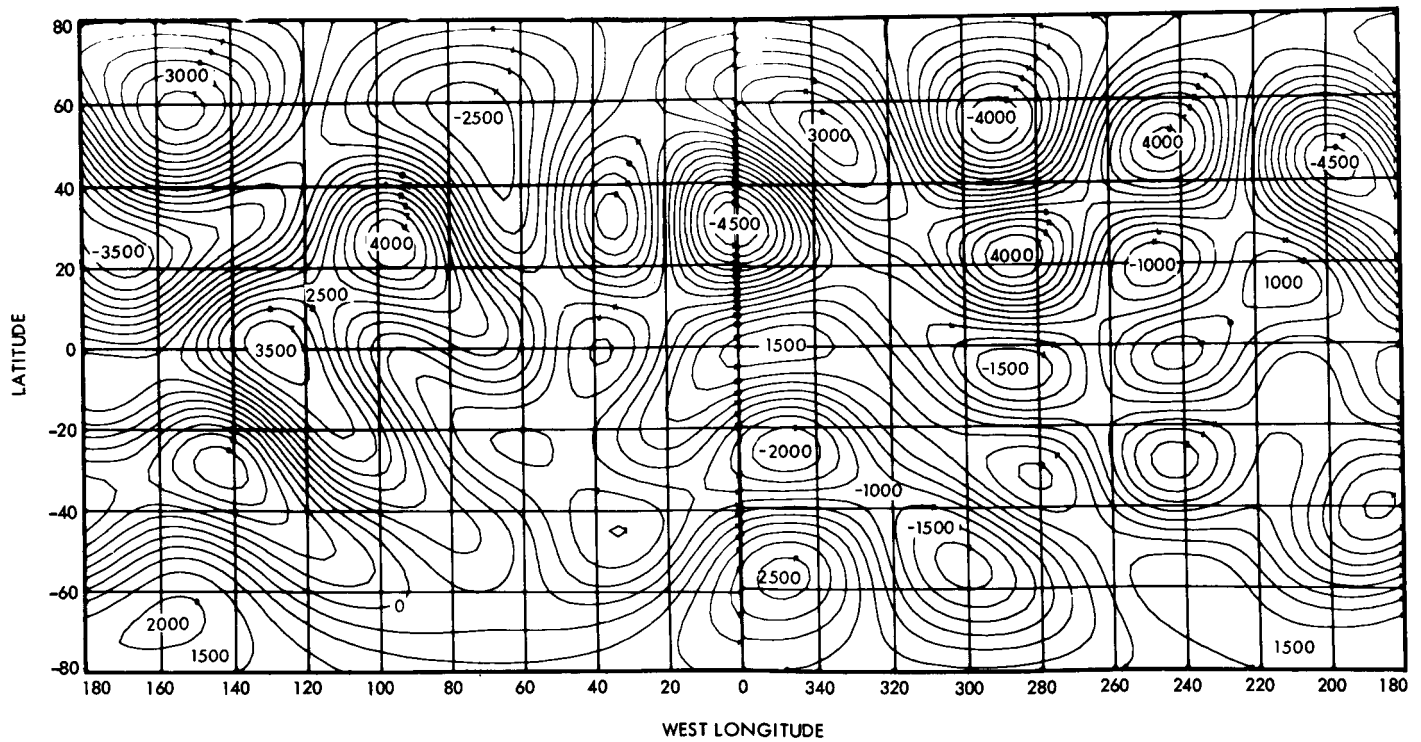


Fig. II-2. Equivalent surface mass distribution, based on interim eighth-degree model (see Table II-2). Contours at 500-m intervals.

Table II-2. Interim eighth-degree harmonic model for the gravity field of Mars<sup>a</sup>

Index	J (Not normalized)			
2.	.1974-02			
3.	.7305-04			
4.	-.1032-03			
5.	.4392-05			
6.	.3734-04			

Index	C (Normalized)	S (Normalized)	J (Normalized)	$\theta$ , deg
22.	-.8400-04	.4621-04	.9587-04	.7559+02
31.	.4673-05	.2315-04	.2362-04	.7859+02
32.	-.2458-04	.4497-05	.2499-04	.8482+02
33.	.3684-04	.2426-04	.4411-04	.1112+02
41.	-.5158-05	-.3041-05	.5988-05	-.1495+03
42.	-.3682-05	-.6341-05	.7332-05	-.6007+02
43.	.5921-05	-.2399-05	.6388-05	-.7351+01
44.	-.4310-05	-.1878-04	.1926-04	-.2573+02
51.	-.2273-04	-.1004-04	.2485-04	-.1562+03
52.	.2200-04	.9236-05	.2386-04	.1138+02
53.	.8852-05	-.5199-05	.1027-04	-.1014+02
54.	-.1767-04	.2008-05	.1778-04	.4338+02
55.	-.4947-05	-.1329-07	.4947-05	-.3597+02
62.	.4181-04	.3261-05	.4193-04	.2230+01
63.	.1258-04	-.1071-04	.1652-04	.1347+02
64.	.8869-07	.3804-05	.3805-05	.2217+02
65.	-.2943-05	-.1616-05	.3357-05	-.3025+02
66.	-.1808-05	-.3659-06	.1845-05	-.2809+02
73.	.2691-04	-.7317-05	.2788-04	-.5071+01
74.	-.9179-05	.9955-05	.1354-04	.3317+02
75.	-.1185-04	-.1129-04	.1637-04	-.2728+02
76.	-.1328-04	.3166-05	.1365-04	.2776+02
77.	-.6095-05	-.2976-05	.6783-05	-.2200+02
84.	-.1617-05	.3416-04	.3419-04	.2318+02
85.	-.1954-04	-.7645-05	.2099-04	-.3173+02
86.	-.1612-04	.1212-04	.2017-04	.2384+02
87.	-.4454-05	.9455-05	.1045-04	.1646+02
88.	-.1012-05	-.6373-06	.1196-05	-.1848+02

<sup>a</sup>Used as the basis for Figs. II-1 and II-2.

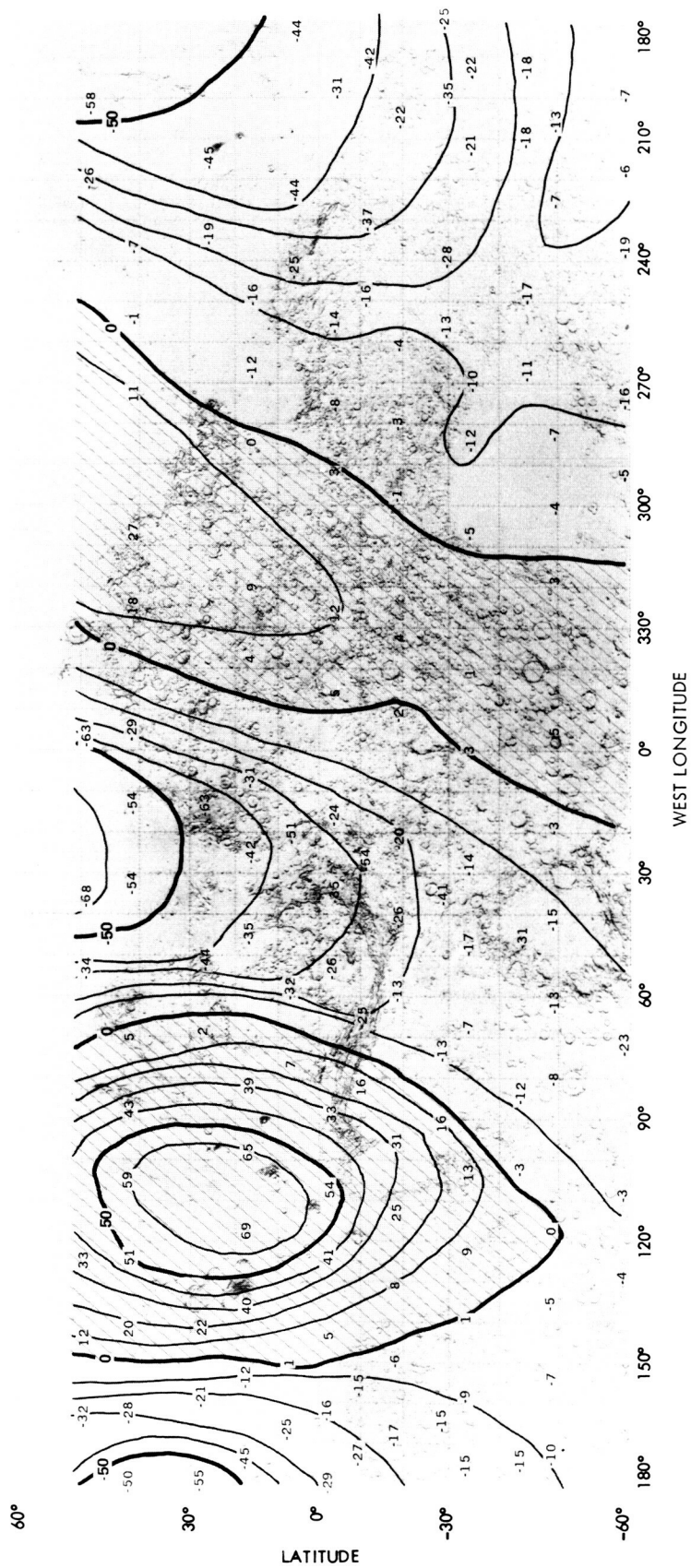


Fig. II-3. Mariner 9 mass point estimate. Units:  $\text{GM} \times 10^{-6}$ . Each unit indicates the size of the disturbing mass at that location. The contours are lines of equal disturbing mass, spaced ten units apart.

c. **Spin-axis direction results.** As reported in Ref. II-5 the spin-axis direction of Mars has been redetermined using *Mariner 9* data, and the new value agrees with that of Ref. II-3. It differs from the previous best value (Ref. II-2) by approximately  $0.5^\circ$ , and has an uncertainty of approximately  $0.2^\circ$  in each component. Sinclair's slightly earlier result, obtained using Earth-based observations of Phobos and Deimos, is compatible with that from *Mariner 9*; he reported an uncertainty of about  $0.05^\circ$  in each component. The *Mariner 9* data are currently being reanalyzed to improve the spin-axis determination, and possibly also to improve the spin-rate determination. No new results are presently available; the present status is shown in Table II-3.

**Table II-3. Direction of the spin axis of Mars**

Method	$\alpha$ , <sup>a</sup> deg	$\delta$ , <sup>a</sup> deg
<i>Mariner 9</i> (six revolutions)	317.3 $\pm$ 0.2	52.6 $\pm$ 0.2
<i>Mariner 9</i> (38 revolutions)	317.3 $\pm$ 0.2	52.8 $\pm$ 0.2
Landmark: <i>Mariner 9</i> , approach phase	317.5 $\pm$ 0.9	52.9 $\pm$ 0.9
Landmark: <i>Mariner 9</i> , orbit phase	317.3 $\pm$ 0.2	52.7 $\pm$ 0.1
Star-satellite-approach	317.4 $\pm$ 0.2	52.8 $\pm$ 0.2
Earth-based Deimos-Phobos	317.31 $\pm$ 0.05	52.65 $\pm$ 0.03
American Ephemeris and Nautical Almanac	316.85	53.01

<sup>a</sup>Referred to the mean equinox and equator of 1950.0.

### 3. Interpretation of the Gravity Results

The Mars gravity-field model is a description of the gravitational forces in the proximity of Mars. The gravity field reflects the distribution of mass within the planet. Unfortunately, a knowledge of the gravity field does not uniquely determine the mass distribution; it leaves one dimension in the spatial mass density profile that must be evaluated by other means. Thus, for example, if we can assume that most of the deviations from uniformity (say from an oblate spheroid) are due to variations in topography and the crust/mantle profile in conjunction with the crust and mantle densities, then the gravity field can be used in conjunction with the topography to characterize the crust density or crust thickness. Efforts in this direction are being pursued in conjunction with the Surface Properties Working Group (see Section VIII of this Report). Preliminary results suggest only a partial isostatic compensation in the Tharsis region, but perhaps a large fraction compensation in the great lowland region of Hellas.

Another desired result that can be inferred from the gravity model is the value of the second-degree moments of inertia. From the gravity results we have directly

$$J_2 = \frac{C - \frac{1}{2}B - \frac{1}{2}A}{MR^2} = (196.0 \pm 0.9) \times 10^{-5}$$

$$J_{22} = \frac{B - A}{4MR^2} = (63.1 \pm 0.07) \times 10^{-6}$$

$f$  (dynamic flattening) =

$$\frac{3}{2}J_2 + \frac{1}{2}\alpha = (52.3 \pm 0.2) \times 10^{-4}$$

From the theory of gravitation equilibrium of a spinning fluid, we have<sup>2</sup>

$$\frac{C}{MR^2} = \frac{2}{3} \left\{ 1 - \frac{2}{5} \left[ \frac{5}{2} \left( \frac{\alpha}{f} \right) - 1 \right]^{1/2} \right\}$$

$$= (375.7 \pm 0.7) \times 10^{-3}$$

where

$$\alpha = n^2 R^3 / GM = (45840.4 \pm 0.2) \times 10^{-7}$$

$R$  (reference equatorial radius) = 3393.4 km

$$n \text{ (sidereal rotation rate)} = (7088218.8 \pm 0.4) \times 10^{-11} \text{ rad/sec}$$

$$= 350.89202 \pm 0.00002^\circ / \text{day}$$

$$GM \text{ (Mars gravity constant)} = 42828.3 \pm 0.2 \text{ km}^3 / \text{sec}^2$$

The moment-of-inertia ratios are

$$\frac{\left( C - \frac{1}{2}B - \frac{1}{2}A \right)}{C} = (52.2 \pm 0.3) \times 10^{-4}$$

$$\frac{B - A}{C} = (67.2 \pm 0.7) \times 10^{-5}$$

$$\frac{B}{C} = (9951.2 \pm 0.3) \times 10^{-4}$$

$$\frac{A}{C} = (9944.5 \pm 0.3) \times 10^{-4}$$

<sup>2</sup>The value of  $n$  is taken from Ref. II-7, and  $GM$  from Ref. II-8.

The value of  $C/MR^2$  is a measure of the radial density variation in the planet. The value ranges from 0, if all of the mass is concentrated at the center, to  $2/5$  for uniform density to  $2/3$  for a spherical shell. Thus, the value derived previously is consistent with the expectation that the planet has a density gradient increasing somewhat toward the center. We need additional information to identify a more detailed structure.

The value of

$$\frac{\left(C - \frac{1}{2}B - \frac{1}{2}A\right)}{C}$$

can be used to estimate the precession of the Martian pole due to the solar torque. Using the expression (Ref. II-2)

$$\text{Precession rate} = -\frac{3}{2} \left( \frac{C - \frac{1}{2}A - \frac{1}{2}B}{C} \right) \frac{n_0^2 \cos \gamma}{n(1 - e_0^2)^{3/2}}$$

and values of Mars mean motion  $n_0$  and eccentricity  $e_0$  from Ref. II-7, we obtain the value  $7.39 \pm 0.04$  arc sec/yr, or a period of  $(1.754 \pm 0.009) \times 10^5$  years, compatible with other estimates.

### C. Test of General Relativity

In this part of the report, we describe the status of an experiment which is not concerned directly with the planet Mars, but instead which has as its objectives a high-precision test of the theory of general relativity, an improvement in the inner-planet ephemerides, and a study of the plasma in the solar corona during August to October 1972. These goals and the work required to achieve them are intricately interconnected. It is virtually impossible to concentrate on any one without becoming deeply involved with others. For the purpose of discussion, however, we will focus primarily on the relativity test.

The *Mariner 9* tracking data offer the opportunity to test the predictions of general relativity more precisely than ever before; this test may constitute the most important non-null gravity experiment since Leverrier uncovered the first deviation from Newtonian theory in the 1850s. With the ranging system capable of a  $0.1\text{-}\mu\text{sec}$  precision in the measurement of round-trip time delays between the tracking station and the spacecraft, the predicted increase of about  $200 \mu\text{sec}$  in these delays near superior conjunction, attributable directly to the Sun's gravity field, may be determined with an uncertainty of no more than about 1%. At this level of accuracy, the

*Mariner 9* test would provide conclusive discrimination between the predictions of Einstein's purely tensor theory of gravity and those of the scalar-tensor Brans-Dicke theory when the fraction of scalar-field admixture in the latter is set in accord with the Princeton solar oblateness experiment. For this time-delay test, the predicted "excess" delays of the Brans-Dicke theory are about 6% less than for general relativity. The distinction between the two theories is of far-reaching importance for the correct understanding of numerous astrophysical phenomena, ranging from the origin of the universe to the evolution of Earth. The prime goal of our efforts, therefore, has been directed toward the achievement of this discrimination.

Our approach in performing this test of general relativity is to use the generalized Schwarzschild metric as first suggested by Eddington. This line element can be written in isotropic form as:

$$ds^2 = \left[ 1 - (2\alpha r_0/r) + (2\beta r_0^2/r_0^2) + \dots \right] dt^2 - \left[ 1 + (2\gamma r_0/r) + \dots \right] (dx^2 + dy^2 + dz^2) \quad (1)$$

where  $r_0 \simeq 1.5$  km is the gravitational radius of the Sun, where  $\alpha = \beta = \gamma = 1$  in the theory of general relativity, and where  $\alpha = \beta = 1$  in the Brans-Dicke theory, but  $\gamma \simeq 0.84$ . Using Eq. (1), we can easily develop the theoretical expression for the time-delay observable. The "excess" delay that is attributable to the direct influence of solar gravity on the round-trip propagation time is given by

$$\Delta t \simeq \frac{2r_0}{c} (1 + \gamma) \ln \left( \frac{r_e + r_m + R}{r_e + r_m - R} \right) \quad (2)$$

where  $r_e$  and  $r_m$  are the heliocentric distances of Earth and Mars, respectively, and where  $R$  is the Earth-Mars distance. As stated above, Eq. (2) yields a maximum value of about  $200 \mu\text{sec}$  for the conditions of the *Mariner 9* experiment.

In the following subsections we outline our progress toward the placement of the most stringent bound on  $\gamma$  allowable by the *Mariner 9* data, when combined with the existing data from radar observations of the inner planets. The latter are required to aid in the determination of the orbits of Earth and Mars. Two basic approaches have been used to determine  $\gamma$ . In the first method a two-step process is employed. The Doppler

and/or ranging data from the radio tracking of one or several passes of the spacecraft are suitably combined and analyzed to obtain an estimate of the equivalent center-of-Earth to center-of-Mars round-trip light time corresponding to each ranging point. These "normal points" are then combined with the radar data to estimate  $\gamma$  and, simultaneously, the other relevant parameters such as the planetary orbital elements. In the second method, all data are analyzed in a single step; the application of this method has so far been confined to a consideration of only a short arc of data in the vicinity of the superior conjunction of Mars because of enormous practical difficulties. In the remainder of this report we discuss only the first method. Section II-C-1 is devoted to a description of the data-reduction procedures used in producing the normal points, and Section II-C-2 contains a description of the analysis used in the estimation of  $\gamma$  from the normal points. Section II-C-3 contains a brief conclusion.

### 1. Generation of Normal Points

While *Mariner 9* was tracked in orbit from November 14, 1971, until October 27, 1972, more than 300,000 two-way Doppler measurements, taken at 1-min count times, and more than 1300 individual time-delay measurements were made. Most of the latter were obtained in the 8 weeks bracketing superior conjunction. The primary mode of processing these data was: (1) to solve for the spacecraft orbit relative to the center of mass of Mars from short spans (usually a single revolution) of Doppler data, and (2) to combine the resulting spacecraft position vectors relative to Mars at the epochs of the time-delay measurements with the time-delay data and other information to yield pseudo measurements of the time delay from the center of mass of Earth to the center of mass of Mars. These pseudo measurements, referred to as normal points, contain essentially all of the information in the individual time-delay and associated Doppler measurements that can be used to improve the test of general relativity and one's knowledge of the Earth-Mars ephemeris. Angular information content of the Doppler data is relatively weak and has been neglected.

More than 1000 normal points have been generated so far from the Doppler and time-delay data. Most of these, as mentioned, are for epochs within a few weeks of the superior conjunction. For these reductions, the spacecraft orbit was determined from the Doppler data by using the Orbit Determination Program of the Jet Propulsion Laboratory; the normal points themselves were then computed using a technique (Ref. II-9) that introduces errors smaller than  $10^{-3}$   $\mu\text{sec}$ .

The uncertainty in the computations and the noise in the Doppler and time-delay data do not, however, limit the accuracy of the normal points. The accuracy of the normal points is limited (Ref. II-9) by: (1) spacecraft orbit determination errors resulting from the complex gravity field of Mars, and (2) distortions of the Doppler and time-delay measurements produced by electrons in the transmission medium, which retard the group velocity and advance the phase velocity of the radio waves.

The non-spherical portion of the gravity field of Mars, if totally unmodeled, would have produced systematic errors of more than 1  $\mu\text{sec}$  in the normal points. However, the use of gravity models available from multi-revolution fits to the Doppler data (see Section II-B) have considerably reduced the errors in the spacecraft position knowledge. The analysis of residuals from Mars-Earth orbital fits to the normal points indicates that the RMS error of the normal points is about 0.1  $\mu\text{sec}$  in the early part of the mission when Doppler data from the overseas stations were used to assist in the determination of the spacecraft orbit, and is about 0.3  $\mu\text{sec}$  when only DSS 14 data were available.

The most serious limitation in the usefulness of the normal points for planetary ephemeris improvement and relativity parameter estimation is caused by electron-density fluctuations in the signal path. While the signal path to *Mariner 9* passed near the Sun, stochastic variations in the electron density of the solar corona led to normal points that were observed to vary by several microseconds during a single day. The DRVID technique (Ref. II-10) was used to calibrate charged-particle activity in the signal path near superior conjunction and to provide corrections for the computation of the normal points. Although the use of the DRVID calibrations has improved the accuracy of the normal points (as the Doppler data and hence the determination of the spacecraft position vector have been corrected), the calibrations do not yield the total group delay caused by the electrons. Thus, the day-to-day fluctuations due to the changing corona remain in the time-delay measurements, and hence in the normal points. These fluctuations, which are as large as 10  $\mu\text{sec}$  near superior conjunction, currently provide the limiting errors in the reduction of the normal points.

### 2. Status of the Normal-Point Analysis

The normal points from the *Mariner 9* tracking data are being analyzed at both MIT and JPL. The status of these analyses is described in the subsequent paragraphs.

**a. Analysis at MIT.** Analyses of the *Mariner 9* normal points have been pursued by: (1) using only the normal points in a least-squares differential correction of the Earth-Mars ephemeris, and (2) combining planetary radar data with the normal points. The interval covered by the normal points (November 17, 1971, to October 25, 1972) is much too short to allow an adjustment to all orbital elements of Earth and Mars; consequently, only the most relevant elements are differentially corrected when fitting the normal points alone. These elements are the semi-major axis, eccentricity, argument of perihelion, and initial mean anomaly of Mars, and the semi-major axis and eccentricity of Earth. In combined solution with the radar data, a much more complete set of parameters can be adjusted.

The radar data, consisting of observations of Mercury and Venus from 1966 to 1972 and Mars from 1967 to 1972, obtained partly at the Haystack Observatory and partly at the Arecibo Observatory, were down-weighted such that the minimum error in Earth-Mars delay was set at  $10 \mu\text{sec}$ , with the corresponding minimum delays of  $3 \mu\text{sec}$  for Earth-Venus and Earth-Mercury. The actual measurement uncertainties were as low as several tenths of a microsecond in many cases, but these values were not used in an attempt to mute the effects of the high-frequency components of the topography variations. The low-frequency components were modeled with a two-dimensional Fourier series. The number of topography parameters estimated in the solutions was 202, with 122 for Mars and 40 each for Mercury and Venus. Another 38 parameters were composed of the orbital initial conditions for each inner planet, their masses, the astronomical unit, a relativity parameter ( $\gamma$ ), and various bias parameters. The solar corona was represented by an electron-density function that decreased inversely with the square of the distance from the Sun's center. The normalizing factor for the electron density, nominally  $7 \text{ electrons cm}^{-3}$  at the distance of Earth's orbit, was included as a parameter in the solutions.

The most recent *Mariner 9* postfit residual plots from a combined radar and normal-point solution are shown in Figs. II-4 through II-6. For purposes of graphic clarity, only two points per tracking pass are shown, the highest and lowest residual for each.

**b. Analysis at JPL.** Fits to the *Mariner 9* normal points have been accomplished by adjusting the orbital elements of Earth and Mars to fit the data in a least-squares sense. Because the purpose of the fits to date has been to find

procedural errors in the generation of the normal points and to edit the data, it has been adequate to assume the validity of the Einstein theory of general relativity in the computations for the orbits and the observables. In particular, the Einstein prediction of the relativistic delay in the ranging signal at conjunction has been assumed. In addition, the delay in the ranging signal through the solar corona has been represented by a spherically symmetric steady-state model for the electron density. The electron density in this model at a given distance from the Sun is a free parameter which has been estimated from the fits to the normal points. An a priori constraint has been imposed on the electron density so that at Earth it is equal to  $5 \pm 5$  per cubic centimeter. Random fluctuations in the electron density have been accounted for by varying the assumed error on each normal point according to the law that the coronal contribution to the error in range is inversely proportional to the  $3/2$  power of the distance of the ray path from the Sun's center. Thus, normal points obtained within a few degrees of the Sun are assumed in error by a few microseconds. On the other hand, points obtained far from the Sun are assumed in error by only  $0.3 \mu\text{sec}$ .

Rather than determine the orbital elements of Earth and Mars directly from the relatively limited arc of normal points, the eigenvectors of the least-squares normal equations are found, and a new set of orthogonal parameters is defined which represents directions along these eigenvectors. This new set of parameters is adjusted to fit the normal points. It has been found that nine orthogonal parameters, made up of a linear combination of the 12 orbital elements of Earth and Mars and two highly correlated steady-state corona parameters, is sufficient to fit the current set of normal points. The data contain no information on parameters beyond those that lie along the nine most significant eigenvectors.

The residuals that result from the rank nine solution of the normal equations are shown in Figs. II-7 and II-8. In Fig. II-7, a current set of normal points over the entire 11 months of the *Mariner 9* mission is represented by residuals about a zero mean. This mean represents the best fit Earth-Mars orbit and the best electron densities that have been achieved to date under the assumption of the correctness of the Einstein theory. Figure II-8 shows the same residuals, but for the conjunction region on an expanded time scale; more resolution in the plot of the residuals near conjunction is available in Fig. II-8 than in Fig. II-7.

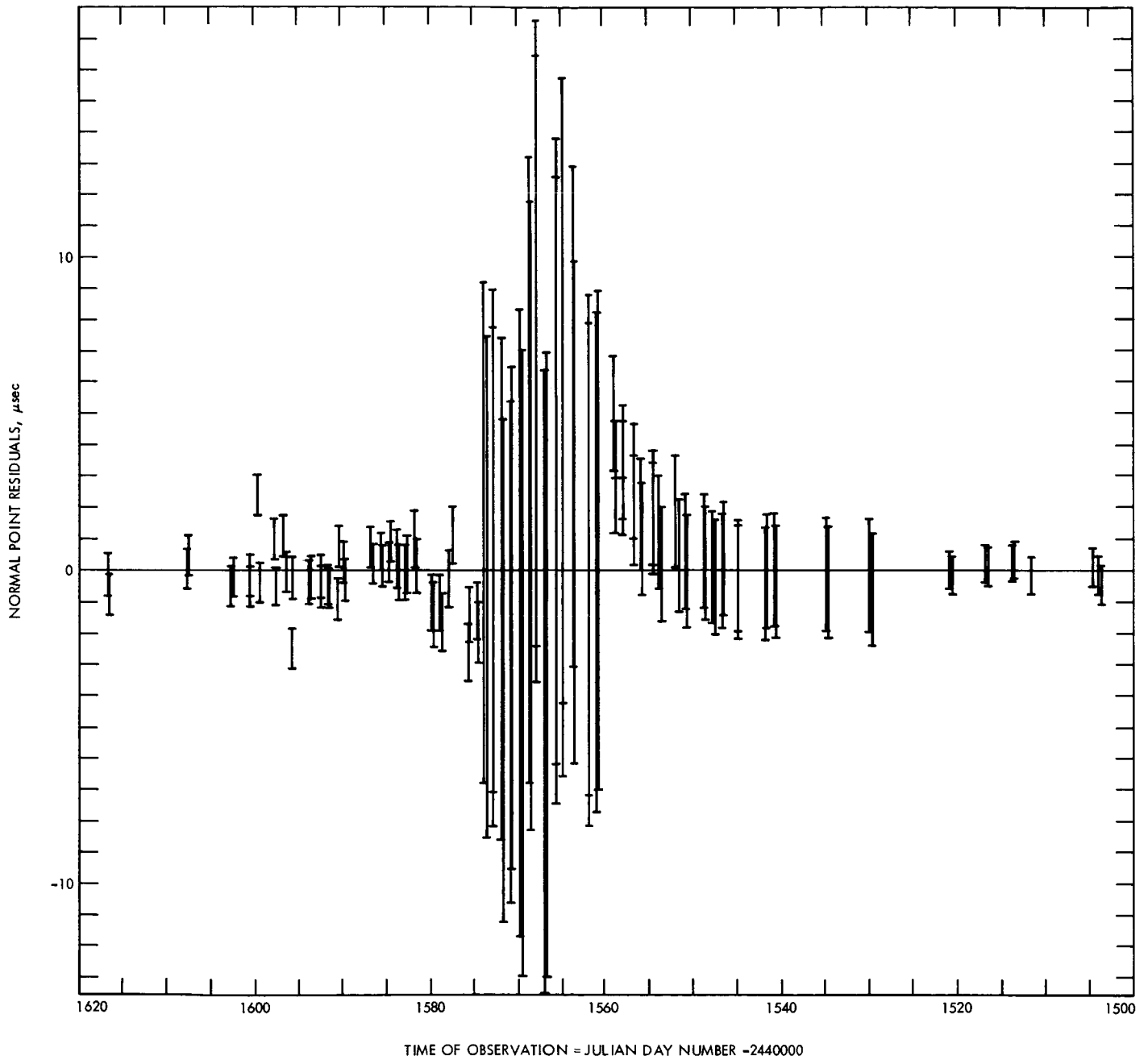


Fig. II-4. Postfit residuals for normal points from an MIT solution that combines planetary radar and *Mariner 9* data.

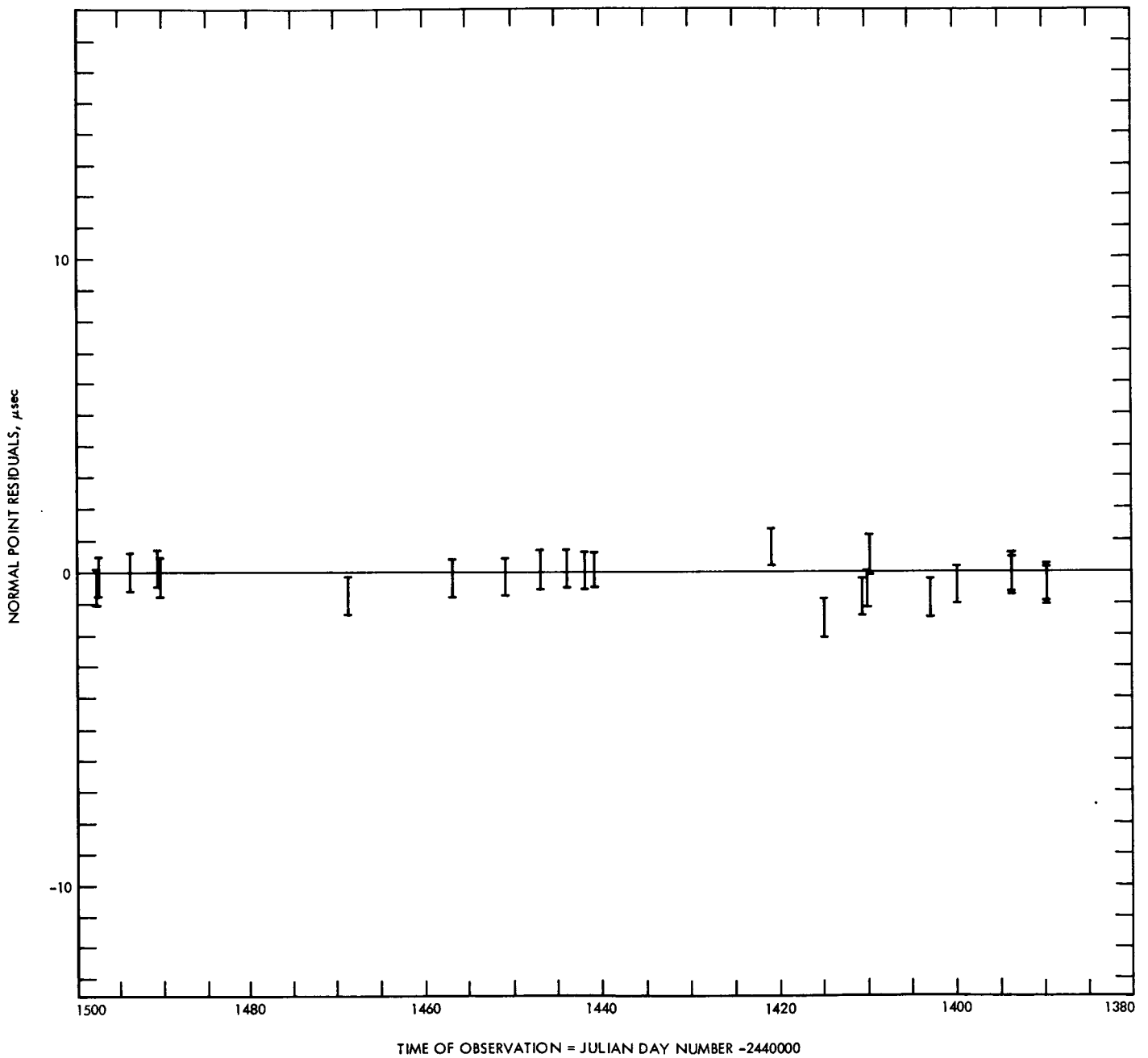


Fig. II-5. Postfit residuals for normal points from an MIT solution that combines planetary radar and *Mariner 9* data.

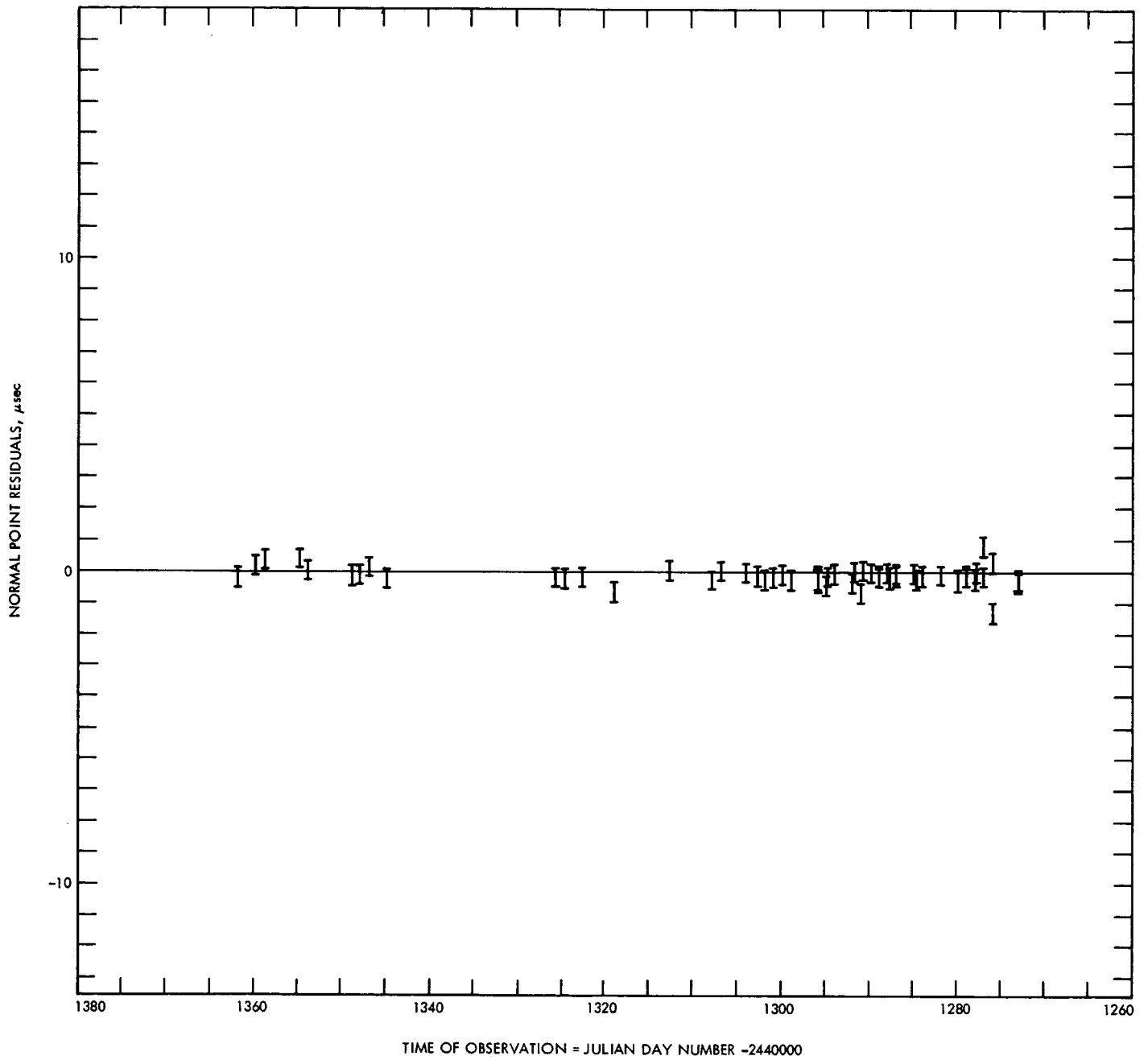


Fig. II-6. Postfit residuals for normal points from an MIT solution that combines planetary radar and *Mariner 9* data.

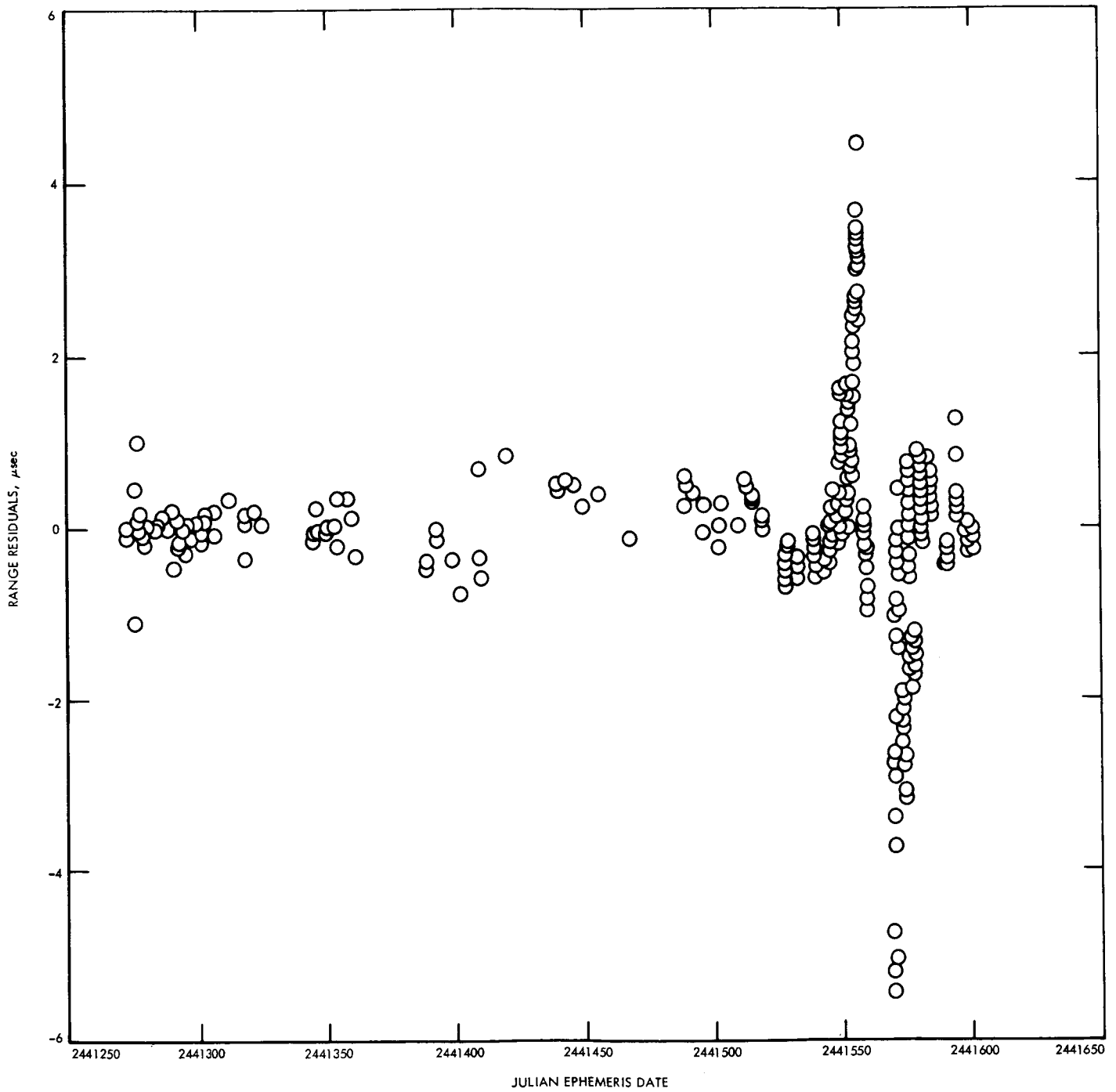


Fig. II-7. Postfit residuals for normal points from a JPL solution for nine orthogonal parameters.

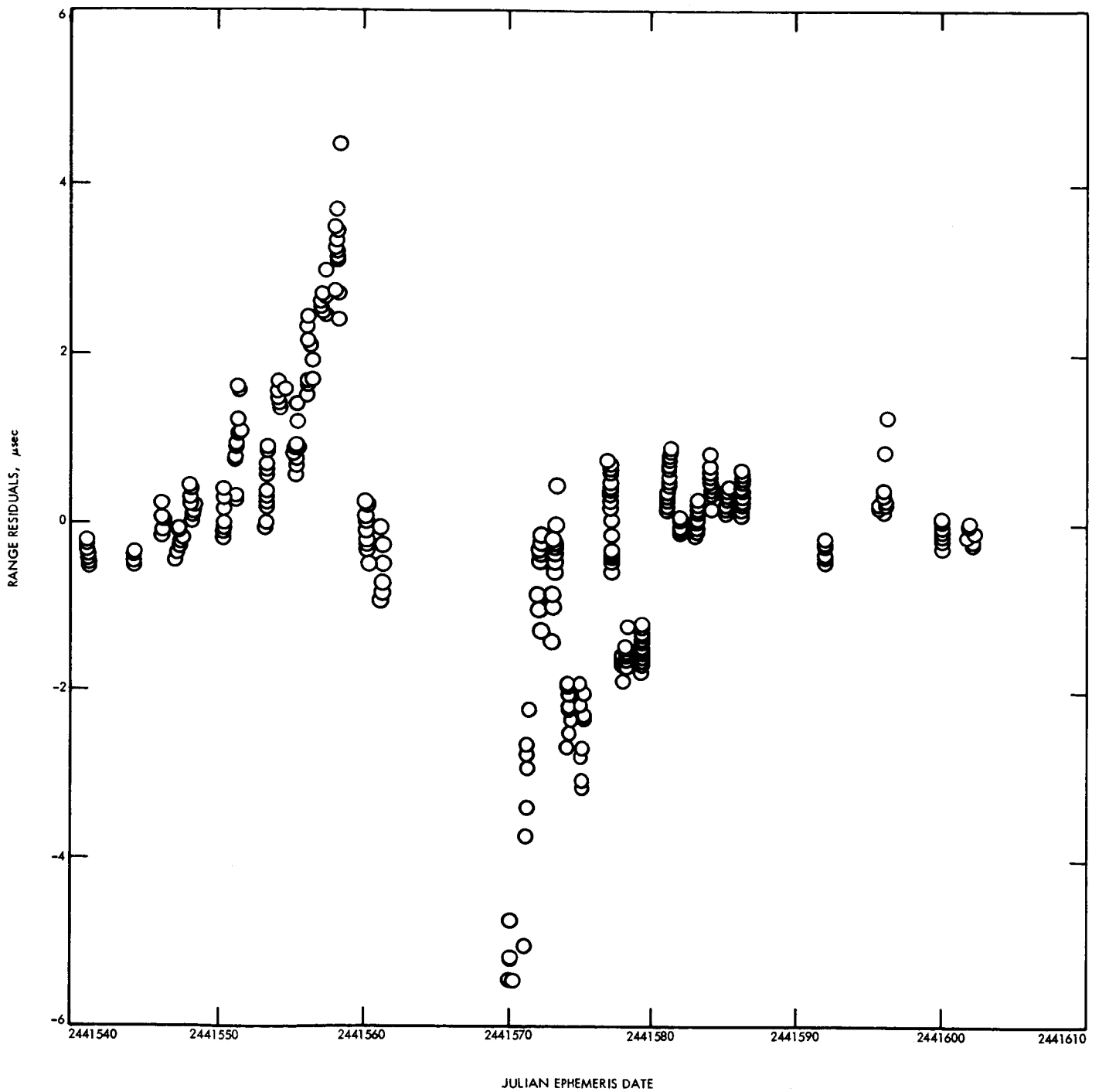


Fig. II-8. Postfit residuals for normal points near conjunction from a JPL solution for nine orthogonal parameters.

### 3. Conclusions

It is obvious that considerably more analysis is required before the goal outlined can be achieved. In particular, cross-checking of each stage of the data reduction through use of the independent software developed at JPL and MIT will be undertaken. More thorough analysis will be made of the possible direct influences of:

(1) Solar corona on the normal points.

(2) Planetary topography on the orbit determination.

The CME Team is guardedly optimistic that the final uncertainty on  $\gamma$  can be reduced at least to 2%, which would represent about a five-fold improvement over current knowledge.

## References

- II-1. Lorell, J., Anderson, J. D., and Shapiro, I. I., "Celestial Mechanics Experiment for Mariner Mars 1971," Vol. 12, pp. 78-81, 1970.
- II-2. de Vaucouleurs, G., "The Physical Ephemeris of Mars," *Icarus*, Vol. 3, p. 326, 1964.
- II-3. Sinclair, A. T., "The Motions of the Satellites of Mars," *Mon. Not. Roy. Astron. Soc.*, Vol. 155, p. 259, 1972.
- II-4. Lorell, J., Born, G. H., Christensen, E. J., Jordan, J. F., Laing, P. A., Martin, W. L., Shapiro, I. I., Reasenberg, R. D., and Slater, G. L., "Mariner 9 Celestial Mechanics Experiment: Gravity Field and Pole Direction of Mars," *Science*, Vol. 175, p. 320, 1972.
- II-5. Lorell, J., Born, G. H., Christensen, E. J., Esposito, P. B., Jordan, J. F., Laing, P. A., Sjogren, W. L., Wong, S. K., Reasenberg, R. D., Shapiro, I. I., and Slater, G. L., "Gravity Field of Mars From Mariner 9 Tracking Data," *Icarus*, Vol. 18, p. 304, 1973.
- II-6. Sjogren, W. L., Muller, P. M., Gottlieb, P., Wong, L., Buechler, G., Downs, W., and Prislun, R., "Lunar Surface Mass Distribution From Dynamical Point-Mass Solution," *The Moon*, Vol. 2, pp. 338-353, 1971.
- II-7. *Explanatory Supplement to the Astronomical Ephemeris, the American Ephemeris, and Nautical Almanac*, Her Majesty's Stationery Office, London, 1961.
- II-8. Null, G. W., "A Solution for the Sun-Mars Mass Ratio Using Mariner 4 Doppler Tracking Data," *Astron. J.*, Vol. 72, p. 1292, 1967.
- II-9. Jordan, J. F., Hylkema, R. K., and Reinbold, S. J., "Determination of Normal Points for the Relativity Test of the Celestial Mechanics Experiment," *Mariner Mars 1971 Final Project Report. Vol. IV: Science Results*, Technical Report 32-1550, Jet Propulsion Laboratory, Pasadena, Calif., 1973.
- II-10. MacDoran, P. F., and Martin, W. L., "DRVID Charged-Particle Measurements With a Binary Coded Sequential Acquisition Ranging System," *Space Programs Summary 37-57*, Vol. II, pp. 72-81, Jet Propulsion Laboratory, Pasadena, Calif., 1969.

## Acknowledgments

Doppler and ranging data used for the *Mariner 9* celestial mechanics experiment were acquired as part of the normal tracking operations of the Deep Space Network. In the time period encompassing superior conjunction (August 29 through September 14), the tracking signal was masked by noise from the solar corona, requiring the application of extraordinary techniques to obtain usable data. A programmable local oscillator was brought on line; it was interfaced to the DSS 14 receiver and operated during the 2 crucial weeks of superior conjunction.

Because of the influence of the solar corona, neither the standard receiver nor the advanced third-order loop could maintain phase lock. The programmable oscillator did work, however, and ranging data were obtained throughout the time of superior conjunction.

The dual polarization spectrograms of *Mariner 9* transmissions that were produced for the solar corona study were helpful in monitoring the corona and in selecting parameters for the ranging measurements.

For the success of these efforts, we especially thank R. Emerson, R. Goldstein, I. MacConnell, R. Sydnor, H. Wilck, C. Stelzried, and D. Spitzmesser of the Jet Propulsion Laboratory; and R. Cannon of the University of California, Berkeley.

# III. S-Band Occultation Experiment: A Summary

A. J. Kliore, D. L. Cain, G. Fjeldbo, B. L. Seidel, M. J. Sykes, and P. M. Woiceshyn  
Jet Propulsion Laboratory/California Institute of Technology, Pasadena, California 91103

S. I. Rasool

National Aeronautics and Space Administration, Washington, D.C. 20546

The S-band occultation experiment was proposed to the Mariner Mars 1971 Program Office on June 17, 1968, with A. J. Kliore as the Principal Investigator and D. L. Cain, B. Seidel, and G. Fjeldbo as Co-Investigators. The objectives of the experiment were stated as follows:

- (1) To obtain a better determination of the surface density and pressure in the atmosphere of Mars and its variation with altitude above many locations on the planet's surface, making it possible to observe possible variations with latitude and provide data for atmospheric circulation models.
- (2) To obtain an improved determination of the electron density profile of the Martian ionosphere at many locations above the planet's surface under varying solar illumination conditions.
- (3) To obtain a precise measurement of the radius of Mars at many points on the surface, thus yielding information on the shape of the planet.
- (4) To investigate surface characteristics by means of studying reflected signals.

The proposal was accepted on October 18, 1968. On September 29, 1970, Dr. S. I. Rasool was added as a Co-Investigator. Among the requirements submitted to the

Mission Design Team for the S-band occultation experiment were:

- (1) Orbits to be selected so that each spacecraft provided not less than 30 pairs of occultation opportunities.
- (2) Occultations to occur over a wide range of latitudes and different longitudes.
- (3) Occultations to occur under varying solar illumination conditions.
- (4) Real-time digitization of data at DSS 14 (Goldstone, Calif.) for open-loop data acquisition.
- (5) Incorporation of data analysis and reduction programs into the Mission Operations System.
- (6) A suitably stable auxiliary oscillator in the radio subsystem (i.e., 1 part in  $10^{10}$  over a 10-sec period).

For investigation of surface electromagnetic characteristics by studying the reflected signals, a system communications margin in excess of 50 dB was required. There was also a requirement to provide for the extension of the mission beyond the nominal lifetime to make use of recurring occultation opportunities. Most of these requirements were met, contributing greatly to the success of the experiment.

As initially designed, the orbit for *Mariner 8* (which subsequently was lost at launch) would provide 42 occultation pairs or 84 occultation measurements, and that for *Mariner 9* approximately 47 occultation pairs for a total of 94. The combined missions, therefore, would comprise 178 occultation measurements during the standard mission. *Mariner 8* would cover the near-equatorial and north polar regions; *Mariner 9* would cover a wider range of northern latitudes.

The failure of *Mariner 8* dictated a new choice of orbit which provided a total of 160 occultations during the standard mission and an opportunity for an additional 160 during extended missions I and II.

### A. Objectives and Achievements

The results from the standard mission and the first extended mission are described in Refs. III-1 through III-5 (also see Sections XXXVI and XXXVII of Vol. IV of this Technical Report).

The first objective of the S-band occultation experiment called for better determination of the surface density and pressure in the atmosphere of Mars and its variation with altitude above many locations in the planet's surface. From a possible 320 such measurements, 260 were obtained. Table III-1 is a summary of all possible occultation measurements during the standard mission, as well as during extended missions I and II. It is immediately obvious that during the extended missions, 35 out of a possible 160 measurements were lost because of conflicting activities at DSS 14. Only 25 of a possible 320 measurements were lost because of operational problems, which include bad or noisy data as well as operational difficulties at the station, such as the inability to obtain open-loop data. Thus, including the tracking conflict, a total of 81.3% of all possible measurements was successfully recovered. However, as the loss of data during DSS 14 tracking conflicts was inevitable, the true percentage of recovered data is about 91.3%.

A detailed summary of the results as they apply to the first, second, and third objectives is given in the subsequent paragraphs. The fourth objective, investigation of surface characteristics by means of studying reflected signals, has not yet been satisfied, primarily because of lack of time. The data, in the form of digital open-loop recordings, do exist, and the achievement of this objective is the goal of a great part of our activities during the reduced data analysis phase of Fiscal Year 1974.

Table III-1. Summary of S-band occultation measurements

Mission phase	Number of possible measurements	Lost		Successful
		Operational problems	Tracking conflict	
Standard	160	7	0	153
Extended mission I	100	8	20	72
Extended mission II	60	10	15	35
Total	320	25	35	260
Percent	100.0	7.8	10.9	81.3

### B. Atmosphere and Ionosphere

Detailed results relating to the atmosphere and ionosphere objectives are described in Refs. III-1, III-2, and III-4 (also see Section XXXVI of Vol. IV of this Technical Report).

During the standard mission, the occultation measurements were made when Mars was enveloped by a severely obscuring dust storm. The effect of the dust in the atmosphere was apparent in the greatly reduced temperature gradients that were measured in the daytime near-equatorial atmosphere. This was interpreted as indicating the heating of the atmosphere by solar radiation being absorbed by the dust. The temperature gradients increased somewhat with time, possibly indicating a gradual clearing of the atmosphere during the standard mission. However, the gradients never fell below about  $-3.5^{\circ}\text{K/km}$ .

Measurements made at  $+65^{\circ}$  latitude near the morning terminator showed temperatures consistent with the condensation of carbon dioxide, which was expected at this time of the year in the northern hemisphere (northern hemisphere winter). The surface pressure in the near-equatorial regions ranged from a high of 8.9 mb in Hellas to a low of 2.8 mb in the Claritas and Tharsis areas, with a mean pressure of 4.95 mb. The pressures deduced from measurements at  $+65^{\circ}$  latitude ranged from 7.2 to 10.3 mb, with an average of 8.9 mb.

The pressure altitudes computed with the reference to the 6-1-mb level showed a range in the equatorial regions from a low of  $-4.4$  km in Hellas to a high of 9.6 km in Claritas, with a net excursion of 14.0 km and a mean altitude of 2.7 km. In contrast, the region at  $+65^{\circ}$  latitude showed uniformly negative altitudes with a mean of  $-2.6$  km. This disparity in pressure, which was also reflected in the measured radii between the near-equatorial

and +65° latitude measurements, at that time suggested that the physical shape of Mars may be more oblate than the shape of gravitational equipotential surface, leading to a higher atmospheric pressure at high altitudes than at the equator. However, it was felt that more measurements at high latitudes were necessary to support this hypothesis.

A daytime ionosphere with a peak density of about  $1.5$  to  $1.7 \times 10^5$  electrons/cm<sup>3</sup> was measured at an altitude of 140 to 134 km over a range of solar zenith angles of 56° to 47°, showing some correlation between the variations in the peak density and the terrestrially measured solar flux. The average topside plasma scale height was 38.5 km, showing little correlation with solar flux and solar zenith angle.

A second set of occultation measurements, obtained during May and June 1972 (extended mission I), yielded extensive data on the north and south polar regions.

The daytime temperature profiles, representative of a clear atmosphere, showed gradients averaging  $-2.3^\circ\text{K}/\text{km}$ , far smaller than those expected under conditions of radiative-convective balance in a carbon dioxide atmosphere. The measured gradients were, however, in good agreement with some computed radiative-dynamical models.

The near-surface temperatures measured in the Martian spring daytime on the north polar cap were about 180 to 190°K, possibly indicating that it may consist of water ice. However, it may also be possible that large temperature discontinuities of 30° or 40°K may exist between the surface and the altitude of the last occultation measurement, which is about 1 km.

Temperatures in the south polar area measured at nighttime were low enough for condensation of carbon dioxide to take place, which is to be expected during the southern hemisphere fall when deposition of the southern polar cap presumably occurs.

Measurements of the daytime ionosphere at solar zenith angles greater than 72° showed much lower than expected heights of the ionization peak, possibly indicating about a 25% cooling of the lower atmosphere between November and December 1971 and May to June 1972, which would also be consistent with a clearing of the atmosphere.

A third set of data was obtained during September and October 1972 (extended mission II period). Of these data, most of the entry measurements were taken at  $-65^\circ$  latitude covering the entire range of longitudes. In contrast to the measurements made at +65° during the standard mission, these measurements yielded surface pressures of about 4 to 5 mb and correspondingly higher radii than in the northern hemisphere. The temperatures measured in this region, representing nighttime conditions during the southern polar winter, were extremely low, averaging about 150°K near the surface.

### C. Radius and Shape

Detailed results on the radius and shape of Mars are contained in Refs. III-3 and III-5.

The accuracy of the occultation radius measurements depends on three quantities: (1) precision of the orbit used for analysis, (2) precision with which the time of occultation can be measured, and (3) geometry of the occultation. During the standard mission the precision of the orbit with respect to time of closest approach, or periastron, was about 0.1, and the uncertainty in the determination of the time of occultation was about 0.07 sec. This yielded a total uncertainty of about 0.35 km in radius measurements. During extended missions I and II, the timing of the occultation events could be determined only to an accuracy of 0.7 sec. This, in extended mission I, combined with an uncertainty of 0.6 sec in orbit determination, yielded a radius uncertainty of about 1 km, when the decreased velocity of the radio beam relative to Mars was taken into account. For extended mission II, the timing uncertainties in orbit and time of occultation remained approximately the same. However, the velocity of the radio beam was greater by a factor of 2, yielding an uncertainty of approximately 2 km. These uncertainties should be remembered when discussing radius measurements resulting from the three phases of the S-band occultation experiment.

All surface occultation data were fitted to a triaxial ellipsoid, the parameters of which appear in Ref. III-5 (also see Section XXXVII of Vol. IV of this Technical Report) as well as in Section VIII of this Report. As expected, when one fits the raw radii to an ellipsoid, large residuals result from the great variations in local topography. This and the fact that the south polar region, as well as the entire southern hemisphere, is higher by about 3 to 4 km than the

northern hemisphere indicate that a triaxial ellipsoid is not a good representation of the physical surface of Mars.

In addition, the radius corresponding to the level of 6.1-mb pressure was computed from the measured pressures, temperatures, and radii. An ellipsoid fitted to these data could approximate a geoid. However, it must be remembered that dynamical corrections were not applied to these data and that the effects of atmospheric circulation may produce rather sizable effects.

The 6.1-mb constant pressure radii were also fitted to a spherical harmonic expansion which provided coefficients comparable in size to those derived from the radio tracking of the spacecraft, within the uncertainties introduced by neglecting Martian atmospheric dynamics.

As mentioned, local topography plays a major role on Mars, with Hellas lying about 6 km below its surroundings and one of the shield volcanoes, Middle Spot, lying about 13.5 km above the surrounding terrain.

#### D. Work in Progress

Although the basic data of the S-band occultation experiment have been reduced, there are some tasks in

progress which will extend beyond the formal lifetime of the Project. These include:

- (1) Correction of the 6.1-mb isobaric surface for the effect of Martian atmospheric dynamics in order to supply data for the construction of a geoid.
- (2) Analysis of the variations in the S-band occultation pressure data to obtain wind magnitudes during the dust storm.
- (3) Analysis of selected portions of the digitized open-loop data to obtain surface-reflected signals, possibly yielding information on the small-scale properties of the Martian surface.
- (4) Correction of latitude/longitude and radius data for a nonspherical Mars, taking into account aberration and relativistic effects.
- (5) Microfilming of data, including the uncorrected and corrected frequency and phase residuals, the refractivity data and the derived atmospheric quantities, which is to be maintained as the master reduced data record in addition to the raw data on magnetic tape.

### References

- III-1. Kliore, A. J., Cain, D. L., Fjeldbo, G., Seidel, B. L., and Rasool, S. I., "Mariner 9 S-Band Martian Occultation Experiment: Initial Results on the Topography and Atmosphere of Mars," *Science*, Vol. 175, pp. 313-317, 1972.
- III-2. Kliore, A. J., Cain, D. L., Fjeldbo, G., Seidel, B. L., Sykes, M. J., and Rasool, S. I., "The Atmosphere of Mars from Mariner 9 Radio Occultation Measurements," *Icarus*, Vol. 17, pp. 484-516, 1972.
- III-3. Cain, D. L., Kliore, A. J., Seidel, B. L., and Sykes, M. J., "The Shape of Mars from the Mariner 9 Occultations," *Icarus*, Vol. 17, pp. 517-524, 1972.
- III-4. Kliore, A. J., Fjeldbo, G., Seidel, B. L., Sykes, M. J., and Woiceshyn, P. M., "S-Band Radio Occultation Measurements of the Atmosphere and Topography of Mars with Mariner 9: Extended Mission Coverage of Polar and Intermediate Latitudes," *J. Geophys. Res.*, Vol. 78, 1973.
- III-5. Cain, D. L., Kliore, A. J., Seidel, B. L., Sykes, M. J., and Woiceshyn, P. M., "Approximations to the Mean Surface of Mars and Mars Atmosphere using Mariner 9 Occultations," *J. Geophys. Res.*, Vol. 78, 1973.

## IV. Infrared Radiometry Experiment

S. C. Chase

Santa Barbara Research Center, Goleta, California 93017

H. H. Kieffer

Department of Planetary and Space Sciences  
University of California, Los Angeles, California 90024

E. Miner

Jet Propulsion Laboratory/California Institute of Technology, Pasadena, California 91103

G. Münch and G. Neugebauer

Division of Physics, Math, and Astronomy  
California Institute of Technology, Pasadena, California 91109

### A. Objectives

The objectives of the infrared radiometry experiment were to:

- (1) Measure the thermophysical properties of the Martian surface on a global scale.
- (2) Isolate large-scale irregularities in the global picture.
- (3) Isolate small-scale hot or cold spots on the surface.

#### 1. Global Thermophysical Structure

The global thermophysical structure is essentially defined by the radiometric albedo,  $A$ , and the thermal inertia,  $I$ , plus a simple thermal model. The parameters  $I$  and  $A$  were strongly affected by the Martian dust storm, but the parameters converged late in the mission to values that are in good agreement with those determined from the *Mariner 6* and *7* data. A plot of inertia versus albedo as a

function of time is shown in Fig. IV-1; each number represents the best fit, in a least-squares sense, to the data of 10 revolutions.

#### 2. Large-Scale Irregularities

Two major deviations from the simple thermal picture defined above were found. (1) After the dust storm had settled it was found that the late afternoon temperatures (about 16:00 to 18:00 hr local time) were significantly too cold relative to the noon temperature as predicted on a simple thermal model. The effect may be related to winds or other atmospheric phenomena. (2) Pre-dawn data (3:00 to 6:00 hr local time), where the temperatures depend primarily on thermal inertia, show that there is no definite correlation between thermal inertia and the visual albedos, as determined qualitatively from the television pictures. Examples of large inertias with high and low albedos are present.

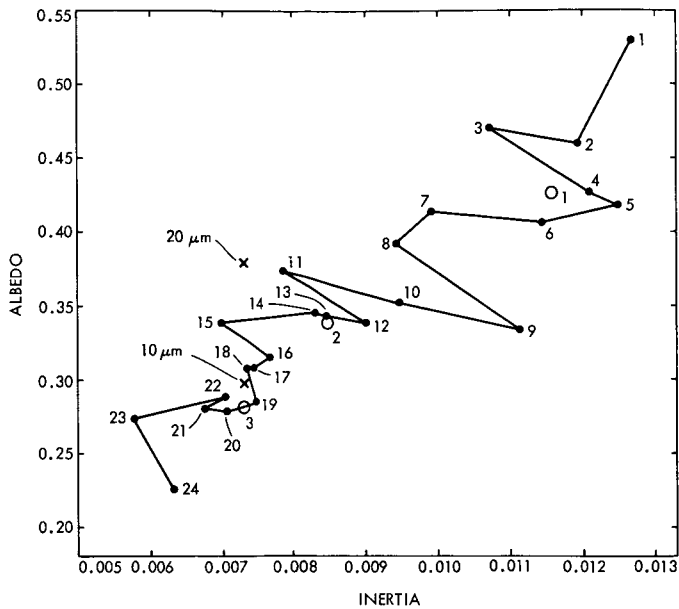


Fig. IV-1. Surface thermal inertia vs bolometric albedo as a function of time.

### 3. Small-Scale Hot or Cold Spots

No hot spots comparable to or larger in spatial extent than the infrared radiometer's field of view (12 km minimum), and at a temperature of 300°K or greater, have been viewed by the infrared radiometer. A hand search of the infrared radiometer data yielded a list of 27 anomalies (Table 2 of Ref. IV-1; also see Table XXI-2 of Vol. IV of this Technical Report). The areas containing these anomalies differ in temperature from their surroundings by from 8° to 13°K. Only 11 of the 27 are warmer than their surroundings. Probable causes, in terms of modest variations in thermal inertia, bolometric albedo, and/or local topography can explain all but two: one measured during Martian mid-morning at the southwest edge of the Argyre basin, and one measured late in the Martian afternoon in a distinctive channel near Nilokeras. Even in these two cases, it is not unreasonable to assume that they are due to somewhat more extreme changes in thermal inertia, bolometric albedo, and/or topography. Neither falls in an area classified as volcanic by the *Mariner 9* geologists.

### B. Significant Additional Results

Two significant additional results beyond the achievement of the originally stated objectives were:

- (1) The *Mariner 9* data, having been obtained from outside Earth's atmosphere and being absolutely calibrated, provide an independent means of calibration for astronomical 10- and 20- $\mu\text{m}$  infrared

photometry. *Mariner 9* data were checked against Earth-based observations of Mars made to provide a backup calibration for the *Mariner 9* data. In fact, the radiometer gains, as derived from onboard checks, were well within 1% of the Earth-based prelaunch calibrations. Hence, it is significant to use the *Mariner 9* data as a basis for the stellar calibration rather than vice versa. The results of this calibration are that at 20  $\mu\text{m}$ ,  $\alpha$  Sco emits  $6.4 \times 10^{-15} \text{ W m}^{-2} \text{ Hz}^{-1}$ , while  $\alpha$  Ori emits  $16 \times 10^{-15} \text{ W m}^{-2} \text{ Hz}^{-1}$ . The 10- $\mu\text{m}$  calibration is in agreement with that derived from model calculations.

- (2) Measurements obtained of Phobos and Deimos show that the surfaces act as extremely poor thermal conductors. With nominal values of specific heat ( $c = 0.2 \text{ cal g}^{-1} \text{ }^\circ\text{K}^{-1}$ ) and density ( $\rho = 1.5 \text{ g cm}^{-3}$ ) the conductivity must be on the order of  $10^{-7} \text{ cal cm}^{-1} \text{ sec}^{-1} \text{ }^\circ\text{K}^{-1}$ , an extremely low value implying a dust-covered rather than a solid surface for the satellites. Photometric data, obtained at phase angles 35° to 80°, show good agreement with thermal model calculations. The most stringent definition of the conductivity, however, comes from an eclipse of Phobos by Mars; data and theoretical curves corresponding to conductivities of  $2 \times 10^{-5}$ ,  $2 \times 10^{-6}$ , and  $2 \times 10^{-7}$  are shown in Fig. IV-2. The errors shown are not only statistical, but incorporate the lack of pointing knowledge in the absence of television pictures. Thus, the points represent lower limits, with the exception of the last two which were accompanied by television pictures. The point shown a few minutes after the exit from the shadow of Mars (the arrow in Fig. IV-2) and on a flux level that equals the final value implies a conductivity of less than  $2 \times 10^{-7}$ .

### C. Problem Areas

Major problem areas encountered involved data reduction and an instrumental uncertainty. Problem areas are:

- (1) Accuracy of the pointing of the science platform was too low to allow a unique correlation between visual features determined on one revolution and infrared features determined at an appreciably later time. This is most serious with the analysis of the pre-dawn data, as the features with significantly different inertias appear on scales smaller than the absolute pointing accuracy.
- (2) Response of the 20- $\mu\text{m}$  channel outside the nominal field of view has been determined, from scans off of and on to the planet, to be wider than predicted

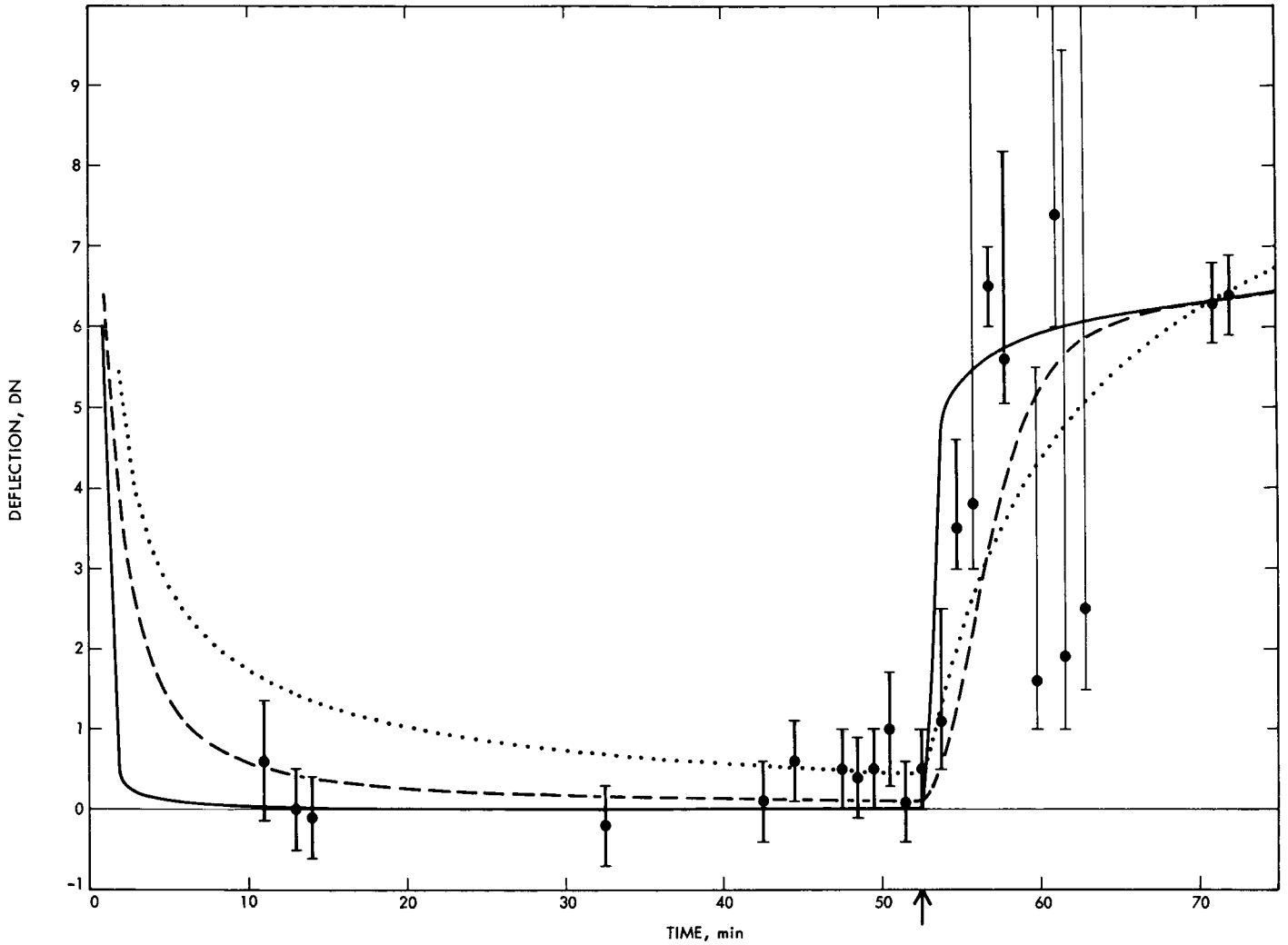


Fig. IV-2. Theoretical eclipse cooling curves for Phobos for surface conductivities of  $2 \times 10^{-5}$  (dotted line),  $2 \times 10^{-6}$  (dashed line), and  $2 \times 10^{-7}$  (solid line). Deflection in data numbers is given for the  $10\text{-}\mu\text{m}$  channel of the radiometer.

from measurements made before launch. This was most serious: (a) in investigating the residual polar caps, because they were so small and surrounded by hotter areas, and (b) in trying to determine effects of variations of emissivity with phase near the limb of the planet.

- (3) A third more general problem was in the nature of Mars itself; no strong and remarkable thermal structures appeared. As a result, the preliminary data reduction using the quick-look "user" data was

too crude to show scientifically definitive results that were at variance with previously established ideas about Mars. The more refined supplementary experiment data record (SEDR) program came too late to affect any serious interpretation within the first year. In retrospect, a net saving of time would have resulted in analyzing all data three times: (a) using the user data for quick-look analysis, (b) using the user data to clean the data with regard to bit errors, etc., and (c) combining the corrected data with the SEDR.

## Reference

- IV-1. Kieffer, H. H., Chase, S. C., Miner, E., Münch, G., and Neugebauer, G.,  
"Preliminary Report on Infrared Radiometric Measurements From the  
Mariner 9 Spacecraft," *J. Geophys. Res.*, Vol. 78, 1973.

# V. Infrared Spectroscopy Experiment: An Overview

R. Hanel, B. Conrath, R. Curran, W. Hovis, V. Kunde, P. Lowman, W. Maguire,  
J. Pearl, J. Pirraglia, C. Prabhakara, and B. Schlachman  
Goddard Space Flight Center, Greenbelt, Maryland 20771

G. Levin  
Biospherics, Inc., Rockville, Maryland 20853

T. Burke  
Jet Propulsion Laboratory/California Institute of Technology, Pasadena, California 91103

The instrumental and scientific objectives of the infrared spectroscopy experiment were presented before *Mariner 9* was launched (see Ref. V-1). The purpose of this report is to provide a retrospective look at the operation and results of the experiment. Because the success of the scientific investigations depends strongly on the performance of the instrument, a brief comparison of proposed and achieved instrument parameters is given first. Following this, the scientific results obtained up to June 1, 1973 (Refs. V-2 through V-5; also see Section XX of Vol. IV of this Technical Report) are summarized and compared with anticipated achievements.

## A. Instrumentation

The design and the performance of the infrared interferometer spectrometer (IRIS) on *Mariner 9* are discussed in Ref. V-6. A comparison of selected parameters, as predicted and as actually achieved, is given in Table V-1. The proposed values are from Ref. V-1, while the achieved values are from Ref. V-6 and from more recent evaluations.

Table V-1. Instrument parameters

Parameter	As proposed	As achieved
Spectral range, $\text{cm}^{-1}$	200 to 1600	210 to 2000
Number of samples per interferogram	4096	4096
Reference wavelength, $\mu\text{m}$	6929	6929
Optical path difference, cm	0.85	0.85
Width of resolved spectral intervals apodized (unapod), $\text{cm}^{-1}$	2.4(1.2)	2.4(1.2)
Area of aperture, $\text{cm}^2$	15	15
Solid angle, sterad	$4.7 \times 10^{-3}$	$4.7 \times 10^{-3}$
Field of view, deg	4.5	4.5
Frequency in data channel, Hz	9.5 to 75.8	9.5 to 95
Noise-equivalent-radiance, $\text{W cm}^{-2} \text{sterad}^{-1}/\text{cm}^{-1}$	$3 \times 10^{-8}$	3 to $5 \times 10^{-8}$

Most of the proposed instrument parameters have been achieved; in addition, the investigated spectral range was extended from 1600 to 2000  $\text{cm}^{-1}$ . Although this capability

existed in the design from the beginning, it was not originally emphasized because the signal-to-noise ratio of an individual spectrum was expected to be poor beyond  $1600\text{ cm}^{-1}$ . However, as shown below, averaging of spectra has permitted the extraction of useful information between  $1600$  and  $2000\text{ cm}^{-1}$ . A consequence of the increased spectral range was an increase in the electrical bandwidth required in the data channel; this was accommodated by a slight reduction in the margin of oversampling.

The noise-equivalent-radiance (NER) of the instrument (Fig. V-1) is derived from the standard deviation of more than 1700 pairs of calibration spectra obtained throughout the orbital phase of the mission. The standard deviation is a measure of the instrument stability and includes the effects of noise in the detector, bias supply, and preamplifier as well as of the temperature drift of the reference blackbody and instrument itself. Near  $300\text{ cm}^{-1}$  and  $400\text{ cm}^{-1}$ , the design goal of  $3 \times 10^{-8}\text{ W cm}^{-2}\text{ sterad}^{-1}/\text{cm}^{-1}$  has been achieved. Over the rest of the range, the NER is within a factor of 2 of the design goal, except below  $250\text{ cm}^{-1}$  where absorption in the CsI of the beamsplitter and entrance window causes a gradual deterioration of the instrument response. Spikes near  $356\text{ cm}^{-1}$  and at multiple frequencies are due to harmonics of the  $8\frac{1}{3}$  and  $33\frac{1}{3}$  Hz engineering multiplexer frequency of the spacecraft telemetry subsystem.

The calibration procedure, based on observations of deep space and an onboard blackbody, has worked well. A small correction for the emissivity of the paint on the

reference blackbody has been included in the calibration. Comparison of calibration data from prelaunch tests with data acquired near the end of the mission reveals no detectable change of responsivity, spectral resolution, or NER. Because of the stability of the instrument it has been possible to apply the same final calibration to all Martian spectra. Included were 1767 pairs of calibration spectra; consequently, random errors from this source are insignificant even for averages of data involving over a thousand spectra.

As a result of the excellent performance of the instrument, the proposed scientific objectives were met, and several unanticipated results were obtained.

## B. Scientific Objectives and Results

The basic scientific objective of the infrared spectroscopy experiment (Ref. V-1) was to utilize the thermal emission spectra to infer atmospheric and surface parameters. Such quantities provide the basis for studies of the physical behavior of the atmosphere, investigations of the surface composition and structure, and biological studies.

During the first 100 days of the mission, about 200 spectra were obtained each day, providing extensive coverage of the entire planet. During the extended mission, which lasted another 8 months, much fewer data were obtained; however, as these spectra extend the time base of the data to nearly half of a Martian year, they have been extremely valuable.

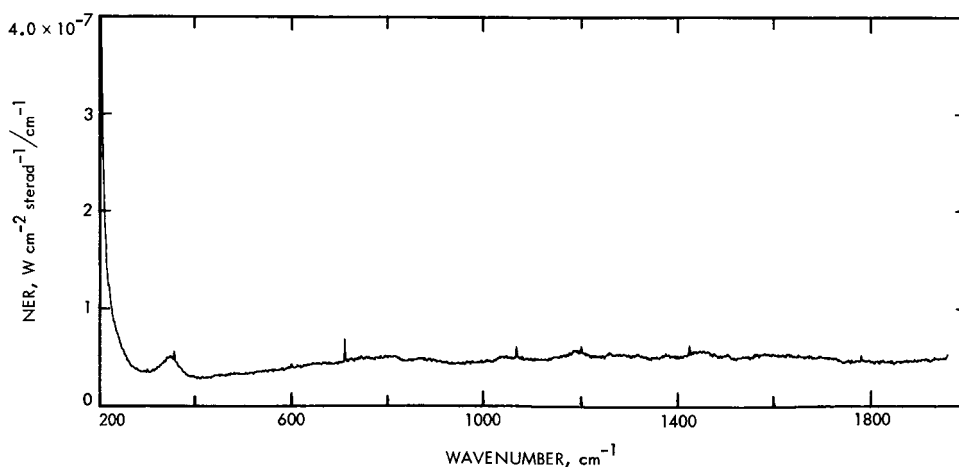


Fig. V-1. Noise-equivalent-radiance (NER) of the spectrometer based on 1767 pairs of calibration spectra. Spikes at multiples of  $356\text{ cm}^{-1}$  are caused by harmonics of the  $8\frac{1}{3}$  and  $33\frac{1}{3}$  Hz engineering multiplexer frequencies of the spacecraft's telemetry subsystem. Degradation below  $250\text{ cm}^{-1}$  is caused by absorption in the CsI of the beamsplitter and entrance window.

## 1. General Atmospheric Composition

Most of the features in the spectrum have been identified with gaseous  $\text{CO}_2$  and  $\text{H}_2\text{O}$ , entrained dust, and ice crystal clouds in the Martian atmosphere. Synthetic data in the  $225$  to  $800\text{ cm}^{-1}$  region are compared in Figs. V-2 and V-3 with an observed spectrum from revolution 174. Numerous rotational absorption lines due to atmospheric water vapor are evident in the  $200$  to  $500\text{ cm}^{-1}$  region (Fig. V-2). The comparison of the observed and the theoretical spectrum shows good spectral correspondence even for the weak lines in the  $500\text{ cm}^{-1}$  region. No unidentified or anomalous features are evident in this spectral interval.

Strong molecular absorption by atmospheric  $\text{CO}_2$  appears between  $500$  and  $800\text{ cm}^{-1}$ , as shown in Fig. V-3. Various isotopes of  $\text{CO}_2$  are evident in the spectrum. The relative strengths of these observed bands are in general agreement with the corresponding theoretical bands; as terrestrial abundances were assumed in the calculations, this indicates that the  $\text{C}^{12}:\text{C}^{13}$  and  $\text{O}^{16}:\text{O}^{18}$  ratios for Mars are close to the terrestrial values. No unidentified or anomalous features are evident in this spectral interval.

Beyond  $800\text{ cm}^{-1}$  the observed spectrum exhibits features due to weak  $\text{CO}_2$  bands ( $800$  to  $2000\text{ cm}^{-1}$ ), to silicate dust ( $900$  to  $1200\text{ cm}^{-1}$ ), and to the  $1595\text{ cm}^{-1}$   $\text{H}_2\text{O}$  band ( $1400$  to  $1800\text{ cm}^{-1}$ ). For a comparison in this spectral region, 3816 individual spectra have been averaged to improve the signal-to-noise ratio (Fig. V-4). Anomalous features appear at  $844$ ,  $1194$ ,  $1236$ , and  $1440$

$\text{cm}^{-1}$ . Investigations to date have not yielded a satisfactory explanation of these features, either in terms of unknown Martian constituents or instrumental effects.

Although no new gaseous minor constituents have been identified, the high radiometric precision and resolution of IRIS will allow present upper limits on several minor constituents to be lowered, thereby placing more rigid constraints on photochemical equilibrium investigations of the Martian atmosphere. The low NER of IRIS has allowed the minor constituent scientific objectives to be attained at a level exceeding that anticipated in the original proposal.

## 2. Atmospheric Water Vapor

Another important scientific objective was to detect atmospheric water vapor. Water vapor has been identified from numerous rotational lines in the  $200$  to  $500\text{ cm}^{-1}$  region. From these data, gross seasonal and spatial trends in the water vapor distribution have been determined.

The water vapor abundances are summarized in the lower three sections of Fig. V-5 for the north polar, mid-latitude and south polar regions, with the upper section of the figure illustrating the classical polar cap regression curves. The values determined from IRIS are indicated by vertical bars. The horizontal dashed lines represent mean values from the Earth-based observations of Tull and Barker (Ref. V-7) for the entire Martian disk during the

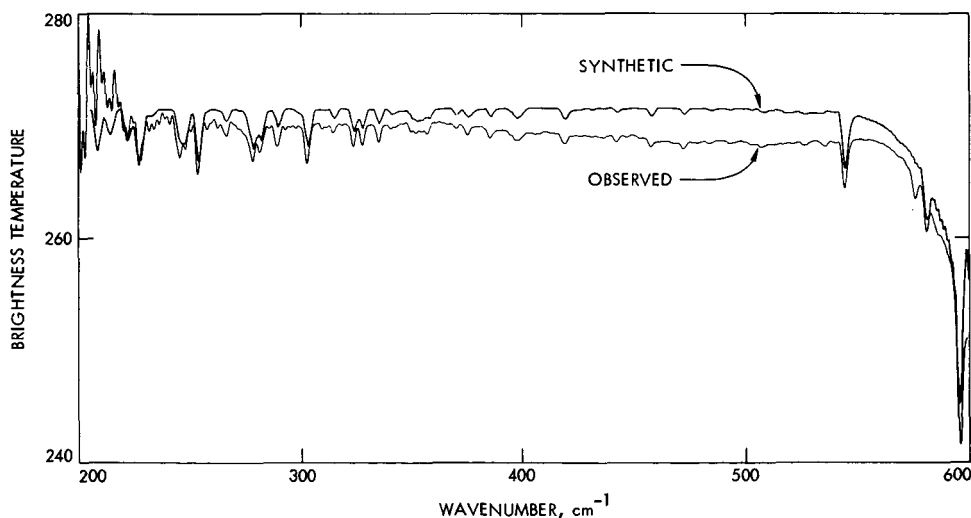


Fig. V-2. Comparison of measured (revolution 174,  $-30^\circ$  latitude,  $32^\circ$  longitude, 14:00 hr local time) and synthetic spectra between  $200$  and  $600\text{ cm}^{-1}$ . Many lines of water vapor are evident;  $10\text{ }\mu\text{m}$  of precipitable water vapor were assumed in the synthetic spectrum. The shift in overall levels is due to broad surface and suspended dust features that were not modeled in the theoretical spectrum.

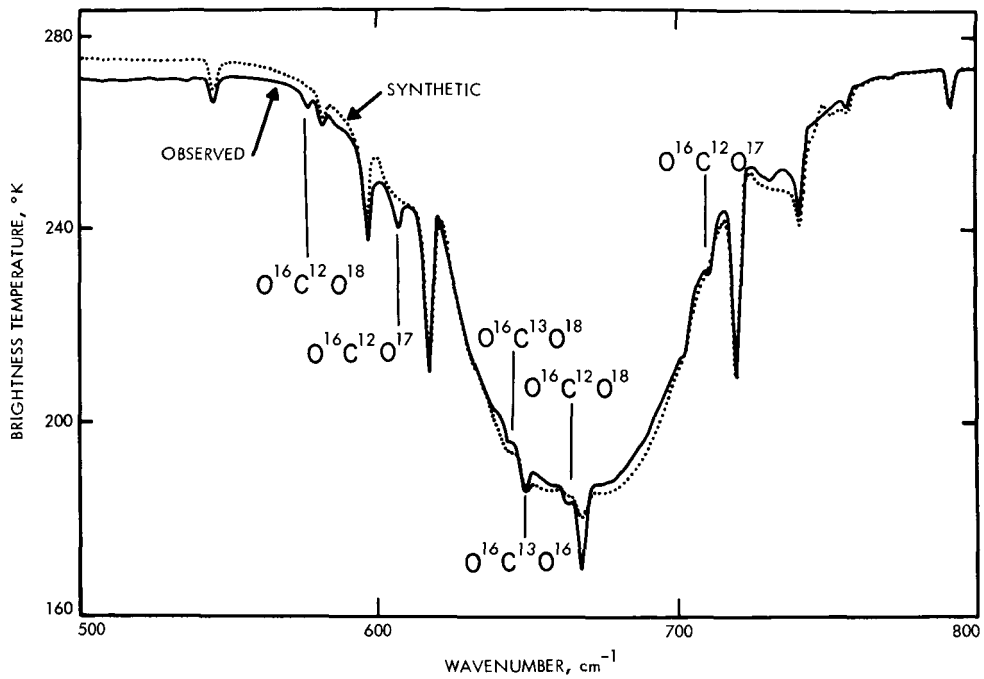


Fig. V-3. Comparison of measured (revolution 174,  $-30^\circ$  latitude,  $32^\circ$  longitude, 14:00 hr local time) and synthetic spectra between  $500$  and  $800\text{ cm}^{-1}$ . The principal feature is the  $667\text{ cm}^{-1}$  band of  $\text{CO}_2$ , on which several branches due to various isotopic variants of the molecule are indicated. The shift in overall levels is due to broad surface and suspended dust features that were not modeled in the theoretical spectrum.

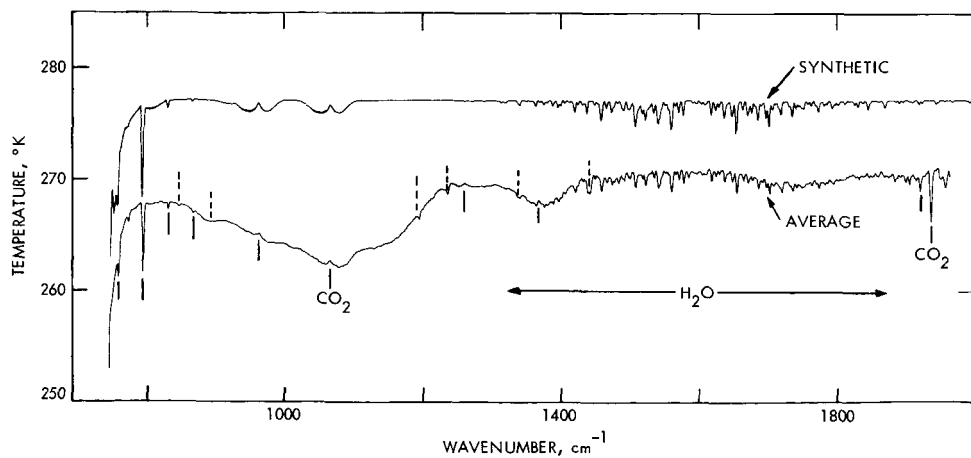


Fig. V-4. Comparison of theoretical spectrum with an average of 3816 spectra for the range  $800$  to  $2000\text{ cm}^{-1}$ . The broad feature caused by dust suspended in the atmosphere has not been modeled in the calculation. Various bands of  $\text{CO}_2$  and lines of water vapor are evident. The anomalous features at  $894$ ,  $1194$ ,  $1236$ , and  $1440\text{ cm}^{-1}$  are indicated by the vertical dashed lines.

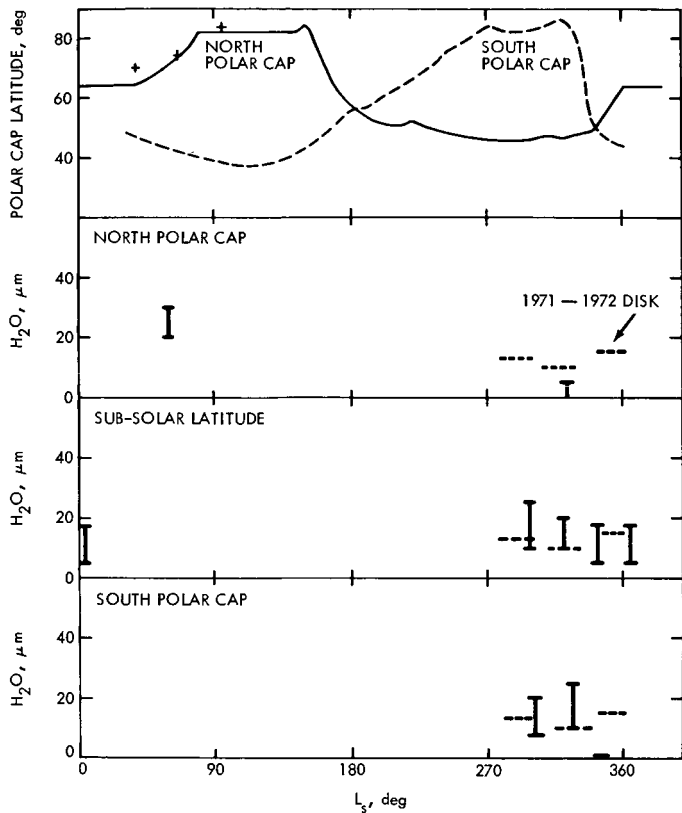


Fig. V-5. Latitudinal and temporal distribution of water vapor, correlated with polar cap regression curves. (a) Classical polar cap regression curves. (b) Water vapor amounts in north polar region. (c) Water vapor amounts at mid-latitudes. (d) Water vapor amounts in south polar region. Vertical bars represent IRIS measurements; horizontal lines represent contemporaneous Earth-based measurements of Tull and Barker (see Ref. V-7).

same time period. The results indicate that during the southern summer season the water vapor content was fairly constant at about 10 precipitable micrometers over all of the planet except the north polar region. Of significance is the low average abundance of water vapor during this opposition, a value considerably lower than measured by Earth-based methods during previous oppositions. This anomalous behavior of the water vapor during this season is probably associated with the dust storm.

Water vapor results obtained during the extended mission in the northern hemisphere during its spring and summer season are summarized in Fig. V-6. The largest amounts of water vapor observed during the *Mariner 9* mission, about 20 to 50  $\mu\text{m}$ , occurred in the north at this time and are associated with the retreating north polar cap. These amounts are consistent with Earth-based determinations made during previous oppositions.

In summary, the water vapor behavior during the southern summer was anomalous, being essentially constant in latitude and low in average amount, probably due to the dust storm. By the time of northern spring, the latitudinal and seasonal behavior of atmospheric water vapor was generally consistent with the source of the vapor being in the retreating polar cap. It may be concluded that the atmospheric water vapor objective matched or even exceeded original expectations.

### 3. Surface Pressure

One result that was not fully anticipated in the proposal was the determination of the surface pressure. Values of the surface pressure have been derived for many points spread over more than half of the planet (Refs. V-3 and V-4). Surface pressures were obtained from the degree of attenuation of surface radiation by the wings of the  $667\text{ cm}^{-1}\text{ CO}_2$  band, assuming a 100%  $\text{CO}_2$  atmosphere. A low-resolution pressure map has been constructed (Fig. V-7) for latitudes  $+20^\circ$  to  $-60^\circ$ , in which the areas of highest pressure ( $\sim 8\text{ mb}$ ) are Hellas and Isidis Regio. The Tharsis ridge was found to be a large-scale area of low pressure ( $\sim 3\text{ mb}$ ), with the summit of South Spot (the only volcanic structure suitably observed by the IRIS) at significantly lower pressure ( $< 1.5\text{ mb}$ ). These pressure excursions correspond to a topographic variation over the planet of at least two atmospheric scale heights ( $\sim 20\text{ km}$ ).

### 4. Atmospheric Temperature Fields

One of the major objectives of the infrared spectroscopy experiment was to obtain atmospheric temperature profiles on a global basis (Ref. V-1). Measurements in the  $667\text{ cm}^{-1}\text{ CO}_2$  band were employed, and profiles were derived by taking advantage of the varying atmospheric opacity from the center of the band through the wing. A  $\text{CO}_2$  mixing ratio of 100% was assumed for this purpose, and the required surface pressures were obtained using the methods described above. This objective has been met with a high degree of success, with atmospheric temperatures obtained from the surface up to approximately the 0.1-mb level.

During the early part of the mission, while the great dust storm was in progress, the atmosphere was found to be in a highly perturbed thermal state. One of the most significant discoveries made during this period was the identification of a migrating diurnal thermal wave at all atmospheric levels up to at least 40 km (Ref. V-3). The maximum peak-to-peak amplitude was about  $30^\circ\text{K}$  at  $-60^\circ$  latitude with a phase lagging the Sun by about 6 hr

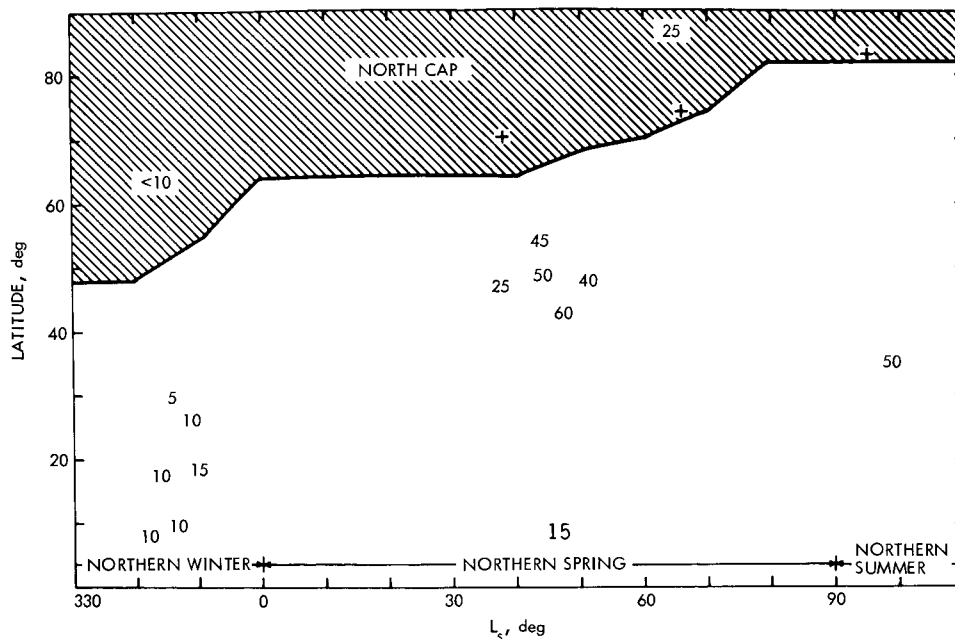


Fig. V-6. Total water vapor amount (in precipitable micrometers) as a function of season. Data are for the northern hemisphere, covering the time period of the extended mission.

(Fig. V-8). Diurnal mean stratospheric temperatures were found to be as much as  $50^{\circ}\text{K}$  warmer than predictions based on radiative-convective clear atmosphere models such as those in Ref. V-8, but in rough agreement with models which include atmospheric heating due to the presence of dust (Ref. V-9). With dissipation of the dust, the amplitude of the diurnal wave decreased, as did the diurnal mean stratospheric temperatures. During the extended mission, the stratospheric temperatures stabilized at a value of about  $155^{\circ}\text{K}$ .

Lapse rates during the dust storm were found to be extremely low, with a value of about  $1.5^{\circ}\text{K}/\text{km}$  at middle and low southern latitudes. A strong temperature inversion was found over the south polar region (Ref. V-2). As the dust dissipated, the south polar temperature inversion weakened; the mid- and low-latitude lapse rates increased, but remained substantially sub-adiabatic even through the extended mission.

## 5. Atmospheric Circulation

As had been proposed, the thermal emission spectra yielded results from which the general circulation of the planet could be studied. Although the circulation models are still evolving, a reasonable picture of the general circulation has been developed (Refs. V-3 and V-4; also see Section XX of Vol. IV of this Technical Report).

The measured temperature field, rather than the atmospheric heating, is used as the dynamic driving term in the momentum equation; the heating is then deduced from the temperature field and the dynamics. This approach has been applied to a modified form of tidal theory. Tidal theory is used because the diurnal behavior of the temperature field suggests that tidal modes may be the dominant circulatory process, at least during the dust storm and its decay period. As it was not possible to obtain temperature measurements over the entire planet, the temperature field existing during the dust storm was modeled by a low-order spherical harmonic expansion consisting of one symmetric and one asymmetric mode each for the diurnal and polar symmetric parts of the field. Use of these data in the tidal theory leads to the surface pressure fluctuations shown in Fig. V-9. The near-surface winds associated with the temperature and pressure fields are shown in Fig. V-10.

The dynamic calculations thus far have not included orographic, viscous shear, or instability effects. The large topographic variations on the planet demand that the topography be considered in more sophisticated circulation models. As the diurnal temperature variations decrease, the dynamics are increasingly influenced by the latitudinal temperature gradient and by turbulent viscosity; in addition, instabilities become very important. Orographic and viscous shear effects are currently under

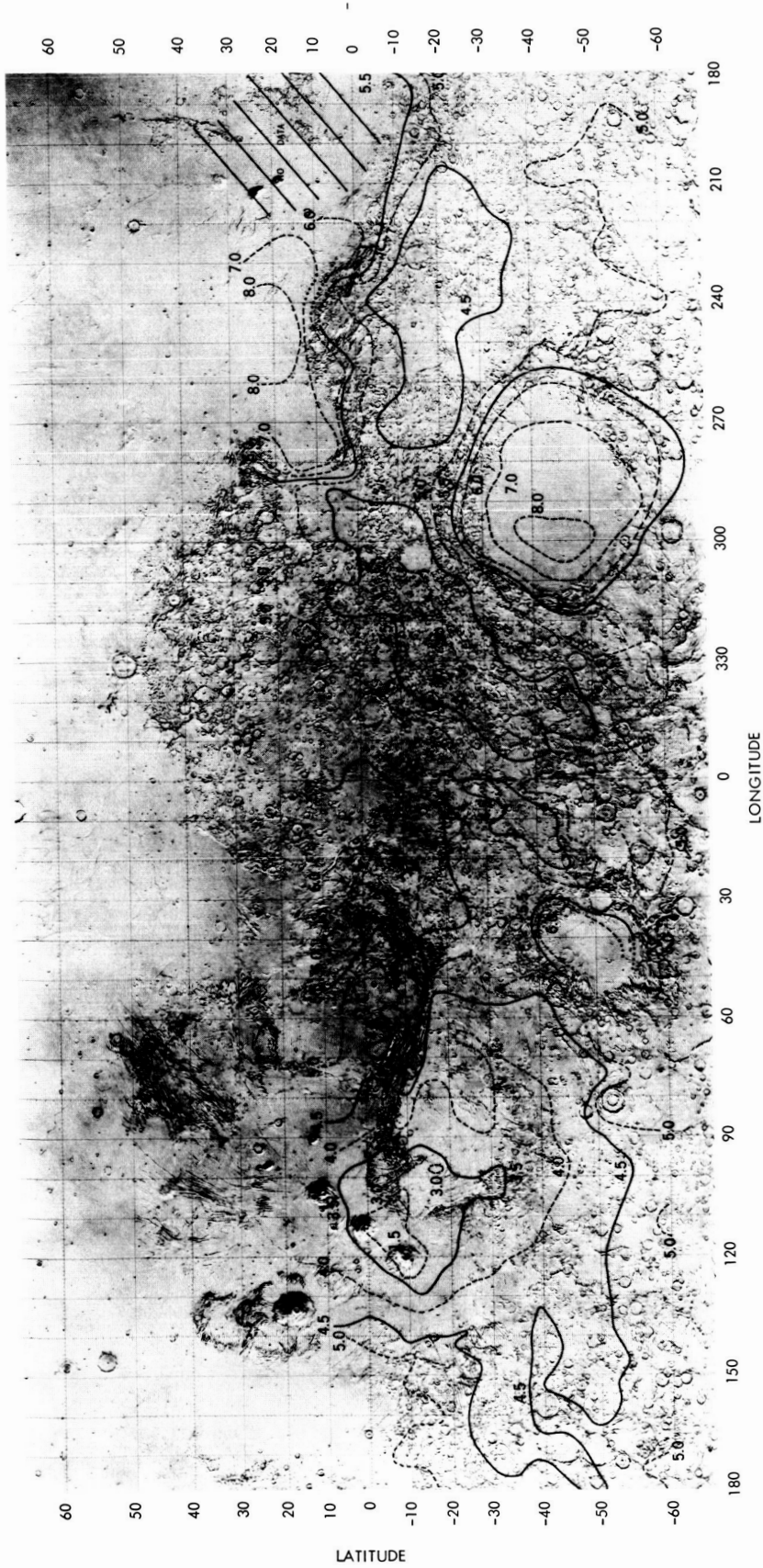


Fig. V-7. Pressure contours (in millibars) superimposed on USGS Martian feature map. Contours corresponding to integer pressures are dashed, and to half-integer pressures are solid; dotted portions represent interpolations across data gaps. Contours based on pressures averaged over areas 5° on a side; accuracy of the pressure determinations is 10 to 15%.

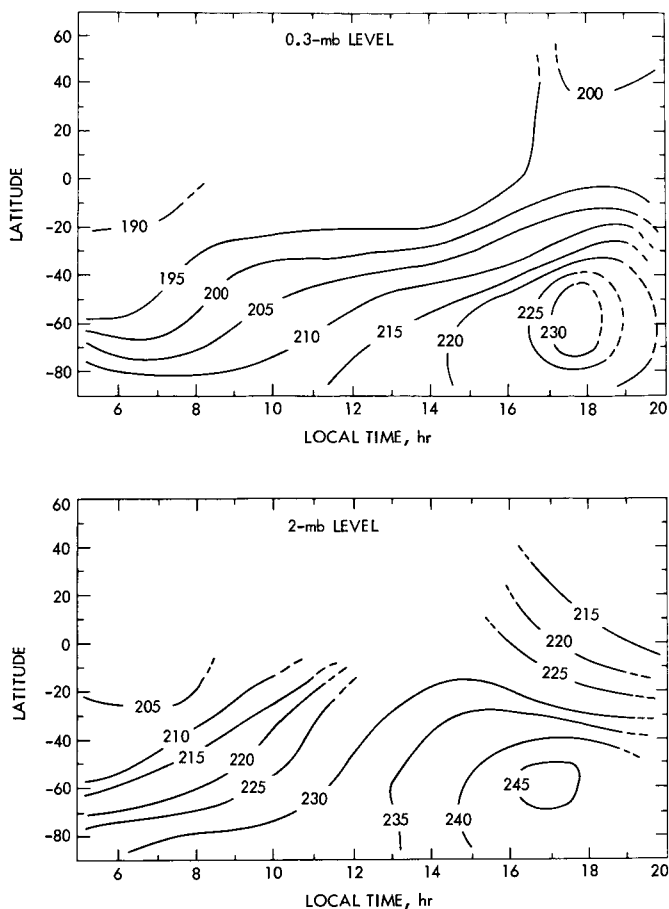


Fig. V-8. Dependence on latitude and Martian local time of atmospheric temperatures at the 2-mb ( $\sim 10$ -km) level, and at the 0.3-mb ( $\sim 30$ -km) level. The temperatures (in degrees Kelvin) represent averages over data obtained during the dust storm on revolutions 1 through 85.

investigation, and the results will be published elsewhere. The study of instabilities is in an incipient stage.

## 6. Particulate Matter

Two results of major significance that had not been anticipated in the original experiment objectives are related to the identification of atmospheric particulate matter. Perhaps the most important of these is an estimation of the chemical composition of the Martian dust. Many of the spectra obtained during the first 50 days of the mission show strong, broad features near 480 and 1090  $\text{cm}^{-1}$  which have been identified with silicates (Fig. V-11a). These spectra, together with standard deviations of sets of spectra (Fig. V-11b), have been used to accurately determine the absorption maxima and minima of

the dust. By utilizing the fact that the frequencies of the transmission maxima and minima are functions of the  $\text{SiO}_2$  content, it has been possible to estimate the  $\text{SiO}_2$  content of the Martian dust to be  $60 \pm 10\%$ . This value, comparable to that of Earth's continental crust and significantly higher than that of a chondritic body, suggests that Mars has undergone geochemical differentiation (Refs. V-2 and V-3). This suggestion is further confirmed by the existence of large volcanic structures on Mars (Refs. V-10 and V-11).

The wide spectral range of the instrument permitted the observation, in many spectra, of a relatively sharp feature centered at 227  $\text{cm}^{-1}$  and a broad feature centered at 900  $\text{cm}^{-1}$ ; these features appeared in low-latitude spectra on revolution 676 ( $L_s = 90^\circ$ ), where they were associated with portions of the W-cloud (Fig. V-12). Comparison of these features with radiative transfer calculations in which the scattering and emissive properties of water ice were included confirmed that the particles consisted of water ice, and permitted the inference that the particles were about 2  $\mu\text{m}$  in radius. The observation of the same spectral features at high latitudes during late northern spring ( $340^\circ < L_s < 355^\circ$ ) confirmed that the southern portions of the north polar hood consist of clouds of water ice. These clouds were observed to extend from about  $+45^\circ$  to about  $+60^\circ$  latitude.

## 7. Surface Properties

An objective in the original proposal was to look for variations in surface emissivity (reststrahlen) in order to identify the composition and granularity of the Martian surface material. Up to the present time no striking reststrahlen effects have been observed in the spectra. This is explained in part by the persistence of the atmospheric dust aerosol, which exhibits emissivity variations in the same general spectral regions as the bulk material, and by the fine-grained nature of the surface dust layer. As mentioned, however, it has been possible to infer a  $60 \pm 10\%$   $\text{SiO}_2$  content for the suspended dust, and arguments have been presented that this should be representative of the average crustal composition of the planet (Ref. V-3). In addition, radiative transfer calculations for a model  $\text{SiO}_2$  dust cloud suggest that the mean radius of the aerosol particles is on the order of a few micrometers (Ref. V-4). Coupled with the absence of strong surface emissivity variations, this further supports the idea that, on the average, the Martian surface is covered by fragmental material ranging down to very small sizes. Surface heating

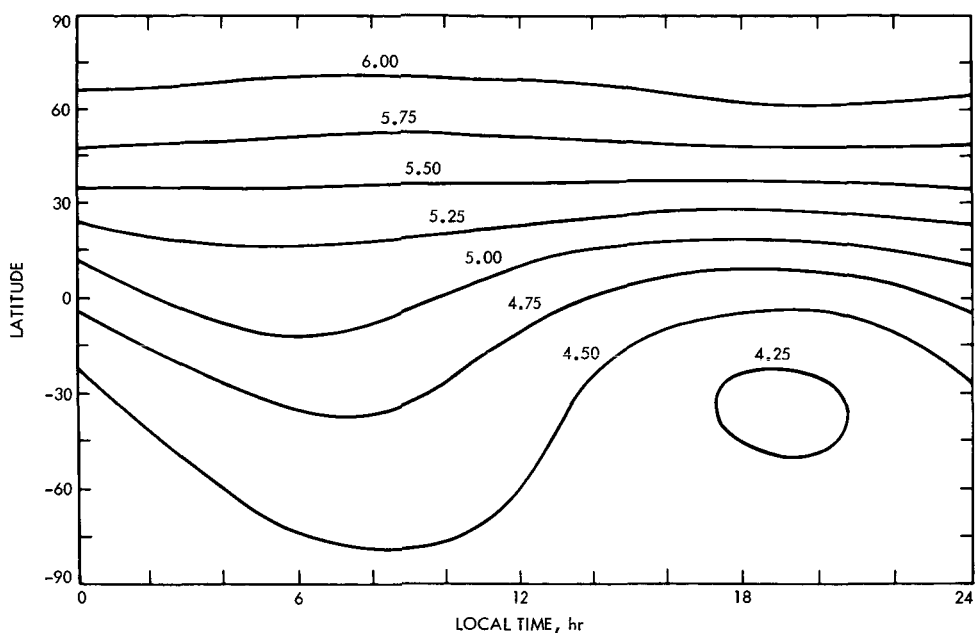


**Fig. V-9.** Calculated dependence of surface pressures on latitude and Martian local time taking into account tidal atmospheric motions. The pressures (in millibars) are the sum of the diurnal tidal pressures and a latitude-dependent seasonal pressure field; an average surface pressure of 5 mb is assumed. Topographic and surface frictional effects are not included in the calculations.

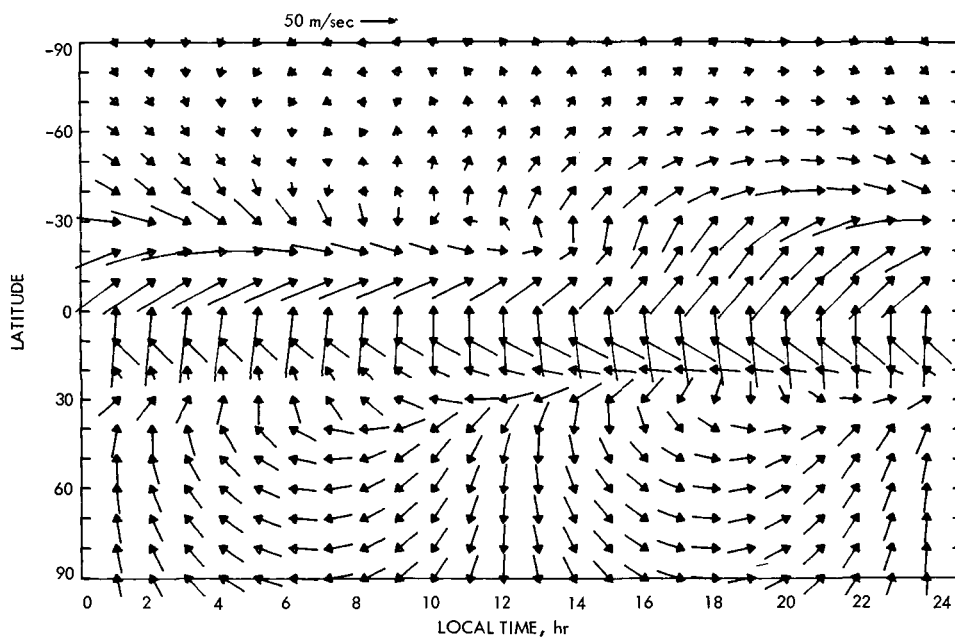


**Fig. V-10.** Calculated near-surface winds during the great dust storm. The wind field, just above the surface boundary layer, is evaluated using the measured temperature field and the associated tidal surface pressure. Wind amplitudes are scaled to the labeled vector.

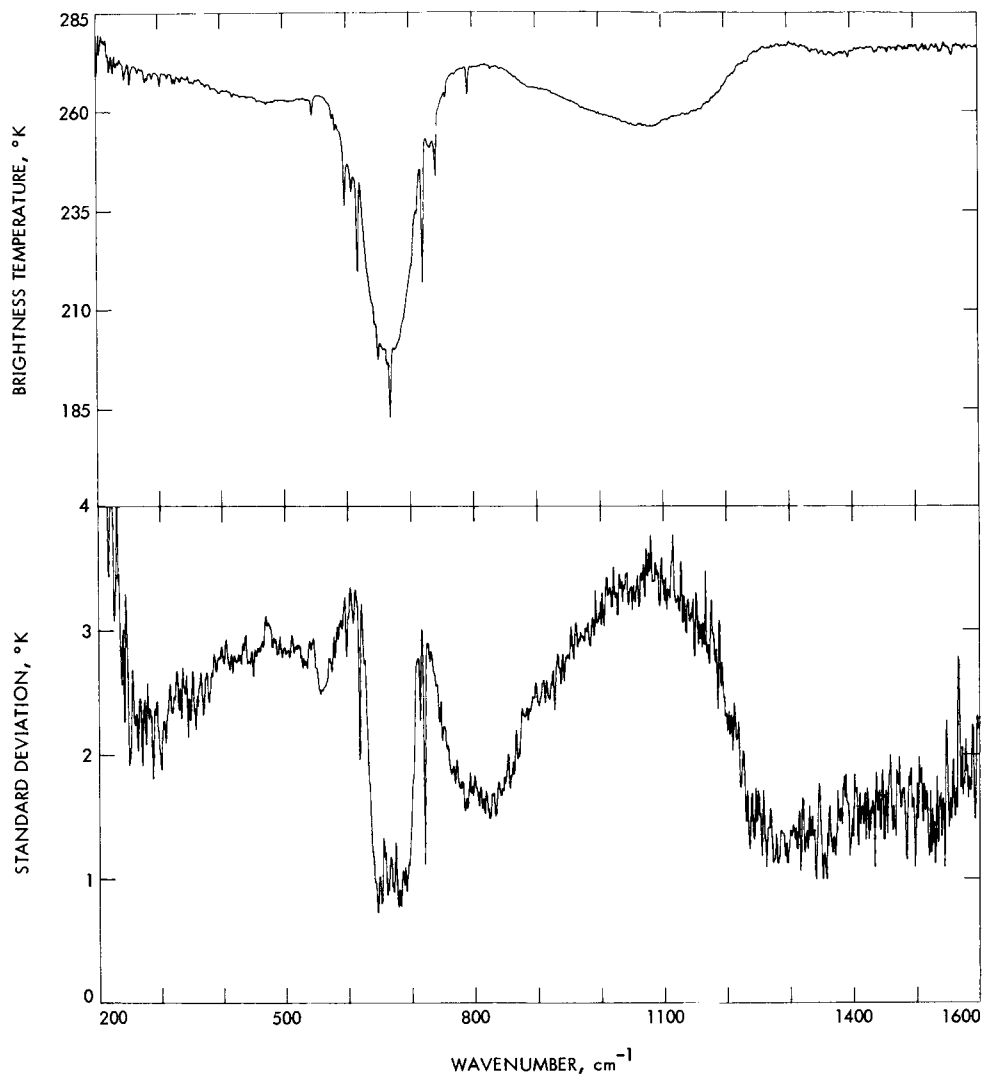


**Fig. V-11. Spectra from revolution 92 showing features due to atmospheric dust aerosol. (a) Brightness temperature average (in degrees Kelvin) of 16 spectra showing broad silicate absorption features centered near 480 and 1090 cm<sup>-1</sup>. (b) Standard deviation of brightness temperature spectra within the ensemble showing enhancement of dust absorption features caused by variations in cloud thickness.**

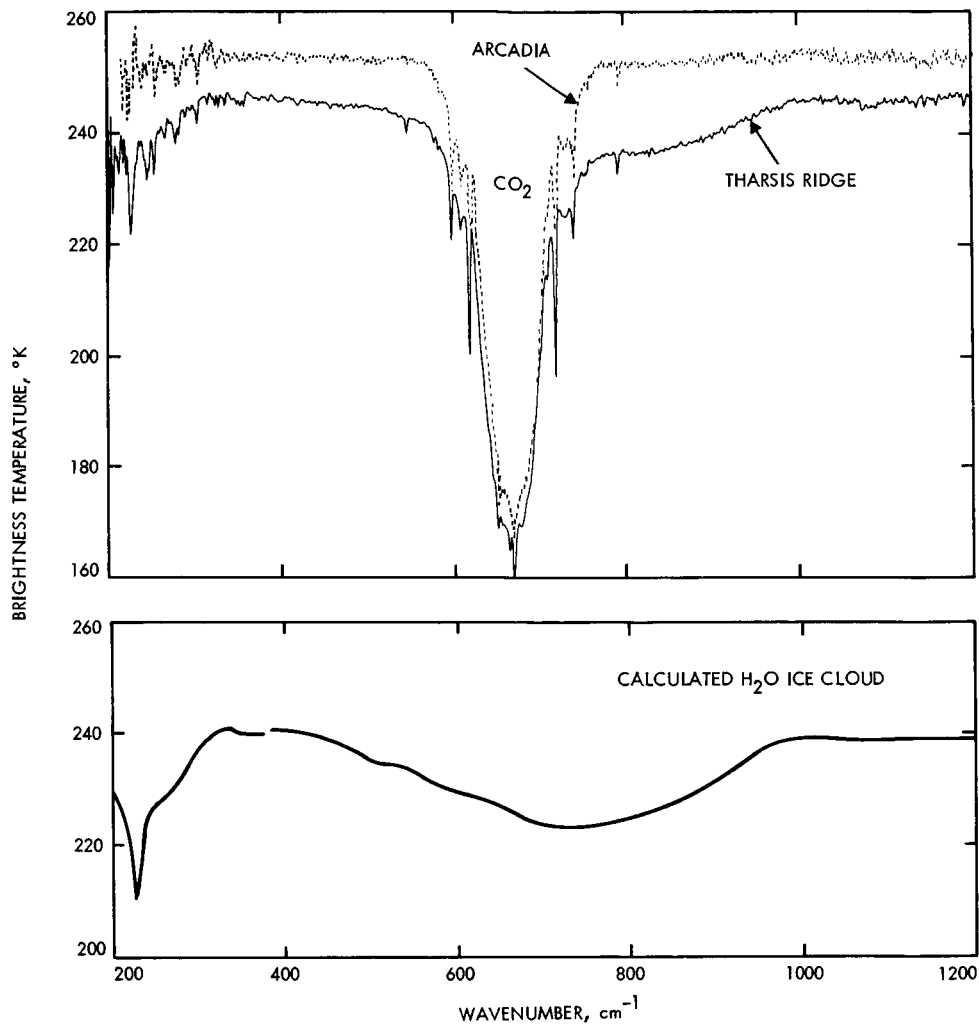


Fig. V-12. Measured and calculated brightness temperature spectra showing evidence for ice crystal cloud over the Tharsis ridge. The Arcadia spectrum shows essentially no ice features, while the ridge spectrum shows strong features centered at 227 and 800  $\text{cm}^{-1}$ ; these features correlate very well with the theoretical ice cloud spectrum shown in the lower portion of the figure.

and cooling data have not yet been analyzed. With this exception, therefore, the surface objectives stated in the proposal have already been accomplished.

### C. Summary

The infrared spectroscopy experiment has provided more than 20,000 high-quality spectra of Mars which are widely distributed in latitude, longitude, local time, and season. This has formed an extensive data base from which the originally anticipated scientific results have been obtained, and which has provided significant unanticipated information in several additional areas.

The composition of the atmosphere has been investigated, providing evidence of water vapor and carbon dioxide with approximately the terrestrial abundances of carbon and oxygen isotopes; no evidence has been found for species suggestive of biological activity. Atmospheric thermal structure has been studied, revealing strong tidal components in the atmospheric circulation and surface pressures. Particulate matter has been identified in the atmosphere consisting of water ice clouds in the vicinity of the volcanic shields and in the north polar hood and of silicate dust distributed widely over the planet. The surface consists largely of fine-grained material with a composition which is essentially the same as that of the dust.

## References

- V-1. Hanel, R. A., Conrath, B. J., Hovis, W. A., Kunde, V., Lowman, P. D., Prabhakara, C., Schlachman, B., and Levin, G. V., "Infrared Spectroscopy Experiment for Mariner Mars 1971," *Icarus*, Vol. 12, pp. 48-62, 1970.
- V-2. Hanel, R. A., Conrath, B. J., Hovis, W. A., Kunde, V. G., Lowman, P. D., Pearl, J. C., Prabhakara, C., Schlachman, B., and Levin, G. V., "Infrared Spectroscopy Experiment on the Mariner 9 Mission: Preliminary Results," *Science*, Vol. 175, pp. 305-308, 1972.
- V-3. Hanel, R., Conrath, B., Hovis, W., Kunde, V., Lowman, P., Maguire, W., Pearl, J., Pirraglia, J., Prabhakara, C., Schlachman, B., Levin, G., Straat, P., and Burke, T., "Investigation of the Martian Environment by Infrared Spectroscopy on Mariner 9," *Icarus*, Vol. 17, pp. 423-442, 1972.
- V-4. Conrath, B., Curran, R., Hanel, R., Kunde, V., Maguire, W., Pearl, J., Pirraglia, J., Welker, J., and Burke, T., "Atmospheric and Surface Properties of Mars Obtained by Infrared Spectroscopy on Mariner 9," *J. Geophys. Res.*, Vol. 78, 1973.
- V-5. Curran, R. J., Conrath, B. J., Hanel, R. A., Kunde, V. G., Pearl, J. C., "Mars: Mariner 9 Spectroscopic Evidence for H<sub>2</sub>O Ice Clouds" (submitted to *Science*).
- V-6. Hanel, R. A., Schlachman, B., Breihan, E., Bywaters, R., Chapman, F., Rhodes, M., Rodgers, D., and Vanous, D., "The Mariner 9 Michelson Interferometer," *Appl. Opt.*, Vol. 11, p. 2625, 1972.
- V-7. Tull, R. G., and Barker, E. S., "Ground-Based Photoelectric Measures of H<sub>2</sub>O on Mars during the Mariner 9 Encounter," *Bull. Am. Astron. Soc.*, Vol. 4, p. 372, 1972.
- V-8. Gierasch, P., and Goody, R., "A Study of the Thermal and Dynamical Structure of the Martian Lower Atmosphere," *Planet. Space Sci.*, Vol. 16, pp. 615-646, 1968.
- V-9. Gierasch, P. J., and Goody, R. M., "The Effect of Dust on the Temperature of the Martian Atmosphere," *J. Atmos. Sci.*, Vol. 29, pp. 400-402, 1972.
- V-10. Masursky, H., Batson, R. M., McCauley, J. F., Soderblom, L. A., Wildey, R. L., Carr, M. H., Milton D. J., Wilhelms, D. E., Smith, B. A., Kirby, T. B., Robinson, J. C., Leovy, C. B., Briggs, G. A., Young, A. T., Duxbury, T. C., Acton, C. H., Jr., Murray, B. C., Cutts, J. A., Sharp, R. P., Smith, S., Leighton, R. B., Sagan C., Veverka, J., Noland, M., Lederberg, J., Levinthal, E., Pollack, J. B., Moore, J. T., Jr., Hartmann, W. K., Shipley, E. N., de Vaucouleurs, G., and Davies, M. E., "Mariner 9 Television Reconnaissance of Mars and its Satellites: Preliminary Results," *Science*, Vol. 175, pp. 294-305, 1972.
- V-11. McCauley, J. F., Carr, M. H., Cutts, J. A., Hartmann, W. K., Masursky, H., Milton, D. J., Sharp, R. P., and Wilhelms, D. E., "Preliminary Mariner 9 Report on the Geology of Mars," *Icarus*, Vol. 17, pp. 289-327, 1972.

## VI. Ultraviolet Spectrometer Experiment

C. A. Barth, C. W. Hord, and A. I. Stewart  
University of Colorado, Boulder, Colorado 80302

A. L. Lane  
Jet Propulsion Laboratory/California Institute of Technology, Pasadena, California 91103

### A. Scientific Objectives

The original scientific objectives of the ultraviolet spectrometer experiment (Ref. VI-1) may be briefly stated as follows:

- (1) *Ultraviolet cartography.* To map the surface and lower atmosphere of the planet Mars in the near ultraviolet spectral region, using measurements taken with the instrument pointed at the illuminated disk. This objective included: the measurement of local atmospheric pressure over a major part of the planet; the measurement of Mars' photometric function in the near ultraviolet; the mapping of the occurrence of ozone on the planet; and the study in the ultraviolet of classical Mars phenomena, including the wave of darkening, white and yellow clouds, and blue hazes and blue clearings. Implicit in the measurement of ozone was the search for evidence of biological activity which might occur in favorable Martian micro-environments.
- (2) *Ultraviolet aeronomy.* To study the composition and structure of Mars' upper atmosphere by the techniques of ultraviolet spectroscopy, using instru-

ment pointings designed to record airglow emissions while discriminating against the bright light scattered from the lower atmosphere. This objective included: measurement of the composition and structure of the upper atmosphere as a function of latitude, longitude, and time; measurement of ionospheric composition and its variations; measurement of the distribution of atomic hydrogen and of its rate of escape from the exosphere; and the search for ultraviolet aurorae and night airglow emissions.

Additional scientific objectives, determined in the light of opportunities presented by the final mission profile and by the planet itself, were to study:

- (1) The great dust storm: measurements of the distribution, evolution, and settling of the dust clouds; and measurements of their photometric properties in the near ultraviolet.
- (2) The seasonal variations in the occurrence of ozone.
- (3) The Martian moon, Phobos, in the near ultraviolet.
- (4) The several types of stars in the near and middle ultraviolet.

## B. Scientific Results

### 1. Original Objectives

The degree of success in achieving the original scientific objectives, and the principal scientific results, is briefly stated in the subsequent paragraphs.

**a. Ultraviolet cartography.** The goal of measurement of local atmospheric pressure over a major portion of the planet was achieved. The measurements were converted to relative altitude measurements via the barometric law (detailed procedures are described in Refs. VI-2 and VI-3), and topographic maps were prepared of the entire surface of Mars between  $+50^\circ$  and  $+20^\circ$ , with an extension northward to  $+40^\circ$  between  $180^\circ$  and  $330^\circ$ W longitude (Fig. VI-1). The south polar region (latitudes higher than  $-65^\circ$ ) was also extensively studied, and preliminary contour maps have been prepared. The north polar region was not mapped because of obscuration by the north polar hood and consequent limited coverage. In addition to these small-scale maps, instrument track topographic profiles have been prepared for a large number of surface features of special interest, including the canyonlands, Nix Olympica, and Middle Spot. The canyonlands were found to be as much as 6 km deep in places, while Nix Olympica was found to rise 25 km above the surrounding plain. These profiles have been correlated with the corresponding wide-angle-camera mapping pictures (see Figs. VI-2 and VI-3). Other mapping products include 1:25,000,000 clay and plastic models of the surface of Mars between  $-50^\circ$  and  $+20^\circ$ , and a 1:5,000,000 plastic topographic profile montage on a wide-angle mosaic of the canyonlands.

The photometric function of Mars in the near ultraviolet was determined from the same data set used in the mapping. The method and preliminary results are described in Ref. VI-3. At  $3000 \text{ \AA}$  the variations in the observed signal were found to be due to variations in the atmosphere (Ref. VI-2).

Detection and mapping of ozone on Mars were successfully accomplished, and in addition its seasonal variation was measured (Refs. VI-4 and VI-5). No ozone was found at low latitudes, and its appearance at high latitudes was seasonal. It appeared in the fall, reached a maximum during winter, and disappeared by early summer. It was always found in association with the polar hoods, and also in clear atmospheres when sufficiently cold. When present, ozone exhibited large latitudinal and time variations. Observed amounts varied from  $60 \mu\text{m-atm}$  down to the detection limit of about  $2 \mu\text{m-atm}$ . Figure VI-4

shows ozone measurements made in a region of both variable cloud cover and atmospheric temperature. The interpretation is that the temperature, rather than the clouds, influences the amount of ozone in the atmosphere.

The presence of ozone was correlated with the occurrence of cold, dry atmospheric conditions. No local concentrations of ozone were found that might be correlated with photosynthetic production of molecular oxygen. However, it was found that there are regions on Mars where the ultraviolet environment varies, in a manner analogous with what might have happened on Earth before biological activity began (Ref. VI-5).

Of the classical Martian dynamic features, nothing was seen in the ultraviolet that corresponds to the wave of darkening or the blue clearing. Yellow and white clouds and blue hazes, however, were detected and studied. Yellow clouds formed the great dust storm discussed previously. Terminator measurements poleward of the 50th parallels showed yellow clouds distributed in the atmosphere to have a scale height of between 6 and 8 km; the effective particle albedo was between 0.3 and 0.6 (Refs. VI-6 and VI-7). An extensive yellow dust cloud, having optical depth 0.2 to 0.3 (compared with about 0.05 in the normal "clear" atmosphere), remained in the Hesperia region after the great dust storm had settled (Ref. VI-2). White clouds, seen in wide-angle television pictures, are bright in the near ultraviolet; the polar hoods are composed of such clouds, which also occur at various times and places, apparently under meteorological influences. In the case of the polar hoods, they are associated with the presence of ozone. Hazes were detected many times in the ultraviolet; detailed study of terminator measurements shows that a haze layer of approximate optical depth 0.005 exists at altitudes varying between 60 and 90 km, between  $-50^\circ$  and  $+50^\circ$ . This haze was detected at 70 km on the limb of the planet on one favorable occasion near the equator (Refs. VI-6 and VI-7).

**b. Ultraviolet aeronomy.** The goal of measurement of the composition and structure of the upper atmosphere as a function of place and time was partially accomplished. The mission profile, developed after the loss of *Mariner 8* and onset in the light of the great dust storm, permitted 56 measurements of limb airglow profiles in the first 208 revolutions and none thereafter; most of the measurements could not be made at optimum viewing geometry, and most were made at  $-40^\circ$  to  $-50^\circ$  latitude in the late morning.

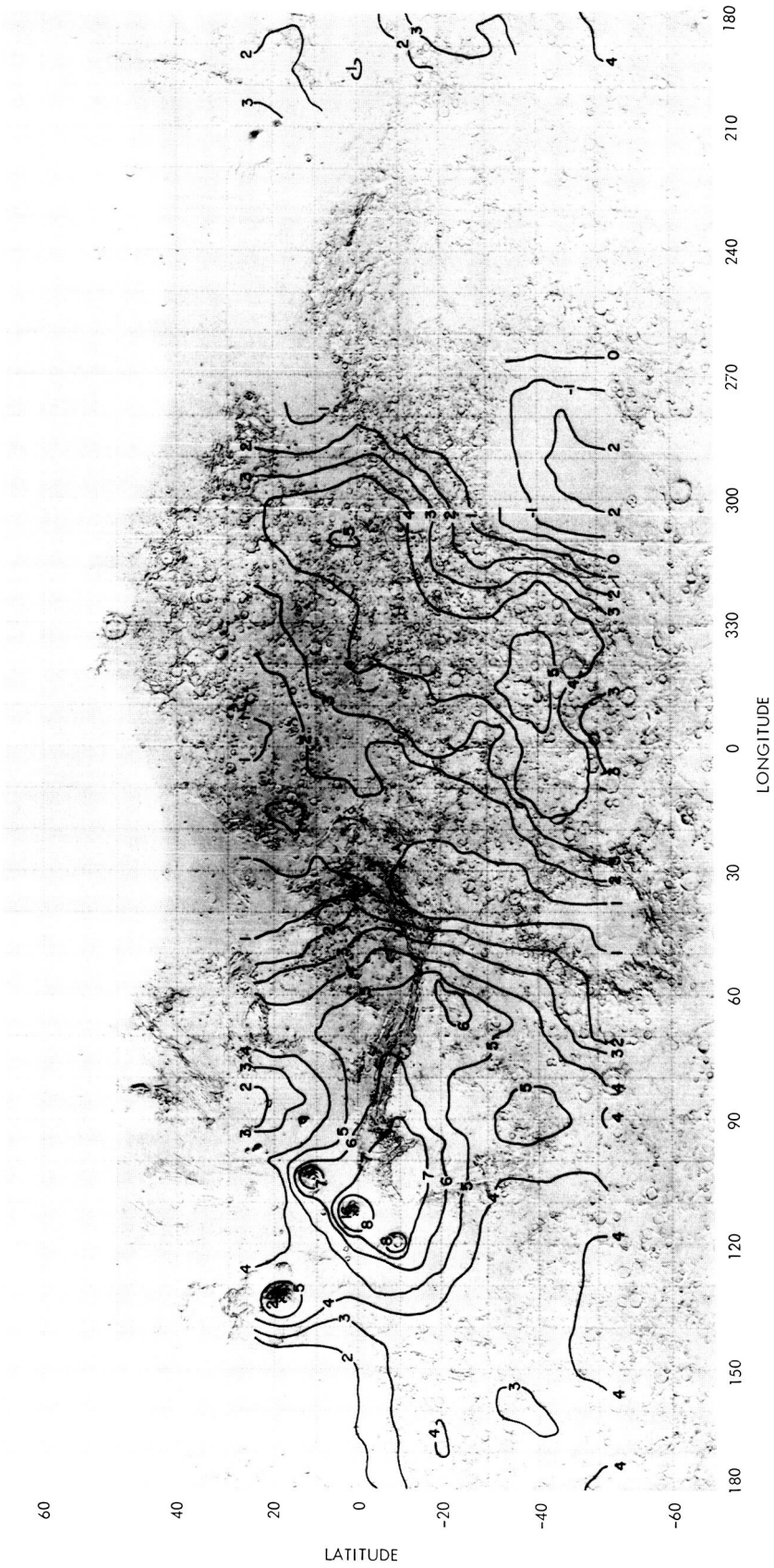


**Fig. VI-1. Ultraviolet pressure altitude contour map of Mars. The measurements have been smoothed to 10° in longitude and latitude except for the volcanoes Middle Spot and Nix Olympica, where more detail is shown. The region from longitude 210° to 270° was dusty at the time the measurements were made.**

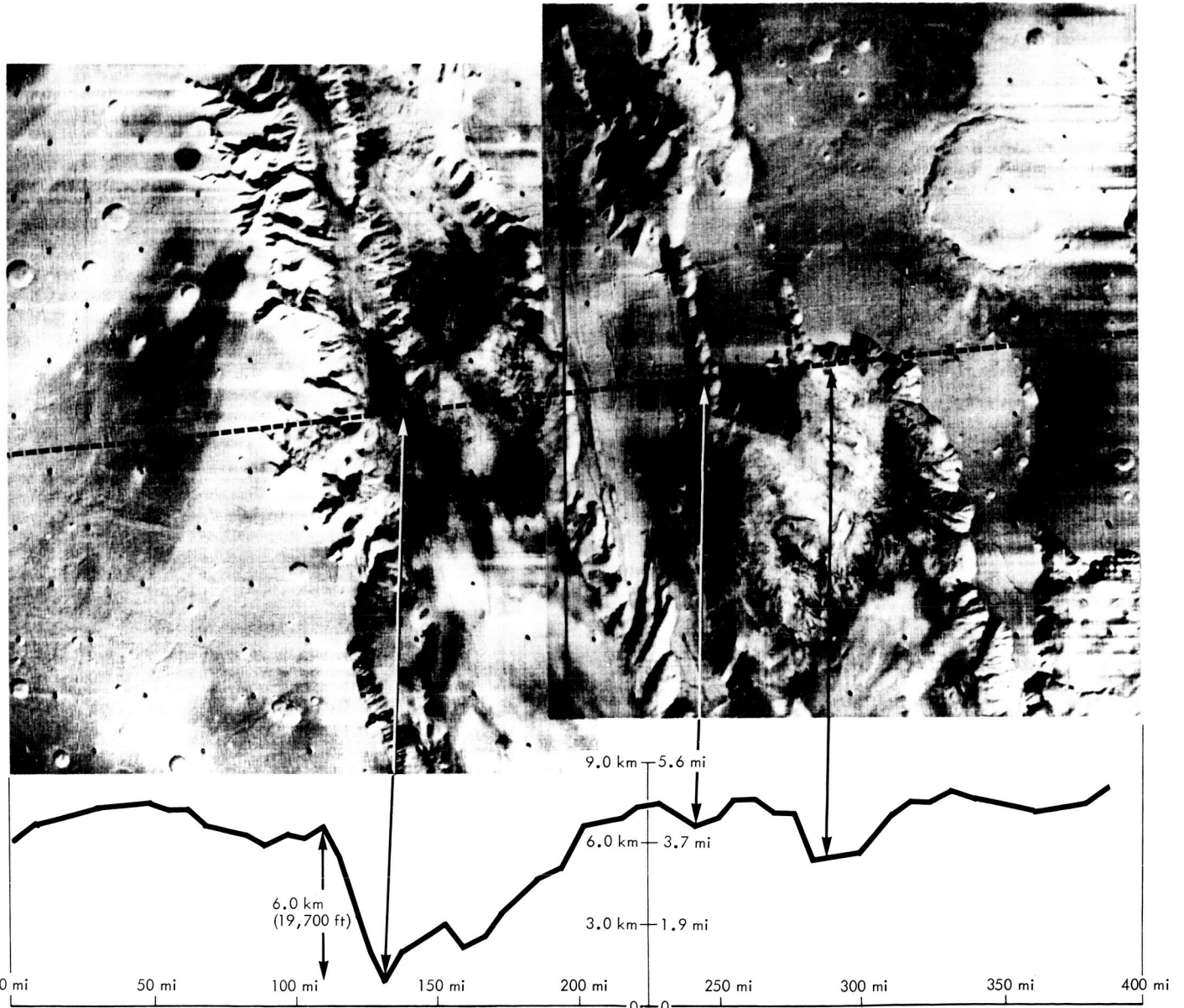


Fig. VI-2. Ultraviolet pressure altitude profile across the rift region shown with *Mariner 9* television pictures of the same region.

This limited coverage on the limb in the near ultraviolet was offset, from the point of view of mission success, by the good quality of measurements in the middle ultraviolet looking downward at the disk of the planet. The upper atmosphere was found to have a rather variable temperature, with a mean exospheric temperature of 325°K. It is composed predominantly of carbon dioxide, with small amounts (~1%) of atomic oxygen and carbon monoxide, and still smaller amounts of atomic hydrogen. The amount of atomic oxygen exhibits a pronounced afternoon enhancement (Fig. VI-5). The brightest airglow emissions were found to be well correlated with solar

activity (Fig. VI-6). Ionized carbon dioxide was not the dominant ion in the ionosphere; the likely alternative is ionized molecular oxygen (Refs. VI-8 through VI-11).

Atomic hydrogen was measured extensively in the exosphere and upper atmosphere. It has a density of about  $2.5 \times 10^4 \text{ cm}^{-3}$  and a temperature of about 300°K at the base of the exosphere. Variations in the intensity of its resonance emission, Lyman alpha, were found to be correlated with solar activity. The rate of thermal evaporation into space was about  $2 \times 10^8 \text{ cm}^{-2} \text{ sec}^{-1}$  (Refs. VI-8 through VI-11).

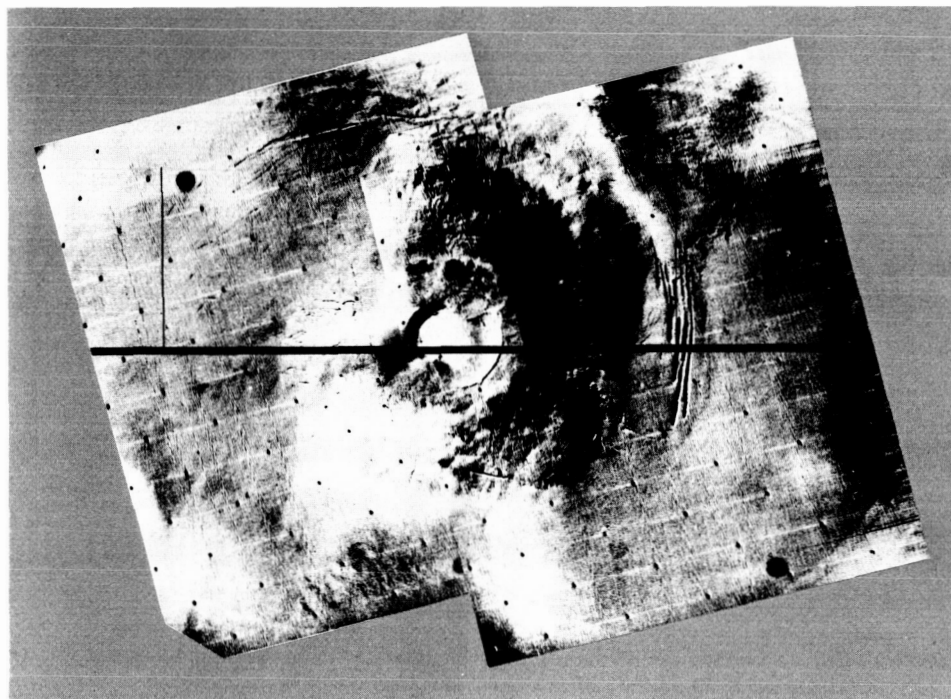
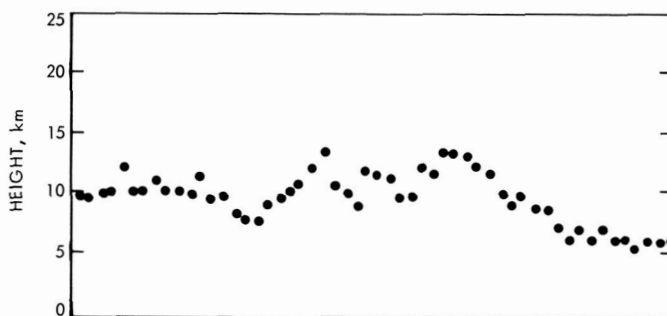


Fig. VI-3. Ultraviolet pressure altitude profile across the volcano Middle Spot. The local slope has been taken into account in computing the surface scattering effect used to find local pressure.

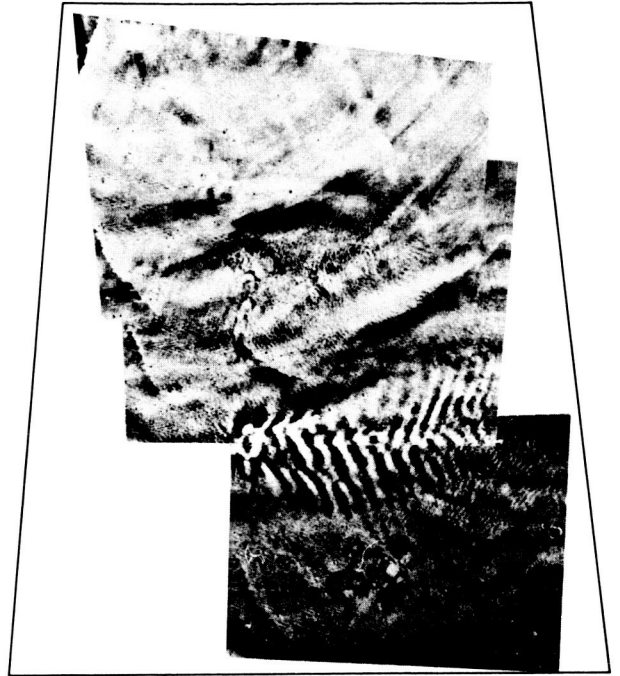
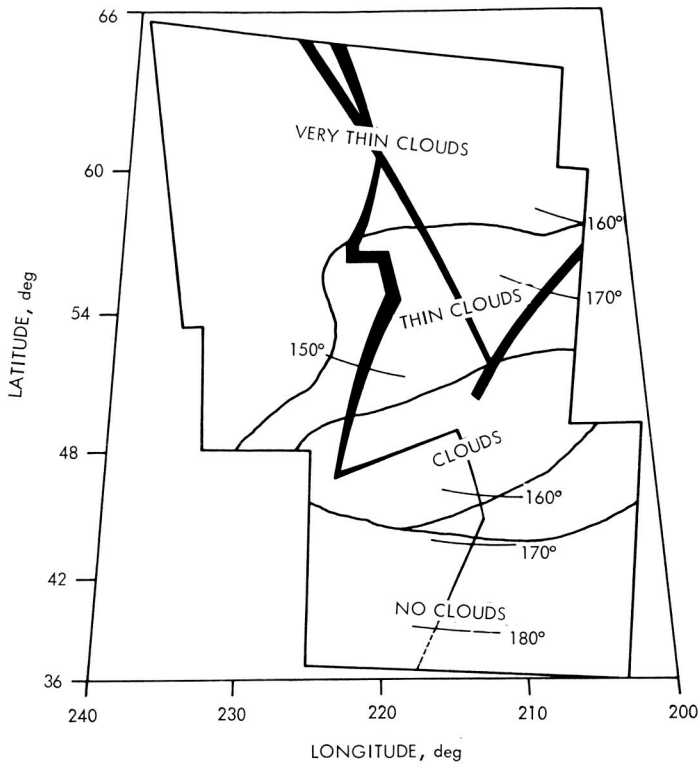


Fig. VI-4. Ultraviolet spectrometer measurements of ozone. The right-hand panel is a mosaic of three rectified wide-angle pictures showing a variety of cloud forms and cover. The left-hand panel shows the corresponding UVS track; the thickness of the line is proportional to the measured amount of ozone. Also shown are IRIS atmospheric temperature measurements.

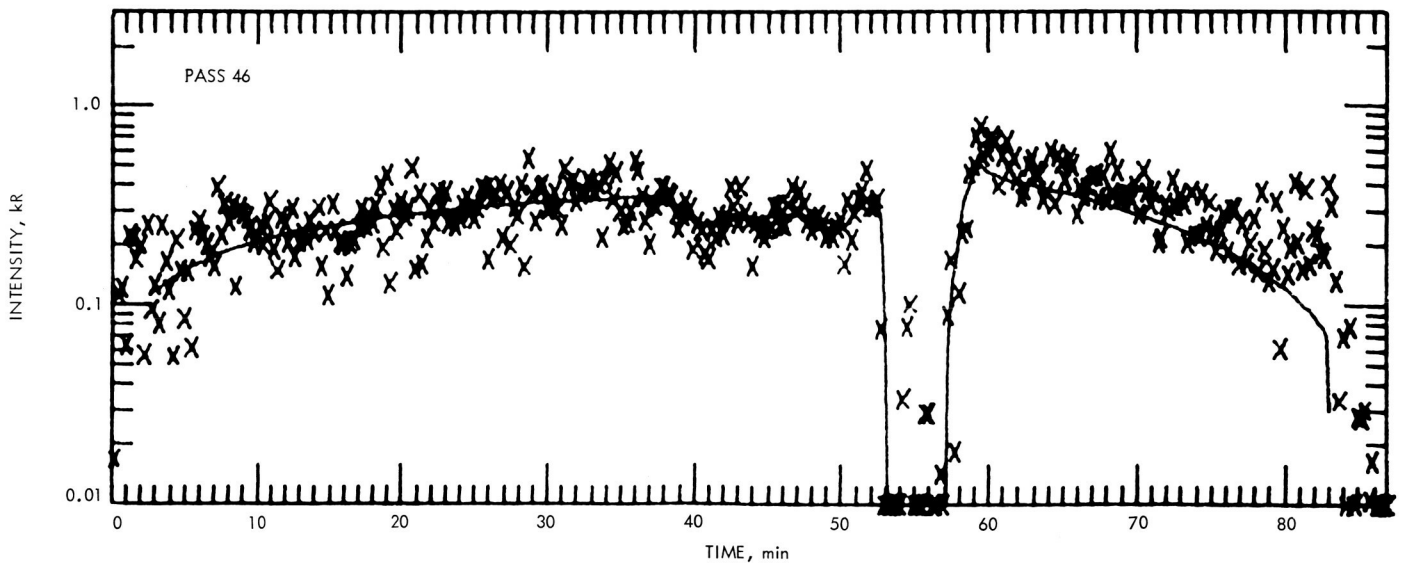


Fig. VI-5. Ultraviolet spectrometer measurements of atomic oxygen  $1304\text{-}\text{\AA}$  airglow emission on revolution 46. Spacecraft time is indicated along the bottom (arbitrary zero); Mars time at the point being observed increases from sunrise on the left to sunset on the right. Except for a bright limb observation near 55 min spacecraft time, all data were taken while looking at the disk of the planet. The crosses are data points, and the line is a theoretical simulation which uses a model atmosphere having 1% atomic oxygen at an altitude of 135 km. The data points lie above this line in the afternoon and evening (Mars time), indicating an afternoon enhancement in the amount of atomic oxygen present in the atmosphere.

Although the data search is incomplete, no auroral or night airglow emission has yet been found.

## 2. Additional Scientific Objectives

a. **The great dust storm.** At orbit insertion, the dust cloud was essentially opaque in the near ultraviolet at equatorial latitudes, but the south polar cap could be seen clearly through it. Limb observations of the cloud near the equator suggested a vertical optical depth of 3, while south polar cap observations suggested a value of 1. This latitudinal variation was confirmed spectroscopically. The dust particles were found to have an albedo of 0.2, and from the spectral scattering characteristics their size was less than  $5\ \mu\text{m}$ . The cloud settled with a characteristic time of 60 days, indicative of  $5\text{-}\mu\text{m}$  particles (Refs. VI-3, VI-6 through VI-8, and VI-12).

b. **Seasonal variations in ozone.** This study was performed during the extended mission, in northern winter and spring and southern summer and fall (see Section VI-B-1; also see Refs. VI-4 and VI-5).

c. **Phobos.** An ultraviolet spectrum of Phobos was obtained. The moon was found to have approximately the same color as Martian dust, but to be very dark, with a reflectance less than 0.01 (Ref. VI-8).

d. **Stellar observations.** At times when the instruments could not view Mars, ultraviolet spectra of stars and measurements of the Lyman alpha sky background were obtained. The spectra are of comparable or superior quality to those obtained from other spacecraft (Refs. VI-13 through VI-16).

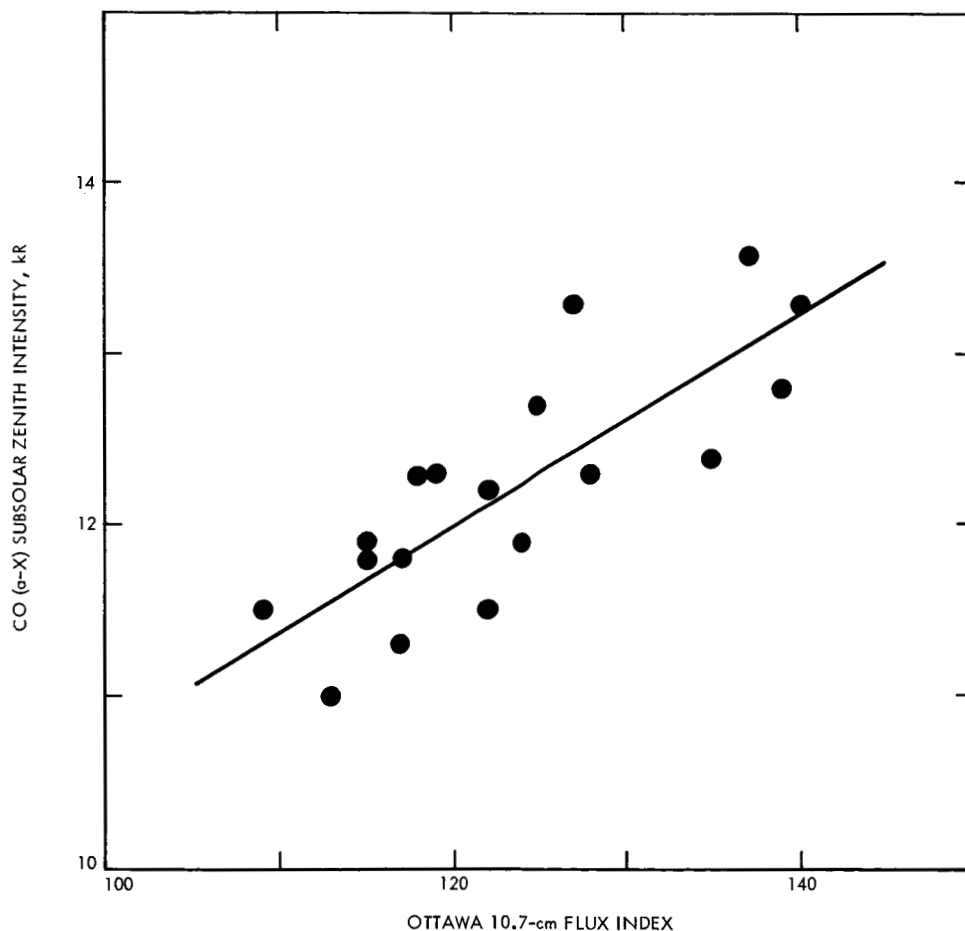


Fig. VI-6. Variation of airglow intensity with solar activity. The intensity of the Cameron bands of carbon monoxide (the brightest airglow emission) is plotted against the solar 10.7-cm flux index (believed to be an indicator of solar extreme ultraviolet activity). The quantities are significantly correlated, in a way that supports the view that this airglow emission is produced by the action of solar extreme ultraviolet radiation on carbon dioxide in the Martian upper atmosphere.

## References

- VI-1. Hord, C. W., Barth, C. A., and Pearce, J. B., "Ultraviolet Spectroscopy Experiment for Mariner Mars 1971," *Icarus*, Vol. 12, pp. 63-77, 1970.
- VI-2. Hord, C. W., "Mariner 9 Ultraviolet Spectrometer Experiment: Pressure Altitude Measurements on Mars" (in preparation).
- VI-3. Hord, C. W., Barth, C. A., Stewart, A. I., and Lane, A. I., "Mariner 9 Ultraviolet Spectrometer Experiment: Photometry and Topography of Mars," *Icarus*, Vol. 17, pp. 443-456, 1972.
- VI-4. Lane, A. L., Barth, C. A., Hord, C. W., and Stewart, A. I., "Mariner 9 Ultraviolet Spectrometer Experiment: Observations of Ozone on Mars," *Icarus*, Vol. 18, pp. 102-108, 1973.
- VI-5. Barth, C. A., Hord, C. W., Stewart, A. I., Lane, A. L., Dick, M. L., and Anderson, G. P., "Mariner 9 Ultraviolet Spectrometer Experiment: Seasonal Variation of Ozone on Mars," *Science*, Vol. 179, pp. 795-796, 1973.
- VI-6. Ajello, J. M., Hord, C. W., Barth, C. A., Stewart, A. I., and Lane, A. L., "Mariner 9 Ultraviolet Spectrometer Experiment: Afternoon Terminator Observations of Mars," *J. Geophys. Res.*, Vol. 78, 1973.
- VI-7. Ajello, J. M., and Hord, C. W., "Mariner 9 Ultraviolet Spectrometer Experiment: Morning Terminator Observations of Mars" (submitted to *J. Atmos. Sci.*).
- VI-8. Barth, C. A., Hord, C. W., Stewart, A. I., and Lane, A. L., "Mariner 9 Ultraviolet Spectrometer Experiment: Initial Results," *Science*, Vol. 175, pp. 309-312, 1972.
- VI-9. Stewart, A. I., Barth, C. A., Hord, C. W., and Lane, A. L., "Mariner 9 Ultraviolet Spectrometer Experiment: Structure of Mars' Upper Atmosphere," *Icarus*, Vol. 17, pp. 469-474, 1972.
- VI-10. Strickland, D. J., Stewart, A. I., Barth, C. A., Hord, C. W., and Lane, A. L., "Mariner 9 Ultraviolet Spectrometer Experiment: Mars Atomic Oxygen 1304-Å Emission," *J. Geophys. Res.*, Vol. 78, 1973.
- VI-11. Barth, C. A., Hord, C. W., Stewart, A. I., and Lane, A. L., "Mariner 9 Ultraviolet Spectrometer Experiment: Mars Airglow Spectroscopy and Variations in Lyman Alpha," *Icarus*, Vol. 17, pp. 457-468, 1972.
- VI-12. Pang, K. D., and Hord, C. W., "Mariner 9 Ultraviolet Spectrometer Experiment: 1971 Mars' Dust Storm," *Icarus*, Vol. 18, pp. 481-488, 1973.
- VI-13. Lillie, C. F., Bohlin, R. C., Molnar, M. R., Barth, C. A., and Lane, A. L., "Mariner 9 Ultraviolet Spectrometer Experiment: Stellar Observations," *Science*, Vol. 175, pp. 321-322, 1972.
- VI-14. Bohlin, R. C., "Mariner 9 Ultraviolet Spectrometer Experiment: Interstellar Absorption at Lyman Alpha in OB Stars," *Astrophys. J.*, Vol. 182, p. 139, 1973.

## References (contd)

- VI-15. Bohlin, R. C., Henry, R. C., and Swandic, J. R., "Mariner 9 Ultraviolet Spectrometer Experiment: Upper Limits on Lyman Alpha Flux From Clusters of Galaxies," *Astrophys. J.*, Vol. 182, p. 1, 1973.
- VI-16. Bohlin, R. C., "Mariner 9 Ultraviolet Spectrometer Experiment: Measurements of the Lyman-Alpha Sky Background" (submitted to *Astronom. and Astrophys.*).

## VII. Television Experiment

G. A. Briggs, J. A. Cutts, R. H. Steinbacher, T. E. Thorpe, and A. B. Whitehead  
Jet Propulsion Laboratory/California Institute of Technology, Pasadena, California 91103

G. de Vaucouleurs  
Department of Astronomy  
The University of Texas, Austin, Texas 78712

M. E. Davies  
The Rand Corporation  
Santa Monica, California 90401

H. Masursky  
U. S. Geological Survey  
Flagstaff, Arizona 86001

J. B. Pollack  
NASA/Ames Research Center  
Moffet Field, California 94305

### A. Experiment Background, G. A. Briggs, J. A. Cutts, R. H. Steinbacher, T. E. Thorpe, and A. B. Whitehead

The primary objective of the television experiment was to provide imaging data that would complement previous data and that would add to man's knowledge of the planet Mars. To achieve this goal, the *Mariner 9* television studies in orbit consisted of two types of investigations: fixed features and variable features. The objectives of each investigation, as originally stated, were (see Ref. VII-1):

#### *Fixed features investigation*

- (1) To obtain a broad range of image information to be used for regional stratigraphic studies of tectonic features, crater configuration and distribution, and local surface environment.

- (2) To measure, by photometric and photogrammetric analysis, surface slopes and elevations; to determine surface brightness and albedo; and to perform analyses related to improving the accuracy of the photometric function for various regions on Mars.
- (3) To obtain an improved value for the shape of the planet, and thereby investigate possible departures from hydrostatic equilibrium.
- (4) To study the surface characteristics of Phobos and Deimos.

#### *Variable features investigation*

- (1) To obtain information on atmospheric structure and circulation.
- (2) To obtain details of diurnal and seasonal changes.

- (3) To obtain clues regarding the possibility of life on Mars.
- (4) To study the following specific phenomena:
  - (a) Wave of darkening.
  - (b) Polar caps and adjacent areas.
  - (c) Nightside atmospheric and surface fluorescence.
  - (d) Haze in the atmosphere.
  - (f) Dust clouds and dust storms.
  - (g) Phenomena of possible exobiological significance.

The loss of *Mariner 8* at launch required a re-evaluation of the mission plan and of the scientific studies for adaptation to a one-spacecraft mission. All objectives were retained and were successfully accomplished despite the additional setback of a planet-wide dust storm.

At the inception of the Mariner Mars Project in 1968, the experiment's Principal Investigators and Co-Investigators, selected by the National Aeronautics and Space Administration, were organized into a collectively functioning Television Team. Scientific disciplines and technical task groups were formed to provide plans for instrument development and requirements for mission planning. (This early organization is shown in Figure 1 of Ref. VII-1.) The organization of the Team at the arrival of *Mariner 9* at Mars is shown in Fig. VII-1. This figure represents a change from the earlier organization, and reflects the results of new information, the combined interests of many of the experimenters, and the capabilities of *Mariner 9*. The Team concept, utilized for the first time on any project, continued through the end of the *Mariner 9* mission. Science results derived from the mission, presented according to the scientific disciplines, are given in the subsequent paragraphs of this section.

## B. Atmospheric Phenomena, G. A. Briggs

In mid-September 1971, Earth-based telescopes first showed the existence of a dust storm in the southern hemisphere of Mars. Within 1 week it had expanded to global proportions, and almost all of the typical Martian features were obscured. This condition remained through October and into November as *Mariner 9* approached the planet. Pre-orbital pictures showed an almost total absence of detail in the illuminated crescent of Mars.

The persistence of the obscuring dust during the first 6 weeks of the orbital mission eliminated plans for the early study of white cloud activity in the Tharsis region and for observation of the characteristics of morning hazes expected from Earth observations in previous oppositions. Nevertheless, the high-altitude photography planned for this time period proved valuable for monitoring the dust storm's progress, and photometric studies provided estimates of the dust particle sizes (Ref. VII-2). There was visible structure in the dust clouds. Wind directions could be inferred from pictures showing waves in the top of the dust near the morning terminator and showing a curvilinear "wake," extending nearly 1000 km southwest from the most southern volcano (South Spot) on the Tharsis ridge (Ref. VII-3).

Perhaps the most remarkable information learned about the dust storm by means of the television experiment, working in conjunction with the ultraviolet spectrometer experiment, was the determination from limb pictures that the dust reached an elevation of about 4 scale heights (Ref. VII-2). The detached haze layers observed at the limb above the dust pall were located at altitudes of up to 70 km. More complex hazes of this type, assumed to be condensates, were observed in the vicinity of the north polar hood; frequently more than one layer could be observed, generally diminishing farther north. A complete analysis of the many hundreds of limb pictures taken by *Mariner 9* is still in progress.

The north polar hood, which could be seen only with useful viewing geometry from February 1972, proved to be a rewarding object of study. The appearance of the hood clouds was variable, but they consistently indicated formation in air moving eastward, as predicted from circulation studies of Mars (Ref. VII-4). Lee waves were the most common cloud type, often of arcuate form behind impact craters. The persistence of the waves for many hundreds of kilometers downstream indicated that high-velocity winds were present at high altitudes, preventing the dissipation of the wave energy into the upper atmosphere (Ref. VII-2). Frontal movements, consistent with the baroclinic wave circulation predicted for the winter mid-latitudes, also were monitored. On two occasions such movements of cold air southward appeared to be responsible for the generation of short-lived dust storms near the periphery of the hood at about +40° latitude. From correlations with the temperature profiles determined using the infrared interferometer spectrometer

TEAM LEADER H. MASURSKY <sup>a</sup>
DEPUTY B. SMITH <sup>a</sup>

DISCIPLINE GROUPS

ATMOSPHERIC PHENOMENA C. LEOVY G. BRIGGS E. SHIPLEY B. SMITH R. WILDEY J. POLLACK A. YOUNG	GEODESY/ CARTOGRAPHY G. de VAUCOULEURS D. ARTHUR R. BATSON W. BORGESON M. DAVIES R. LEIGHTON A. YOUNG R. WILDEY	GEOLOGY J. McCAULEY M. CARR W. HARTMANN R. SHARP L. SODERBLOM D. WILHELMS J. CUTTS D. MILTON B. MURRAY C. SAGAN	VARIABLE SURFACE FEATURES C. SAGAN J. CUTTS J. LEDERBERG E. LEVINTHAL J. VEVERKA R. WILDEY A. YOUNG G. BRIGGS M. CARR G. de VAUCOULEURS J. POLLACK B. SMITH	SATELLITE ASTRONOMY J. POLLACK D. MILTON M. DAVIES W. HARTMANN C. SAGAN J. VEVERKA B. SMITH A. YOUNG	POLAR PHENOMENA B. MURRAY J. CUTTS R. LEIGHTON J. LEDERBERG C. LEOVY R. SHARP L. SODERBLOM D. MILTON
---	--	---	---	--	--

TASK GROUPS

HARDWARE B. MURRAY W. BORGESON J. CUTTS R. LEIGHTON B. SMITH R. WILDEY A. YOUNG	MISSION ANALYSIS G. BRIGGS W. BORGESON M. DAVIES D. MILTON J. POLLACK C. SAGAN B. SMITH	DATA PROCESSING AND PROCESS CONTROL E. LEVINTHAL <sup>b</sup> D. ARTHUR R. BATSON <sup>b</sup> G. BRIGGS <sup>b</sup> J. CUTTS M. DAVIES E. SHIPLEY <sup>b</sup> B. SMITH <sup>b</sup> L. SODERBLOM <sup>b</sup> J. VEVERKA <sup>b</sup> R. WILDEY <sup>b</sup> A. YOUNG <sup>b</sup>	MISSION OPERATIONS B. SMITH R. BATSON G. BRIGGS M. CARR W. HARTMANN C. LEOVY J. McCAULEY B. MURRAY C. SAGAN
--	--	---	--

<sup>a</sup>Ex-officio members of all groups.

<sup>b</sup>Member of the Process Control sub-group. A. Young and L. Soderblom are chairmen.

Fig. VII-1. Mariner 9 Television Team matrix.

(IRIS), the wave clouds observed between  $+45^\circ$  and  $+60^\circ$  are believed to be composed of water ice, while the more diffuse hazes observed farther north are considered carbon dioxide.

A major goal of the atmospheric studies was to achieve a better understanding of the discrete "white clouds" observed in various regions. Observations of condensate clouds over the summit of the volcano "South Spot," made in February 1972, showed that the brightening observed in this region (an element of the W-cloud) was the result of clouds rather than surface frost. The pictures, which from shadow measurements indicated an altitude of only about 8 km above the caldera, confirmed the theory (Ref. VII-5) that the clouds were composed of water ice. The clouds associated with the Tharsis area and with Nix Olympica were observed over a greater part of their diurnal cycle and at a time of peak seasonal activity during the extended mission in August and October 1972. At this time the clouds were extensive and invariably to the west of the volcanic mountains with which each was associated. (Clouds also were observed over the Coprates canyon complex.) A general lack of shadows suggested that the clouds were low, but this has not been conclusively shown, nor has an entirely acceptable mechanism for their production been proposed. Generally the clouds were fully developed at the earliest time of day at which they were observed (about 13:30), but one view of Nix Olympica acquired in mid-morning has a suggestion of low hazes around the base escarpment of the volcano. IRIS spectra showing an absorption feature of water ice conclusively determine the composition of the clouds; infrared radiometer data on the cloud temperatures will help to determine the elevation of the clouds and to reveal the mechanism of their formation. In this study and in many others the results of the television experiment, combined with those from other *Mariner 9* experiments, has proved to be of great value (see Section X of this Report).

### C. Geodesy/Cartography, G. de Vaucouleurs, M. E. Davies, T. E. Thorpe, and A. B. Whitehead

Approach pictures, taken in the last 48 hr before orbit insertion, are of extreme importance in establishing the global surface geodetic grid and the preliminary surface and albedo maps by which small-area, high-resolution pictures can be accurately mosaicked. The *Mariner 9* mission plan was to establish, within 90 days, a preliminary

control net from approach pictures which would be used for preliminary photomosaics. The control grid then would be refined with orbital pictures so that surface maps could be in production 6 months after orbit insertion. This plan was not carried out because the dust storm prohibited the approach pictures of the surface.

When the planet's surface became visible, efforts to establish the geodetic net were greatly impeded because the planetary viewing geometry of *Mariner 9* had changed, and there were no longer any opportunities to photograph suitably large areas to establish the basic grid. Instead, a grid was constructed by combining a large number of smaller-area mapping frames.

Program modification, computer capacity expansion, and a great amount of effort have provided a control net of 1645 points (10-km accuracy) covering about 80% of the planet (distributed on all 30 sections of the planet described by the 1:5,000,000 map system, although not uniformly; see Ref. VII-6). The control net computation resulted in the determination of a new direction of the spin axis of Mars that differs from the direction given in the Nautical Almanac by about  $\frac{1}{2}^\circ$ . The new spin direction agrees with a recent analysis of the motion of the natural satellites (Ref. VII-7) and is considered to be correct within  $0.1^\circ$ . A new definition of  $0^\circ$  longitude has been incorporated in the coordinate system and uses the center of a crater designated Airy-0 (zero) to locate the prime meridian (Ref. VII-8). It is close to the traditional origin of longitude (center of Sinus Meridiani). The geodetic net has provided coordinates of control points for most of the areas of Mars where maps are needed. Coverage is not uniform, and there are still several areas in which additional effort will be required to complete the task. It may have to await a future photographic mission to complete and improve the *Mariner 9* control net.

Surface mapping, although started, has been hampered from lack of optimum pictures. Both picture mosaics and an airbrush shaded relief map of the entire planet at a scale of 1:25,000,000 (see Fig. VII-2) have been developed (Ref. VII-9). Following the quick-look, variable-scale mosaics assembled almost concurrently with spacecraft photography, a system of 1:5,000,000 maps was defined by dividing the planet into 30 sections (Fig. VII-3). Two Polar Orthographic Projections provide coverage of the north and south poles. Twelve Lambert Projection

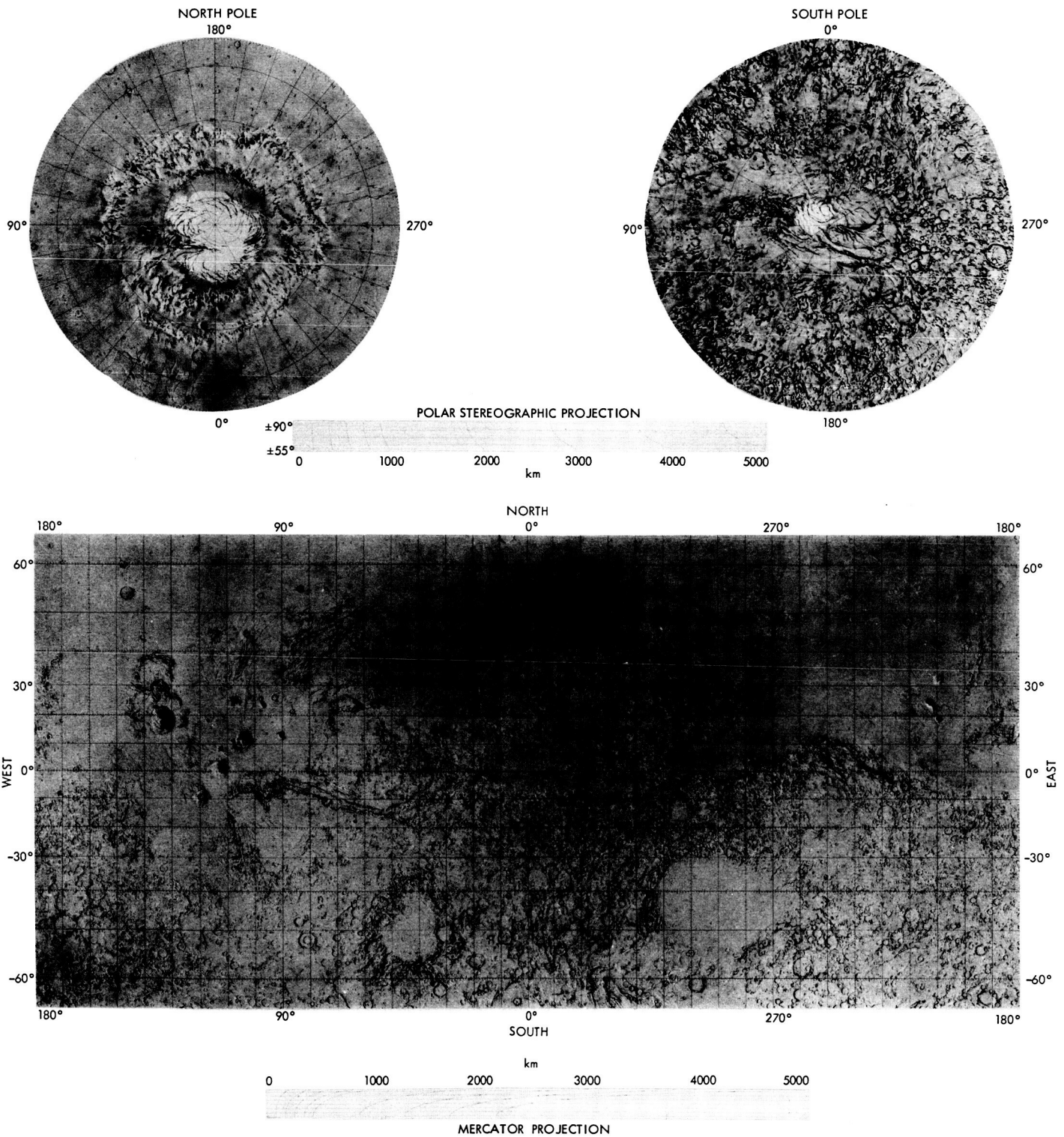


Fig. VII-2. Shaded relief map of Mars showing the entire surface of the planet. The mid-latitudes are in Mercator Projection and the poles in Stereographic Projection. Each polar cap is shown at its minimum size during the summer. The relief map does not show the normal albedo markings, but is an airbrushed rendition with the physical features as they would appear with similar lighting conditions at all parts of the planet. The 1:25,000,000 maps were produced at the U. S. Geological Survey, Flagstaff, Arizona.

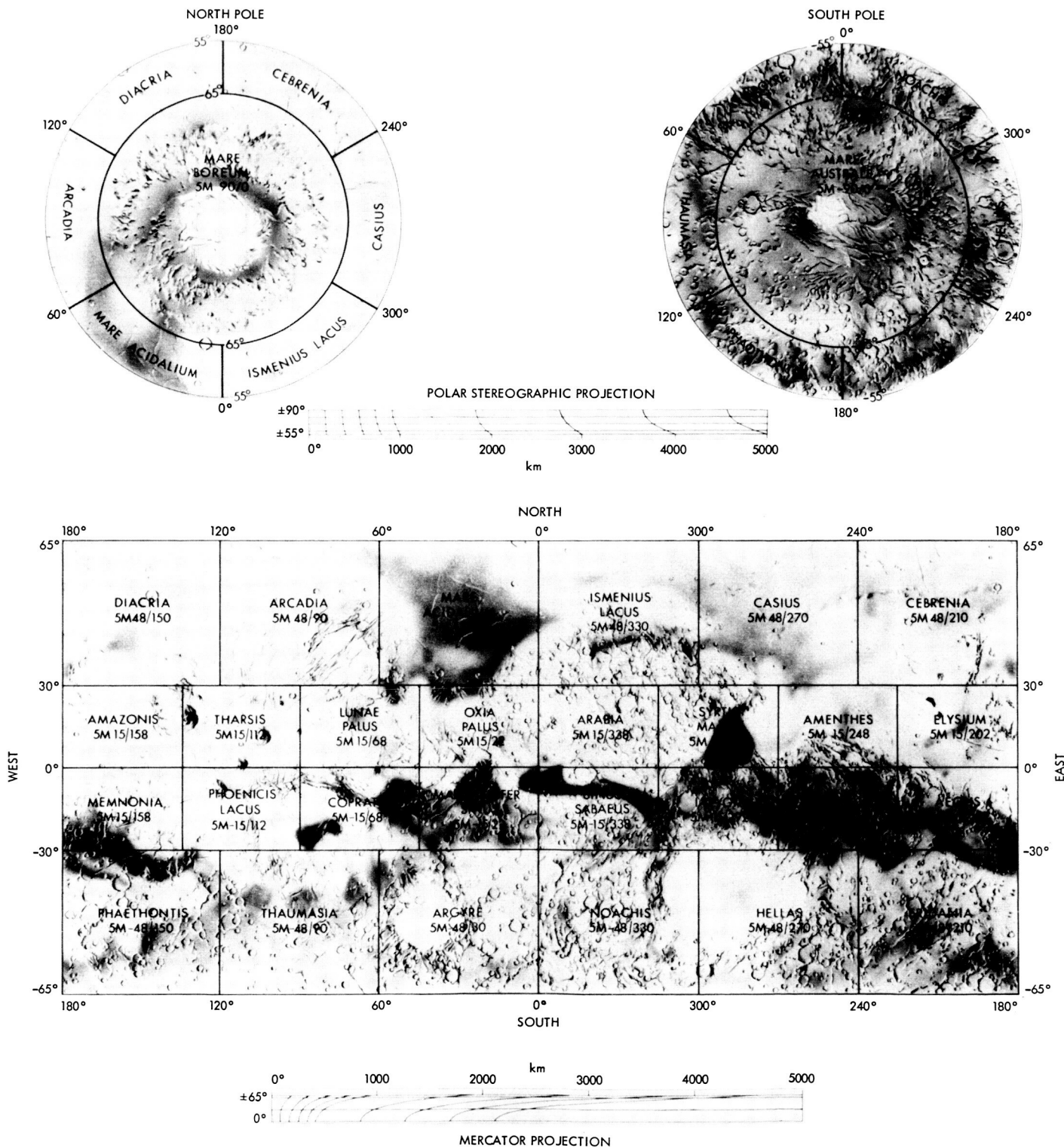


Fig. VII-3. Index chart of Mars showing names and locations of the 1:5,000,000 scale mapping system. There are 30 quadrangles in the set which provide high-resolution detail of the Martian surface in shaded relief and in albedo markings. The equatorial latitudes (+30° to -30°) are in Mercator Projection, the mid-latitudes (+30° to +65° and -30° to -65°) in Lambert Conformal Projection, and the polar regions (+65° to +90° and -65° to -90°) in Stereographic Projection.

quadrangles cover the mid-latitudes of the northern and southern hemispheres; 16 Mercator Projection quadrangles cover the northern and southern equatorial zones. Production and completion of the sections were determined by the scientific need and usefulness for planning purposes of future missions to Mars. The sequence of development was an uncontrolled picture mosaic, a semi-controlled mosaic, and a geodetic controlled mosaic (still in production). An airbrushed geodetic controlled relief map is also planned. High-resolution maps are being produced at scales of 1:1,000,000 and 1:250,000. These high-resolution charts are for specific scientific studies.

A series of albedo maps indicating surface contrast is also being produced. The 1:25,000,000 map (see Fig. VII-4) is based on telescopic data from Earth just before the onset of the dust storm (Ref. VII-10). Six of the maps (MC-9, MC-10, MC-11, MC-17, MC-18, MC-30) for the 30 sections at a scale of 1:5,000,000 (Fig. VII-5) have been completed (Refs. VII-11 and VII-12). High-precision photometric measurements of Martian surface features

were not possible because of the inherent properties of the vidicon (Ref. VII-13). The selection mechanism on the polarizing filter failed, reducing the albedo accuracy capabilities of the camera subsystem because only a partial calibration had been performed, and inflight checks showed a marked change from that calibration. An additional deterrent to the measurement of the surface albedo was that the picture budget constraints resulting from the dust storm prohibited acquisition of special high Sun pictures. However, attempts have been made at the Image Processing Laboratory (IPL) of the Jet Propulsion Laboratory to construct albedo maps from the mapping pictures. The contrast on the existing albedo maps was guided by observations made in 1971 (Ref. VII-10).

Counts of small-scale albedo markings visible on wide-angle pictures have been used to derive contour maps of the fractional area coverage and the average area of dark surface features, which allows interesting comparisons with the large-scale albedo features known from Earth-based telescopic data.

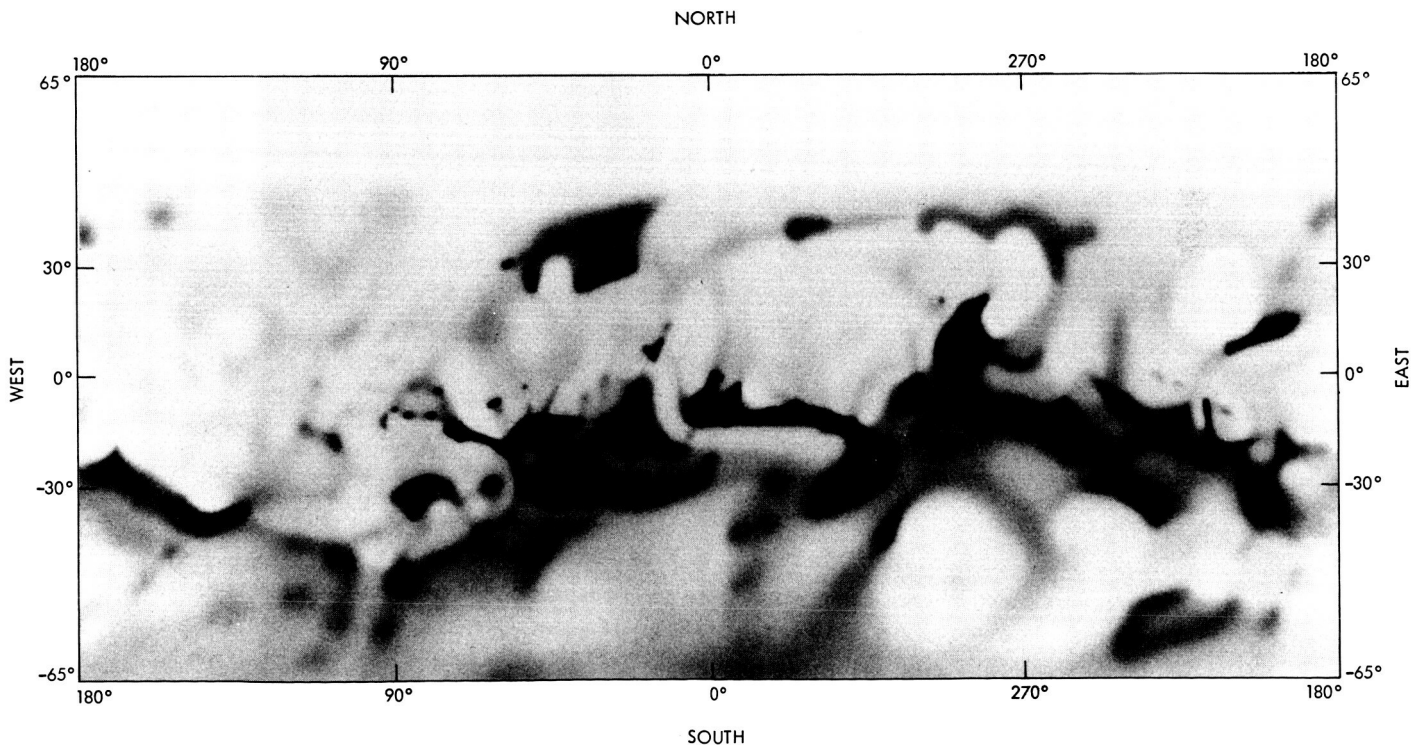


Fig. VII-4. This map represents the large-scale albedo (bright and dark) patterns on the surface of Mars near its perihelic opposition (August 1971). It is based on visual and photographic observations. Originally produced at a scale of 1:25,000,000 by the Department of Astronomy, University of Texas.



Fig. VII-5. Albedo map of the Coprates quadrangle (MC-18), combining information for the 1971 opposition from Earth-based observations with the high resolution of the *Mariner 9* pictures. Originally produced at a scale of 1:5,000,000 by the Department of Astronomy, University of Texas.

#### D. Geology, G. A. Briggs, J. A. Cutts, and H. Masursky

If *Mariner 9* had survived only for the 90-day mission for which it had been designed, many discoveries such as the volcanic and tectonic regions on Mars still would have been made, but the vast amount of information derived from the systematic mapping of the planet would have been lost. Although 100% of the planet's surface was photographically mapped, the delay in beginning the systematic mapping, caused by the dust storm, led to the mapping pictures being taken farther from the terminator than originally planned. This meant that the effective resolution of these pictures was less than desired.

Because of the loss of *Mariner 8* and the resulting reduction in picture budget, fewer high-resolution, narrow-angle camera pictures were obtained to assist in the interpretation of the wide-angle coverage. However, results from the *Mariner 9* Geology Discipline Group exceeded expectations primarily because of the successful efforts to surmount various operational setbacks and because Mars proved to be a much more varied planet geologically than indicated by results from *Mariners 4, 6, and 7*. Similarly, the almost faultless 1-year operation of *Mariner 9* allowed the entire planet to be photographed instead of the original goal of 70% of the planet's surface. The resolution of the mapping pictures acquired during the extended mission is reduced above a latitude of about +40° because the southern orbital periapsis provided a higher spacecraft altitude for the northern latitude pictures. However, interpretation of the topography of this part of the planet proved to be adequate.

Several major scientific results have emerged from geologic studies of the Martian surface in combination with the planet's shape derived from occultation measurements, infrared and ultraviolet spectrometer pressure mapping, and photogrammetric studies of elevation differences. These major results are:

- (1) Mars is divided into two hemispheres: the southern hemisphere, which consists of dominantly heavily cratered, ancient, continental terrain that represents an early differentiated crust modified by later processes; and the northern hemisphere, which is more than 3 km lower and is covered by what appears to be less cratered, basaltic lava flows of much younger age that are partially mantled by eolian deposits. These areas apparently are almost isostatically balanced, indicating that the crustal style in the two hemispheres differs markedly.

- (2) Basaltic volcanism has blanketed the low-standing "oceanic basins" and has created large volcanic structures, the largest of which is Nix Olympica. The high-resolution pictures of the flank flows of Nix Olympica show that: (a) the form indicates possible basaltic composition, (b) the few impact craters on the flows indicate geologic youthfulness, and (c) the sharpness of terrain detail of the flows confirms the geologic youthfulness of the uppermost flows.
- (3) Examination of the highland areas shows many volcanic centers of different types, which vary from "young" volcanic centers such as those in Hesperia, "the Dandelion," and the center in Alba to ancient centers that are very heavily cratered and degraded. One such structure was found northeast of Hellas; two other structures adjacent to Hellas have been mapped. These observations indicate that volcanism has occurred on Mars from the earliest to the most recently definable geologic times.
- (4) The high central equatorial plateau is composed of sub-horizontal layered rocks visible in many pictures. The uppermost layers of this sequence are cut by faults and are very lightly cratered, indicating their geologic youth. The plateau is cut by fault valleys up to 6 km deep measured by the ultraviolet spectrometer and by Earth-based radar. The lowest layers of this sequence probably are much older than the upper layers, although no technique presently exists for estimating the age of the lowest layers. The terrain sharpness of the faults cutting the upper layers indicates the continuation, up to geologically recent times, of the tectonic activity leading to the faulting.
- (5) Study of the channels indicates that there are at least five types:
  - (a) Sinuous channels without tributaries that resemble lava channels observed on Earth and on the Moon.
  - (b) Broad channels that start in chaotic terrain and run north into the lowlands. These channels may be fluvial and may be derived from melted permafrost. These channels are all in the near-equatorial region.

- (c) Sinuous channels with multiple tributaries that broaden and deepen downstream. These may be fluvial, based on their gross form and the form of the complex braided channels in high-resolution pictures. The channels are most similar to terrestrial intermittent streams; no viable alternate hypothesis for their origin has been proposed.
  - (d) Complex patterns of the channel networks that are widely distributed in the equatorial and temperate regions (Ref. VII-14). Their distribution may imply widespread rainfall, but their form is not entirely consistent with this proposed origin.
  - (e) Channels that may be caused by ground-ice sapping. These channels are abundant along the northern border of the central plateau in the area of the fretted terrain described by Sharp in Ref. VII-15. The channels vary from sparsely cratered channels in new terrain to heavily cratered channels in degraded terrain. The interpretation of the variability in appearance is that there are great variations in age. The oldest channels appear to have been formed early in the history of Mars, so the channel-forming process has occurred many times over a large proportion of the geologic history.
- (6) Photo-interpretation of the equatorial region indicates that eolian erosion is a dominant process (Refs. VII-16 and VII-17). Apparently the material accrues from the equatorial region and is deposited in the polar regions as layered deposits (Ref. VII-18). The circumpolar etch-pitted terrain indicates that strong winds near the ice cap actively erode the layered deposits and scour the underlying older deposits (Ref. VII-19). This eroded material is deposited as dunes and loess blankets that thin equatorward. These deposits comprise the mantled terrain discussed by Soderblom in Ref. VII-20.

## E. Variable Surface Features, G. A. Briggs

Planning of the variable features investigation was based on the expectation that any changes that might be observed during the mission would be subtle, involving a relative change in surface albedo rather than clear-cut changes in the outline of albedo features. On the basis of telescopic observations, the part of Mars expected to be most subject to change in a given season was the southern

tropical belt; therefore, considerable effort was expended to design a low-inclination orbit that would allow the spacecraft to acquire extensive wide-angle camera coverage of the southern hemisphere every few days with similar lighting and viewing geometry. A significant programming effort was undertaken at the Artificial Intelligence Laboratory (AIL) of Stanford University and at the IPL to permit the detection of albedo changes by means of "picture differencing."

The loss of *Mariner 8* was a severe blow to the plans, necessitating curtailment of the picture budget for variable feature studies (a penalty shared by all disciplines). Repeated coverage of a given region was acquired only every 18 days rather than the 5 days planned, and observations of the equatorial region were made more obliquely from the higher-inclination orbit of *Mariner 9*. Initially the dust storm also hampered the experiment in that it prevented the acquisition of approach pictures that would have allowed a detailed comparison of the global-scale albedo features with those observed 2 years earlier by *Mariners 6* and *7*. The first 6 weeks of orbital television data were of little use for the variable features investigation except that they provided additional data on the nature of Martian dust storms. Ultimately, however, the waning stages of the dust storm proved to be the ideal time to perform an experiment designed to study albedo changes.

When the surface became visible, it was saturated with albedo markings resulting from the redistribution of surface material by strong winds prevailing during the storm (Ref. VII-21). The most characteristic markings were "tails" emanating from the lee side of craters and dark "spotches" at the bottom of craters. The distribution of dark streaks corresponds rather well to the classical configuration of dark albedo features as seen by Earth-based observations of Mars. Mapping, over the whole planet, of the light and dark streaks on the surface has proved to be an excellent method for determining the wind directions at the time of the streak formation. The results of this mapping are in close general agreement with the wind directions deduced from an analysis of the temperature and pressure profiles derived from the IRIS data (Ref. VII-22). That these albedo features are caused by the action of wind moving surface material seems established beyond doubt, and thus allows a straightforward explanation of telescopic observations of seasonal and secular changes. Such changes also were observed in many places on Mars, and the analysis of these changes has proved to be greatly facilitated by picture differencing performed at the AIL and at the IPL.

In general, the observed changes have involved increased darkening (Ref. VII-22). For example, Syrtis Major, the most prominent of all classical dark features, was initially observed to be a region full of bright and dark streaks at the start of the observations. Continued observations of this area (one of many areas selected for intensive monitoring during the mission) showed a gradual, but persistent, darkening trend; this trend is interpreted to be the result of the steady removal of a thin layer of dust deposited during the storm. The darkening manifested itself by the appearance, development, and merging of dark crater tails. Elsewhere, and most notably in a cratered region near Promethei Sinus (close to the south pole), the development of dark features was observed. In this region a dark, leaf-shaped region about 10 km across developed at some time between revolutions 99 and 126, a gap of 13 days. This feature remained unchanged thereafter, but development of a scalloped dark feature nearby was later detected. Although changes in dark features were observed at various places on Mars, including the bottoms of channels, no variations were found in the production or dissipation of bright streaks.

Although the general nature of the albedo changes is clear, the details of the processes involved remain uncertain. There is always ambiguity in deciding whether albedo changes are due to the motion of bright material over a dark foundation (which seems a priori more likely, as fines are brighter than larger particles of the same material) or due to movement of dark material. Both theoretical and experimental (wind tunnel) tests are in progress to clarify this matter.

The wind velocities inferred in these studies are at least 50 to 70 m/sec above the surface boundary layer (Refs. VII-21 and VII-22). Sand and dust entrained at such high velocities will be effective agents of eolian abrasion and erosion on Mars (Refs. VII-23).

#### F. Satellite Astronomy, J. B. Pollack and T. E. Thorpe

Observations of the Martian satellites were an important *Mariner 9* science objective relevant not only to knowledge of their physical properties, but to a description of the cratering environment of Mars and possibly into the interior structure of the planet. Before the mission little was known about these objects, with the exception of their orbital elements, and various explanations as to their ori-

gin, rotation, and physical appearance were possible (see Ref. VII-1). *Mariner 7* provided only a few images of Phobos near the resolution limit of the television photography. *Mariner 9*, with repeated close-encounter geometries (5000 to 10,000 km), offered a unique opportunity to greatly enhance man's knowledge of these objects.

Pre-orbital science pictures, taken while the spacecraft was several hundred thousand kilometers from Mars, were used to refine orbit parameters and to permit accurate camera pointing at closer encounters. Some differences from terrestrially determined elements included changes in the mean longitudes (Phobos:  $+2.8^\circ$ , Deimos:  $-0.3^\circ$ ) and the inclination of the orbit of Phobos ( $-0.3^\circ$ ) in relation to Earth's orbital plane (Ref. VII-24). By comparing the mean motion of Phobos observed by *Mariner 9* over 1 year with that found from measurements made during the last century, secular changes in the orbital period are being evaluated. A positive determination of secular acceleration will lead to an estimate of the dissipation function,  $Q$ , for Mars relevant to the interior structure of the planet.

Television images of Phobos and Deimos with up to 150 resolution elements diameter (see Figs. VII-6 and VII-7) show that they are tiny, irregularly shaped objects, 23 km and 13 km in diameter, respectively, well below the limiting size at which hydrostatic equilibrium forms natural spherical shapes. The largest axis of each satellite is about 40% larger than the smallest axis and always points toward Mars as the result of tidal forces. *Mariner 9* observations over a period of 100 days confirmed this synchronous rotation to an accuracy of 1 part in  $10^4$  for Phobos and 1 part in  $3 \times 10^3$  for Deimos.

Both Phobos and Deimos are dark objects, reflecting only 5% of the sunlight falling upon them. Studies of the variation of brightness with luminance geometry suggests that they may be covered with a top layer of fine particles. Such a complex surface texture (indicated by strong back-scattering) also is consistent with polarization measurements of up to 20% polarization at a phase angle of  $75^\circ$ . A regolith deep enough to cover the surfaces of both satellites probably is the result of meteoroid impact. Initially the ejected material produced at impact escapes the satellites' gravitational pull to orbit Mars. The material subsequently is recaptured over a much longer period of time.

Cratering on Phobos and Deimos has produced much larger populations of craters of a size near 1 km than those evident on the surface of Mars and suggests extensive



Fig. VII-6. Computer-processed picture of Phobos taken during revolution 34. Phase angle =  $59^\circ$ , range = 5720 km, predicted sub-spacecraft point =  $70^\circ\text{S}$ ,  $161^\circ\text{W}$ . The illuminated area is about 23 km high and 15 km wide. (IPL Roll 820, 002025)



Fig. VII-7. Computer-processed picture of Deimos taken during revolution 149. Phase angle =  $65^\circ$ , range = 5465 km, predicted sub-spacecraft point =  $28^\circ\text{N}$ ,  $355^\circ\text{W}$ . The illuminated area is about 12 km high and 7 km wide. (Stanford AIL Picture Product STN 0156, 020501)

erosion of Martian craters of similar diameters. Comparison with our moon, allowing for differences in bombardment rates, indicates that the satellites are at least 2 billion years old and probably date back to the early history of the solar system. Both the existence of an apparent linear fracture and a study of the satellite's past collision history suggest that Phobos has survived impact energies capable of disintegrating any object whose interior does not have rock-like cohesive strength. The weak gravity of the satellites, incapable of forming such material, leads to the postulation of the one-time existence of a much larger body that was subsequently fragmented. In this context, a search for additional satellites of Mars was made using pre-orbital approach pictures. The negative result provides an upper limit to possible bodies ranging from 1.6 to 0.25 km in diameter over limited coverage (a small fraction of the possible space-time domain of an unknown satellite).

The Satellite Astronomy Discipline Group now is concerned with the compilation of picture data as well as the refinement of measurements. A catalog containing all *Mariner 9* satellite pictures is being prepared together with latitude/longitude overlays. A three-dimensional globe of Phobos and two-dimensional satellite maps are in production with the assistance of the U.S. Geological Survey. Data from the ultraviolet and infrared spectrometers are also being utilized as part of a program to obtain a composite reflectivity spectrum of Phobos for comparison with laboratory curves relating composition information. It is hoped that future spacecraft photography of Phobos and Deimos, for example from the Viking orbiters, will provide a continuation of this work.

## G. Polar Phenomena, J. A. Cutts

Objectives of the Polar Phenomena Discipline Group were to gain an understanding of the geology of the polar regions and the physical behavior of the annual and perennial frost deposits. Interest in the polar regions as a subject for special attention was first stimulated when Leighton and Murray (Ref. VII-25) showed, on the basis of surface pressure data returned by *Mariner 4*, that a theoretical model of carbon dioxide condensation could account for the gross behavior of the annual frost deposits of Mars. The interest was revived in 1969 when the polar flyby made by *Mariner 7* revealed bright "quasilinear" markings roughly concentric with the pole and strange etch pits within the region of annual frost cover (Ref. VII-26).

On arrival of *Mariner 9* at Mars, the south polar region was one of the few parts of the planet in which surface detail could be discerned. Compared to its springtime appearance when viewed by *Mariner 7*, the actual polar cap was extremely small. It measured only 300 by 400 km, and was offset from the pole by about 6° (Ref. VII-27). The polar cap area was divided by curving dark bands of frost-free ground which, on closer examination, proved to be the same features that *Mariner 7* had viewed as bright "quasilinear" markings approximately concentric with the pole.

During the next few weeks of observations, the only change in the perimeter of the polar frost deposits was the disappearance of a large outlier of frost near 82°S, 30°W. High-resolution pictures showed minor changes in the frost cover in the interior of the residual cap, but no changes were detected after 60 days from insertion into orbit. The formation of a residual nucleus of frost so soon after southern summer solstice has been interpreted to mean that it consists of water ice, which is much less volatile than carbon dioxide (Ref. VII-27). However, contrary views have been expressed, and no satisfactory theoretical model accounting for all aspects of the behavior of the seasonal frost has yet been formulated. Significant observations of the north polar frost cap were also made later in the *Mariner 9* mission; they are discussed in Ref. VII-20 and in Section IX of this Report.

Some of the most exciting results of the polar phenomena investigations emerged from intensive high-resolution photography of the "quasilinear" markings and etch pits viewed by *Mariner 7*. These features now appear to be landforms peculiar to two types of blanketing deposits which overlie the primitive cratered terrains in the south polar region. The "etch pits" are developed in what has been termed the "pitted plains unit," a massive deposit with little evidence of layering. The "quasilinear" markings, however, are developed on remarkable layered deposits, or "laminated terrain," which are seen to stratigraphically overlie both the pitted plains unit and the primitive cratered terrain in contacting areas.

Various ideas on the nature and origin of the layered deposits have been discussed (Refs. VII-18, and VII-24 through VII-31); agreement has been reached that the layered deposits are unique to the polar region and that their formation is connected with the condensation of carbon dioxide. While there are differing opinions on the mechanism of the formation of layering (Refs. VII-28 and VII-30), it is the consensus that the layering is controlled

by perturbations of the Martian orbital elements (Refs. VII-31 and VII-32).

It is not clear whether the rock materials that comprise the pitted plains unit were deposited in a way that was strongly influenced by the polar environment. However, the processes that subsequently indented this massive, smooth, homogeneous blanket and in some cases exhumed underlying surfaces appear to have been strongly influenced by their polar location. Wind erosion, perhaps abetted by ablation of frozen volatiles, has been suggested as one of these processes (Ref. VII-19). The pattern of lineations on the pitted plains (Ref. VII-32) and mantling of craters in mid-latitudes (Ref. VII-33) suggest that winds moving off the polar cap have transported materials from the pitted plains (and also the layered deposits) and have deposited them in a peripheral belt.

Large-scale topographic features of the layered deposits, of which the quasilinear circumpolar markings are one example, have generated considerable curiosity. The large en echelon escarpments that underlie the residual polar caps in both hemispheres have been interpreted as a series of "stacked, slightly concave plates" (Ref. VII-27). Their offset appearance has suggested that the plate edges are aligned along fossil latitudinal circles corresponding to former pole positions during an era of polar wandering (Ref. VII-34). An alternative idea is that the offset plates and the offset polar caps can be explained by atmospheric rotational motions (Ref. VII-19).

Descriptions of the layered deposits, fits of the behavior of the polar caps to theoretical models, and investigations of the effects of orbital perturbations on the polar caps will continue in the post mission period.

## References

- VII-1. Steinbacher, R. H., and Gunter, S. Z., "The Mariner Mars 1971 Experiments: Introduction," *Icarus*, Vol. 12, pp. 3-9, 1970.
- VII-2. Leovy, C. B., Briggs, G. A., Young, A. T., Smith, B. A., Pollack, J. B., Shipley, E. N., and Wildey, R. L., "The Martian Atmosphere: Mariner 9 Television Experiment Progress Report," *Icarus*, Vol. 17, pp. 373-393, 1972.
- VII-3. Masursky, H., Batson, R. M., McCauley, J., Soderblom, L., Wildey, R., Carr, M. H., Milton, D. J., Wilhelms, D. E., Smith, B. A., Kirby, T. B., Robinson, J. C., Leovy, C. B., Briggs, G. A., Young, A. T., Duxbury, T. C., Acton, C. H., Jr., Murray, B. C., Cutts, J. A., Sharp, R. P., Smith, S., Sagan, C., Veverka, J., Noland, M., Lederberg, J., Levinthal, E., Pollack, J. B., Moore, J. T., Jr., Hartmann, W. K., Shipley, E. N., de Vaucouleurs, G., and Davies, M. E., "Mariner 9 Television Reconnaissance of Mars and Its Satellites: Preliminary Results," *Science*, Vol. 175, p. 294, 1972.
- VII-4. Leovy, C., and Mintz, Y., "Numerical Simulation of the Atmospheric Circulation and Climate of Mars," *J. Atmos. Sci.*, Vol. 26, pp. 1167-1190, 1969.
- VII-5. Smith, S. A., and Smith, B. A., "Diurnal and Seasonal Behavior of Discrete White Clouds on Mars," *Icarus*, Vol. 16, pp. 509-521, 1972.
- VII-6. Davies, M. E., *Mariner 9 Control Net of Mars: June 1973*, R-1309-JPL, The Rand Corporation, June 1973.

## References (contd)

- VII-7. Sinclair, A. T., "The Motions of the Satellites of Mars," *Mon. Not. Roy. Astron. Soc.*, Vol. 155, p. 259, 1972.
- VII-8. de Vaucouleurs, G., Davies, M. E., and Sturms, F. M., Jr., "Mariner 9 Areographic Coordinate System," *J. Geophys. Res.*, Vol. 78, 1973.
- VII-9. Mariner 9 Television-Experiment Team, "The New Mariner 9 Map of Mars," *Sky and Telescope*, Vol. 44, pp. 77-82, 1972.
- VII-10. de Vaucouleurs, G., "Telescopic Observations of Mars in 1971," *Sky and Telescope*, Vol. 42, pp. 134-135, 263-264, 1971; and 20-21, 1972.
- VII-11. de Vaucouleurs, G., Roth, J., and Mulholland, C., "Preliminary Albedo Map of the South Polar Region," *J. Geophys. Res.*, Vol. 78, 1973.
- VII-12. de Vaucouleurs, G., "Mariner 9 Albedo Charts of Mars," *Sky and Telescope*, September 1973.
- VII-13. Thorpe, T. E., "Verification of Performance of the Mariner 9 Television Cameras," *Applied Optics*, Vol. 12, 1973.
- VII-14. Sagan, C., Toon, O. B., and Gierasch, P. J., *Climatic Changes on Mars*, Cornell University CRSR 537, 1973.
- VII-15. Sharp, R. P., "Mars: Fretted and Chaotic Terrains," *J. Geophys. Res.*, Vol. 78, 1973.
- VII-16. McCauley, J. F., "Mariner 9 Evidence for Wind Erosion in the Equatorial and Mid-Latitude Regions of Mars," *J. Geophys. Res.*, Vol. 78, 1973.
- VII-17. Cutts, J. A., and Smith, R. S. U., "Eolian Deposits and Dunes on Mars," *J. Geophys. Res.*, Vol. 78, 1973.
- VII-18. Cutts, J. A., "Nature and Origin of Layered Deposits of the Martian Polar Regions," *J. Geophys. Res.*, Vol. 78, 1973.
- VII-19. Cutts, J. A., "Wind Erosion in the Martian Polar Regions," *J. Geophys. Res.*, Vol. 78, 1973.
- VII-20. Soderblom, L. A., Malin, M. C., Murray, B. C., and Cutts, J. A., "Mariner 9 Observations of the Surface of Mars in the North Polar Region," *J. Geophys. Res.*, Vol. 78, 1973.
- VII-21. Sagan, C., Veverka, J., Fox, P., Dubisch, R., Lederberg, J., Levinthal, E., Quam, L., Tucker, R., Pollack, J. B., and Smith, B. A., "Variable Features on Mars: Preliminary Mariner 9 Television Results," *Icarus*, Vol. 17, pp. 346-372, 1972.
- VII-22. Sagan, C., Veverka, J., Dubisch, R., French, R., Gierasch, P., Quam, L., Lederberg, J., Levinthal, E., Tucker, R., Eross, B., and Pollack, J. B., "Variable Features on Mars II: Mariner 9 Global Results," *J. Geophys. Res.*, Vol. 78, 1973.
- VII-23. Sagan, C., "Sandstorms and Eolian Erosion on Mars," *J. Geophys. Res.*, Vol. 78, 1973.

## References (contd)

- VII-24. Pollack, J. B., Veverka, J., Noland, M., Sagan, C., Duxbury, T. C., Acton, C. H., Jr., Born, G. H., Hartmann, W. K., and Smith, B. A., "Mariner 9 Television Observations of Phobos and Deimos II," *J. Geophys. Res.*, Vol. 78, 1973.
- VII-25. Leighton, R. B., and Murray, B. C., "Behavior of Carbon Dioxide and Other Volatiles on Mars," *Science*, Vol. 193, p. 136, 1966.
- VII-26. Sharp, R. P., Murray, B. C., Leighton, R. B., Soderblom, L. A., and Cutts, J. A., "The Surface of Mars: 4. South Polar Cap," *J. Geophys. Res.*, Vol. 76, p. 357, 1971.
- VII-27. Murray, B. C., Soderblom, L. A., Cutts, J. A., Sharp, R. P., Milton, D. J., and Leighton, R. B., "A Geological Framework for the South Polar Region of Mars," *Icarus*, Vol. 17, p. 328, 1972.
- VII-28. Sagan, C., "Liquid Carbon Dioxide and the Martian Polar Laminae," *J. Geophys. Res.*, Vol. 78, 1973.
- VII-29. Murray, B. C., and Malin, M. C., "Volatiles on Mars: Theory vs Observation" (in preparation).
- VII-30. Briggs, G. A., "Periodic Dust Storms and the Martian Polar Laminae" (submitted to *Science*).
- VII-31. Murray, B. C., Yeung, S. C., and Ward, W. R., "Periodic Insolation Variations on Mars," *Science* (in press).
- VII-32. Sharp, R. P., "Mars: South Polar Pits and Etched Terrain," *J. Geophys. Res.*, Vol. 78, 1973.
- VII-33. Soderblom, L. A., Kreidler, T. J., and Masursky, H., "The Latitudinal Distribution of a Debris Mantle on the Martian Surface," *J. Geophys. Res.*, Vol. 78, 1973.
- VII-34. Murray, B. C., and Malin, M. C., "Polar Wandering on Mars," *Science* (in press).

## VIII. Surface Properties Working Group

A. B. Whitehead and D. L. Cain

Jet Propulsion Laboratory/California Institute of Technology, Pasadena, California 91103

During the *Mariner 9* mission, Science Evaluation Team Working Groups were established to:

- (1) Identify specific problem areas requiring results from more than one experiment, and solve them through correlation of results.
- (2) Expedite reduction of data.
- (3) Coordinate analysis and reporting of results.

One meeting each month was held to perform these functions.

Members of the Working Groups were selected to provide representation from each relevant Experiment Team. The Working Group Chairman was selected by the members.

Three Working Groups were active at the end of the mission:

- (1) Surface Properties.
- (2) Volatiles.
- (3) Atmospheric Phenomena.

This section of this Report concerns the Mars Surface Properties Working Group. Sections IX and X present the activities of the Volatiles and Atmospheric Phenomena Working Groups, respectively.

The initial objectives of the Surface Properties Working Group were to:

- (1) Determine a simple reference surface that would adequately represent the shape of the planet for cartographic purposes.
- (2) Monitor the topographic results being generated by each of the Experiment Teams and to assess the relative calibration and accuracies of these techniques, thereby leading to a composite topographic map of the planet.
- (3) Facilitate the exchange of data in closely connected disciplines.

*Mariner 9* experiments that obtained topographic data were: television (geodesy, concerned with planet-wide shape and orientation parameters; and cartography, relating to determination of local features), infrared spectroscopy, infrared radiometry, ultraviolet spectrometer, celestial mechanics, and S-band occultation. Each of these experiments had a representative member in the Working Group who kept the Group informed on progress regarding, for example, the development of the planet-wide geodetic network (Ref. VIII-1), establishment of secondary control network and production of the cartographic products (Ref. VIII-2), and gravity analysis results and progress in generating a geoidal surface (Refs. VIII-3 and VIII-4).

In addition to the *Mariner 9* experiments, Earth-based radar data furnished valuable topographic information.

## A. Shape of the Planet

It was recognized that the planet could not be well represented by a simple oblate spheroid, and use of the more realistic representation of a triaxial ellipsoid was proposed. The triaxial ellipsoid was fitted to the occultation radii and produced data (Ref. VIII-5), but even this figure did not adequately fit the shape of Mars for some purposes, and higher-order fits were generated and published (Ref. VIII-6). An offset ellipsoid gave a better fit when both the occultation data and the derived ephemeris for the planet were considered. The result of this effort was to provide many reference figures, with the higher-order figures offering significant improvements over the more simple ones.

## B. Topography

Topographic information was derived using seven techniques (see Table VIII-1):

- (1) *Earth-based radar*. The radar data, once corrected for planet ephemeris, are accurate. However, they cover restricted latitude bands.
- (2) *Occultation*. The occultation data are most unique because each occultation provides, independently and simultaneously, a planet radius, a surface pressure, and the atmospheric scale height. Thus, occultation data provide the only direct comparison between the true shape of the planet and the isobaric surface.
- (3) *Geodesy*. The less-than-optimum pictures caused by the dust storm resulted in a struggle to produce a primary control network. The present network contains more than 1600 control points, and has an accuracy of about 5 km.
- (4) *Photogrammetry*. Where stereoscopic image pairs are available, photogrammetry is the best way to obtain the detailed topographic shape of local forms such as volcanoes, valleys, craters, etc.
- (5) *Infrared interferometer spectrometer (IRIS)*. IRIS topography results are derived from interpretation of IRIS spectra. Surface pressures and temperature profiles are derived simultaneously and are highly dependent on carbon dioxide transmittances that

are assumed from theoretical work and laboratory measurements. New carbon dioxide transmittances have been generated, including many weak lines. Presently obtained surface pressures and atmospheric temperature profiles are reasonably accurate, but additional refinements are necessary before final data reduction can proceed.

- (6) *Ultraviolet spectrometer (UVS)*. The basic UVS technique assumes that most of the ultraviolet radiation reaching the spacecraft in a narrow wavelength band at 3050 Å is produced by Rayleigh scattering from the atmosphere, with a small contribution from the surface. The relationship between the detected flux and the surface pressure includes known geometry and four unknown constants, two relating to atmospheric properties and two to surface properties.
- (7) *Infrared radiometer (IRR)*. By assuming an average thermal model of the surface, the IRR measurements can be interpreted as measurements of the inclination of the surface element to the Sun. Under suitable measurement conditions and with the added strength of end-point constraints, these slopes can be integrated to yield elevation changes. The method had limited application.

Intercomparison of results from these techniques proved complicated because of the few opportunities to measure a specific location using several techniques. However, several occultation points fell close enough to radar scans to be used to correct the ephemeris error inherent in the radar measurements.

No correlation between occultation and geodesy points was possible because each geodetic control point was a clearly visible selected feature on the planet's surface, while the occultation point, or the occulting feature, was hard to identify; thus, the "radius" to the point was easiest to interpret when occurring in a featureless, level area.

Extensive large-scale topography was inferred from IRIS and UVS data; however, both techniques measured the atmospheric pressure at the surface with respect to an ambient (time varying) isobaric surface, whose shape was the most complex aspect of topography undertaken by the Working Group. Thus, the problem of using IRIS and UVS data to provide large-scale topography hinged on the ability to relate the ambient isobaric surface to the radius of the planet.

**Table VIII-1. Basic techniques used to measure Martian topography (1971 to 1972)**

Techniques	Quantity measured	Type of measurement	Spatial resolution <sup>a</sup>	Areal coverage
Earth-based radar	Radius	Relative	Good <sup>b</sup>	Dense along narrow latitude strips
Occultation	Radius, surface pressure, scale height	Absolute	Excellent	Sparse; more or less random over planet
Geodesy	Global shape	Absolute	Good	Global
Photogrammetry	Local topography	Relative	Excellent	Very limited
Infrared interferometer spectrometer	Surface pressure, scale height	Relative to isobar	Moderate	Dense along northeast tracks; latitudes $-60^{\circ}$ to $+20^{\circ}$
Ultraviolet spectrometer	Surface pressure	Relative to isobar	Good	Dense along northeast tracks; south pole to $+40^{\circ}$ latitude
Infrared radiometer	Slope	Relative	Excellent	Limited applications

<sup>a</sup>Resolution: more than 25 km = excellent; 25 to 125 km = good; 125 to 200 km = moderate.  
<sup>b</sup>When corrected for ephemeris uncertainties, measurements are excellent.

The unknown constants of item (6) were determined by comparison with occultation and radar points. For about 75% of the planet, the UVS technique was calibrated to be consistent with the known points. For the rest of the planet, the calibration differed primarily because the ultraviolet flux included a significant contribution from Mie scattering from atmospheric dust when the measurements were taken.

### 1. Nix Olympica

In order to focus all of the topographic techniques on one area, the Working Group selected the volcanic feature, Nix Olympica, for more intensive study. Early values for the height of this volcano differed by a factor of 6.

Reports on intensive studies of Nix Olympica topography were made to the Working Group, also using several techniques:

- (1) Local fits to a set of geodetic points.
- (2) Several different convergent stereoscopic techniques (see Ref. VIII-7).
- (3) Limb photography.
- (4) UVS scans.
- (5) Slope photometry.

With refinement of the various techniques, the reported values are more in agreement, and it now appears that the overall height is somewhere between 20 and 25 km, depending on which part of the surrounding plain is used as the base.

### C. Isobaric Surface

The problem of generating an isobaric surface lies in the atmospheric dynamics. The dynamics cause diurnal and seasonal changes which can amount to 15% in surface pressure. In addition, the annual variation in the total amount of carbon dioxide in the atmosphere has not yet been determined. An attempt to model the isobaric surface is being made using data on atmospheric tides and latitudinal temperature effects; these corrections are being applied to the observed pressure at each occultation point. An attempt is being made to generate, from these data, a corrected isobaric surface on which all of the data points fit within statistical accuracy; however, refinements in making the atmospheric corrections are still necessary. It is also possible that the occultation data are not adequately distributed in position over the planet, or that the isobaric surface is, in reality, highly irregular.

### D. Gravity Field

Efforts to achieve a gravitation equipotential, or geoidal, surface from radio tracking data were impeded by: (1) partial degeneracy due to data from a single orbit,

and (2) lack of coverage in the northern hemisphere, because the periapsis remained at  $-23^\circ$  latitude. The Working Group has been engaged in an effort to combine the radio data with the occultation pressure measurements in a simultaneous determination of a geoidal surface which reflects the strength of both data types. A systematic difference has been found, however, between the radio and occultation data in that the radio-determined geoid and the occultation-determined pressure isobar differ by about 1 km in the north. This difference is attributed to the latitudinal variations in pressure caused by atmospheric circulation. Current circulation theories produce pressure corrections that do not alleviate the radio and occultation data inconsistencies. It is concluded that occultation data from a single latitude region may be used in conjunction with the radio data to determine the geoidal shape, unless more accurate atmospheric circulation models become available.

### E. Crustal Density Model

The Working Group hoped to use the final topographic data and the final geoidal shape to generate a surface density model. A limited attempt at such a model was conducted (see Ref. VIII-8) using published topographic and gravity data to provide a crustal density around a narrow latitude band at about  $-20^\circ$ .

### F. Conclusions

The Surface Properties Working Group proved useful to all participants and served an important function in the overall analysis of the data. Meaningful progress was made in each of the areas undertaken. It was found that

there is no simple reference figure for the planetary surface, although an offset, triaxial ellipsoid probably is adequate for most purposes. As yet, topographic data have not been completely assimilated into a single topographic map because of the extremely challenging nature of the task.

At the end of the Mariner Mars 1971 Project, there are many areas that remain as a challenge for future work. Continued analysis of *Mariner 9* data can provide improved topographic maps, improved detailed topography of specific features, and a better understanding of the isobaric surface and of the geoid. The data probably exist to generate a reasonable crustal density model. However, far better data are desirable such as better geodesy coverage of the planet, pressure mapping when there is less dust in the atmosphere, pressure mapping at a different season when the effects of the latitudinal variation can be determined, and more topographic coverage. These measurements will have to await future Mars missions.

### G. Participants in the Working Group

The following members participated in the Surface Properties Working Group:

D. W. G. Arthur	J. F. Jordan	J. Pearl
R. M. Batson	A. J. Kliore	I. I. Shapiro
D. L. Cain	J. Lorell	W. L. Sjogren
M. E. Davies	H. Masursky <sup>1</sup>	L. A. Soderblom
C. W. Hord	E. D. Miner	A. B. Whitehead

---

<sup>1</sup>Working Group Chairman.

## References

- VIII-1. Davies, M. E., and Arthur, D. W. G., "Martian Surface Coordinates," *J. Geophys. Res.*, Vol. 78, 1973.
- VIII-2. Batson, R. M., "Cartographic Products from the Mariner 9 Mission," *J. Geophys. Res.*, Vol. 78, 1973.
- VIII-3. Ferrari, A. J., and Christensen, E. J., "Mars Gravity Derived from Long-Period Motion of Mariner 9," in *Mariner Mars 1971 Project Final Report, Vol. IV: Science Results*, Technical Report 32-1550, Jet Propulsion Laboratory, Pasadena, Calif., 1973.
- VIII-4. Sjogren, W. L., Lorell, J., Reinbold, S. J., and Wimberly, R. N., "Mars Gravity Field Via the Short Data Arcs," in *Mariner Mars 1971 Final Project Report. Vol. IV: Science Results*, Technical Report 32-1550, Jet Propulsion Laboratory, Pasadena, Calif., 1973.
- VIII-5. Cain, D. L., *The Shape of Mars*, paper presented at AAS Meeting, Hawaii, March 20-24, 1972.
- VIII-6. Cain, D. L., Kliore, A. J., Seidel, B. L., Sykes, M. J., and Woiceshyn, P., "Approximations to the Mean Surface of Mars and Mars Atmosphere Using Mariner 9 Occultations," *J. Geophys. Res.*, Vol. 78, 1973.
- VIII-7. Blasius, K. R., "A Study of Martian Topography by Analytic Photogrammetry," *J. Geophys. Res.*, Vol. 78, 1973.
- VIII-8. Phillips, R. J., Saunders, R. S., and Conel, J. F., "Mars: Crustal Structure Inferred from Bouguer Gravity Anomalies" (submitted to *J. Geophys. Res.*).

## IX. Volatiles Working Group

James A. Cutts

Jet Propulsion Laboratory/California Institute of Technology, Pasadena, California 91103

The primary objectives of the Volatiles Working Group, as defined at its inception, were to:

- (1) Provide a forum for interdisciplinary discussion of the physical behavior of water and carbon dioxide on Mars and the physics and chemistry of minor constituents associated with them.
- (2) Encourage the formation of small subgroups to identify and attempt to solve topical problems related to volatiles.
- (3) Promote a standardization of units and nomenclature used in data reduction.

In the seven meetings of the Volatiles Working Group, most of these objectives were met; however, much remains in terms of completing the existing analysis, seeking correlations among different sets of data, and conducting laboratory experiments to facilitate data interpretation.

The Volatiles Working Group also considered problems that lie in the more general area of planetary processes, all of which seem to involve volatiles in some way. Through interaction in the Working Groups members became aware of the rate at which their colleagues were able to reduce their data, and it became possible to set priorities in data reduction. Specific problems were also identified by means of this communication.

Participation of non-*Mariner 9* scientists made available to members of the Working Group new and unpublished results and interpretations derived from Earth-based astronomical observations. Theoretical, experimental, and Earth-analog studies were presented pertinent to processes occurring on the Martian surface. Some recent and unfamiliar planetological ideas were also discussed and provided an expanded framework in which *Mariner 9* observations could be evaluated. Finally, the participation of scientists from the Viking Program enabled evolving ideas regarding Mars to be conveyed and, just as important, served to emphasize our limited knowledge of the surface environment of the planet.

On many topics the Working Group did not reach agreement, and many conflicting views were presented and discussed. These differences in many cases represent alternative hypotheses that additional analyses of *Mariner 9* data or future spacecraft exploration will help to clarify.

A brief review of the progress made on some topical problems is presented in the subsequent paragraphs. Areas of agreement, conflicting interpretations, and anomalous results are discussed, and reference is made to publications that either exist or are in process of preparation.

## A. Physics of Polar Frosts

The Martian polar caps, discovered by seventeenth century astronomers, are still the most apparent indication that the planet's atmosphere has a condensable component. *Mariner 9* made exploratory observations of both polar caps at high resolution using television cameras and special instruments. It monitored the characteristics of the south polar cap between southern summer solstice and fall equinox and the north polar cap from its formation beneath a cloud or "hood" until just beyond northern summer solstice. Many unexpected observations were made and have stimulated many new hypotheses concerning the role of carbon dioxide and water in the frost caps.

Observations in the south polar region were particularly pertinent to the nature of perennial frost:

- (1) Existence was confirmed of a small frost deposit, about 300 by 400 km, surviving all year (Ref. IX-1). Previous Earth-based observations had been equivocal.
- (2) This remnant cap was irregular in shape, divided by curving dark bands of frost-free terrain and offset from the south pole by about 6° (Ref. IX-1).
- (3) Remnant cap remained virtually unchanged in outline throughout the southern summer (Ref. IX-1).
- (4) Average temperature of visible frost deposits (perhaps also including bare ground beyond camera resolution) was less than 160° K (H. Kieffer, personal communication, 1971).
- (5) An anomalous ultraviolet absorption (2000 to 2400 Å) was recorded over the southern cap in late summer; no comparable feature was observed over the northern cap during northern springtime. Photometric properties of the residual south polar cap observed by *Mariner 9* in the ultraviolet part of the spectrum differed from the springtime polar cap observed by *Mariner 7* (K. Pang, personal communication, 1973).
- (6) Preliminary ultraviolet determinations of elevation indicate considerable relief in the south polar region and specifically a large basin offset from the pole (Ref. IX-2).

Observations in the north polar region spanned different seasons and provided important information on annual as well as perennial frost:

- (1) Variable clouds and haze that covered the north polar region during most of the standard mission almost completely disappeared by the resumption of observations on revolution 416 ( $L_s = 35^\circ$ ; Ref. IX-3). Cloud phenomena were observed during the subsequent observations of the springtime cap (Ref. IX-4).
- (2) Large albedo differences were detected within the area of frost cover (Ref. IX-3).
- (3) Frost persisted on the rims of some large craters outside the margin of the receding frost cap (Ref. IX-3). The same frost-rimmed craters had been observed previously through the winter cloud cover.
- (4) North polar cap had a polygonal shape (Ref. IX-3).
- (5) A dark, circumpolar albedo band was observed around the retreating polar cap (Ref. IX-3).
- (6) Deep winter cap had a uniform radiometric temperature of about 150° K, but the margins of the receding cap during the spring season appeared to be somewhat warmer than the interior (H. Kieffer, personal communication, 1973).
- (7) North polar cap near its minimum size consisted of two roughly circular components: one with its center near the pole, and one offset from it. Both were broken up by the pseudo-circular, dark bands of frost-free terrain also observed in the southern polar region (Ref. IX-3).
- (8) Frost-free slopes were truncated in several locations by frost deposits of possibly greater thickness than those viewed in the remainder of the area of the residual frost (Ref. IX-5).

Many contrasting interpretations of these observations have been given in meetings of the Working Groups and in other conferences and seminars. It is generally agreed that annual deposits of frost that vary with the seasons are composed of carbon dioxide. However, the composition of the permanent caps is still a subject of debate. The abrupt arrest of the retreat of the south polar cap halfway between solstice and equinox has been interpreted to mean that this permanent cap is made of water ice (Ref. IX-1); thermal balance arguments also were made in support of this point of view. However, more recent but unpublished work reported in the Volatiles Working Group meetings suggests that this conclusion may have been premature. R. Hanel noted that seasonal variations in the infrared emission from the south polar cap are consistent with

carbon dioxide composition. J. Cutts suggested that the observed arrest in the retreat of the cap would be expected to occur with a permanent carbon dioxide cap as well as with a permanent water ice cap. Unfortunately, the discontinuous nature of the cap makes it difficult to discriminate between carbon dioxide and water on thermal grounds, and no diagnostic absorption bands can be recognized in the infrared or in the ultraviolet. However, the ultraviolet photometric function of the residual cap differs from that of the annual frost and may indicate compositional differences.

Explanations of the irregular shapes of the residual polar caps and their lack of rotational symmetry with respect to the polar axis have also been discussed. An early hypothesis that the complex topography beneath the residual caps provides a location at which the annual insolation is less than that at the pole itself now appears to have been discarded. Instead, polar wandering has been suggested as an explanation of the configuration of the perennial frost (Ref. IX-6). An alternative view is that atmospheric heat transport may determine the site of the perennial polar cap because insolation is an insensitive function of latitude near the pole.

Unexpected phenomena observed during the retreat of the north polar cap also stimulated ideas on physical processes governing the annual frost. The polygonal form of the receding cap has been attributed to longitudinal variations in insolation, surface pressure, surface texture, or atmospheric heat transport (Ref. IX-3). All of these effects must be attributed ultimately to regional topographic differences (Ref. IX-3). The failure of the northern polar frost deposits to develop to latitudes below  $65^\circ$  and the existence of residual frost deposits on crater rims have been interpreted as consequences of the great dust storm (Ref. IX-7).

Albedo differences within the frost cover and radiometric temperature variations add complexities that simple models of the behavior of annual frost on Mars (Refs. IX-8 and IX-9) do not consider. G. Briggs, H. Kieffer, C. Leovy, O. Toon, and W. Ward are developing improved models to examine different aspects of the characteristics of the polar caps. Some of these experimenters are pursuing an improved explanation of the annual behavior of the caps in the present era derived from Earth-based observations as well as from *Mariner 9*; others are attempting to predict the stability and extent of the polar caps under different climatic conditions (see Sections IX-E and IX-F). These theoretical studies are

being complemented by further reduction of polar frost data from *Mariner 7* as well as from *Mariner 9*. C. Leovy, M. Malin, and J. Cutts are continuing to work on *Mariner 7* and *9* television photometric data; H. Kieffer is re-evaluating *Mariner 7* near-infrared data; A. Lane and K. Pang are continuing studies of data from the *Mariner 7* and *9* ultraviolet spectrometers (UVS); and R. Hanel is continuing his analysis of data from the *Mariner 9* infrared interferometer spectrometer (IRIS).

## B. Carbon Dioxide Budget

*Mariner 9* observations of the polar frost caps have resulted in greater interest in, and more speculation about, the history, behavior, and location of carbon dioxide in the Martian surface environment. The processes that control the atmospheric pressure, their modification by long-term variations in the insolation experienced by the planet, and the time scales in which adjustments in atmospheric pressure can be made have been of particular concern.

Leighton and Murray (Ref. IX-8) first pointed out that the measured Martian atmospheric pressure is surprisingly close to that expected if it were controlled by solid-vapor equilibrium with a permanent north polar cap made of carbon dioxide. As observational and theoretical arguments have, at various times, been raised against the possibility of permanent carbon dioxide frost on Mars, it seemed to some that this near equality was merely a minor cosmic coincidence and that the present atmosphere and annual polar caps contain essentially all of the carbon dioxide that ever entered the planet's atmospheric environment. However, G. Briggs has conjectured that water ice could be sealing what would otherwise be unstable carbon dioxide deposits accreted from a thicker atmosphere in a colder climatic era. F. Fanale suggested that atmospheric carbon dioxide could be in equilibrium with a reservoir of carbon dioxide absorbed on the Martian regolith. Yet if evidence and opinion move back toward the existence of at least one perennial carbon dioxide cap, neither a cosmic coincidence nor these more exotic hypotheses will be necessary to account for the mean Martian atmospheric pressure.

One observable of great importance in the understanding of the annual carbon dioxide cycle is the total atmospheric pressure. Large seasonal variations in the total mass of the Martian atmosphere, and therefore in the atmospheric pressure, are predicted by heat-balance models of the annual condensation and sublimation of

carbon dioxide in which atmospheric transport of heat is neglected (Refs. IX-8 and IX-9). Accounting for the contribution of atmospheric heat (Ref. IX-10), these variations will occur, but with a lower amplitude. If the atmosphere is assumed to be in adsorption equilibrium with a 1-km-deep regolith, as suggested by F. Fanale, or with free solid carbon dioxide in the vast hypothetical isothermal polar reservoirs, as proposed by B. Murray, then the mean pressure would be uniform all year. It is questionable, however, on both kinetic and thermodynamic grounds that such reservoirs could be effective buffers for annual carbon dioxide pressure variations. Thus, measurements of seasonal variations in atmospheric pressure should provide important new information on the role of the atmosphere in the polar heat balance.

Efforts are being made by J. Pearl and P. Woiceshyn, using the *Mariner 9* data, to unravel seasonal variations in atmospheric pressure due to changes in total atmospheric carbon dioxide from variations caused by other phenomena. Orographic effects, diurnal tides, seasonal changes in circulation patterns, weather, and uncertainties in the gravity field all produce pressure changes comparable to those that are being sought. There also are observational difficulties in obtaining pressure determinations made in exactly the same location on the planet at different seasons. This particular problem might be one for which Earth-based observations of the mean pressure for large areas on Mars taken at different seasons could provide a solution.

While evidence remains inconclusive and opinion is still divided on the stability of solid carbon dioxide on Mars, new hypotheses continue to evolve. In one of the most elaborate models presented so far (Ref. IX-5) there are permanent water ice caps at both poles, but an additional small thick deposit of carbon dioxide at the north pole. Theoretical and observational evidence has been cited in support of this model. On the one hand it is argued that since occultation observations show the north polar region to be low, then the higher pressures there (Ref. IX-11) will favor it over the south pole as the site for accumulation of excess carbon dioxide. This argument is quite different from that used in Leighton and Murray's original paper (Ref. IX-8), where it was stated that the total insolation experienced by the north pole is less than that at the south. Subsequent analytical solutions have shown that the insolation at the north and south poles are the same whatever the orbital ellipticity or the stage in equinoctial precession. The observational evidence is the

apparently thicker deposit of ice (see Section IX-A, item 8) inferred from *Mariner 9* television pictures of the north pole. The total quantity of carbon dioxide that might be represented by this thicker deposit is estimated to be equivalent to an atmospheric pressure of 30 mb (Ref. IX-5).

This still highly debatable observation of a permanent carbon dioxide north polar cap has once again focused attention on the amount of carbon dioxide that has ever been released into the Martian atmosphere and the quantity that could be cycled back into the atmosphere if climatic conditions changed. O. Toon (Ref. IX-12) has reported the existence of a potential climatic instability which could cause a transition from the present 5- to 6-mb Martian surface pressure to pressures of about 1 bar if sufficient carbon dioxide were available. W. Ward, B. Murray, and M. Malin have considered pressure variations specifically due to astronomical perturbations of the planet's obliquity (Ref. IX-13), assuming equilibrium with a permanent polar cap but without incorporating Toon's atmospheric positive feedback effect. They find variations with periods of up to 2 million years and a maximum pressure of about 100 mb. This is close to predictions (Ref. IX-5) of the total carbon dioxide realized by volatilizing the perennial north polar cap. The agreement is almost surely fortuitous when one considers the inherent errors in both the observations and the model. If observations and model were correct, however, one might regard the agreement as coincidence. A more intriguing, although unlikely, possibility is that the carbon dioxide pressure on Mars, on extremely long time scales of tens of millions of years and more, is controlled by equilibrium with a reservoir of adsorbed carbon dioxide in the deep regolith such that the surface frost cap, although perennial, comes and goes as the planet's obliquity oscillates.

### C. Atmospheric Minor Constituents

*Mariner 9* spectral and television data have been used in the detection of minor atmospheric constituents in the solid state (clouds and hazes) as well as in the gaseous state. These observations are important in understanding the seasonal behavior of water, atmospheric photochemistry, planetary differentiation, and atmospheric evolution.

Measurements of clouds and haze were made in both polar regions and in the elevated volcanic regions of Tharsis and Arcadia.

- (1) Clouds of varying heights and morphologic characteristics were observed in television pictures (Refs. IX-4 and IX-14). The existence of dust, water ice, and carbon dioxide ice clouds was inferred by relating the heights of the clouds to atmospheric temperature profiles (Refs. IX-14 and IX-15) and on morphologic grounds.
- (2) Spectra with absorption features diagnostic of water ice clouds were obtained by the IRIS. Concentrations equivalent to about 1 precipitable micrometer with a particle size of about 2  $\mu\text{m}$  were deduced by R. Curran for the Tharsis ridge region. Water ice clouds were also detected in the boundary of the north polar hood region. IRIS spectra also indicated suspended dust (silicates) in the Martian lower atmosphere (Refs. IX-15 and IX-16). Spectra diagnostic of solid carbon dioxide in the Martian upper atmosphere were obtained in 1969 by *Mariner 7* (Ref. IX-17).
- (3) Areographic variations and the vertical distribution of haze in the atmosphere were inferred from terminator measurements by the UVS (Ref. IX-10).

Information on the areographic distribution and seasonal and diurnal variations in atmospheric water vapor was obtained from *Mariner 9* IRIS data. Because of the complexity of the data reduction, involving uncertainties in carbon dioxide transmission and the precision of atmospheric thermal profiles, many important results emerged in the period of April–June 1973. Some significant results were:

- (1) Low water vapor abundances in late southern summer over the south polar cap and throughout the equatorial regions (Ref. IX-15).
- (2) A maximum abundance of water vapor in the northern hemisphere spring season, with the concentrations greatest near the polar cap edge and decreasing toward the pole and toward the equator (V. Kunde, personal communication, 1973).
- (3) Detection of water vapor near the morning terminator (V. Kunde, personal communication, 1973).

The only other gaseous constituent identified to date in *Mariner 9* spectra is ozone. The UVS observed the 2550-Å adsorption feature, and latitudinal and temporal variations in ozone concentration have been observed.

- (1) Ozone was found in the north polar region beginning at a latitude of  $+45^\circ$  and extending northward (Ref. IX-19).
- (2) Ozone was not observed at any time in the equatorial region nor at the south polar cap during its summer season (Ref. IX-19).
- (3) Ozone later appeared in the southern hemisphere southward of  $-50^\circ$  as the Mars autumnal equinox approached (Ref. IX-19).

Although carbon dioxide, water, and ozone are the only gaseous constituents identified in *Mariner 9* spectra:

- (1) Absorptions corresponding to different carbon and oxygen isotopes in carbon dioxide have been recognized in IRIS data and reported by W. Maguire.
- (2) It will be possible to provide more stringent upper limits for many other molecules of planetological significance.

Efforts have been made to understand both the behavior of water vapor in the Martian atmosphere and also to establish the factors controlling the ozone abundance. Ozone is produced by the photolysis of oxygen. Its formation is preceded by photodissociation of molecular oxygen to form oxygen atoms, which then react with other oxygen molecules to form ozone. However, it is believed that observed variations in ozone concentration do not indicate comparable variations in oxygen abundance. (Oxygen in the lower atmosphere, produced by photodissociation of carbon dioxide and possibly water could not be detected by any of the instruments carried on *Mariner 9*.) One possibility considered before the *Mariner 9* mission was that different surface materials might react in different ways with ozone creating areographic variations in the amount of ozone in the atmosphere (Ref. IX-20). *Mariner 7* observations of ozone only over the south polar cap (Ref. IX-21) suggested that the substance might be concentrated in adsorbed form on carbon dioxide frost (Ref. IX-22). However, ozone was observed by *Mariner 9* outside the polar caps, and the seasonal variations in its concentration and their inverse correlation with temperature and the abundance of water vapor suggest that photochemical processes within the atmosphere must account for the major variations in the ozone abundance (Ref. IX-19).

Whereas photochemical processes permit atmospheric sources and sinks of ozone, the behavior of atmospheric water is constrained by continuity laws. Water vapor can

change state within the atmosphere creating cloud particles. There also can be exchange of these vapor and cloud particles with the surface by diffusion or gravitational fallout. Loss of water vapor from the Martian environment by atmospheric escape does occur at a very slow rate (Ref. IX-23), which is important to water exchange processes taking place over the longest time scales. *Mariner 9* IRIS observations of seasonal and areographic variations in atmospheric water vapor and water ice already discussed, together with information about diurnal variations and vertical distribution still being analyzed, may resolve the many uncertainties regarding atmospheric water.

One area of uncertainty concerns the seasonal migration of water. A theoretical model of the seasonal transport of water presented by C. Leovy in one of the earlier meetings of the Working Group predicted the storage of atmospheric water in intermediate latitudes (Ref. IX-24). Earth-based observations showing peak water vapor concentrations near  $+45^\circ$  latitude in the spring season (Ref. IX-25) support the general features of this model. However, preliminary *Mariner 9* observations of the time history and areographic distribution of water vapor during this same season show peaks at much higher latitudes and are interpreted by V. Kunde to indicate storage of water vapor within the annual deposits of carbon dioxide at the north polar cap.

The diurnal behavior of atmospheric water is another important process for which Earth-based and *Mariner 9* observations have yet to be reconciled. Some Earth-based results suggest a large diurnal variation in water vapor, implying that the atmospheric water vapor is strongly concentrated near the surface and condenses during nighttime (Ref. IX-25). IRIS data may, however, contradict this result, as water lines comparable in strength to those seen over the south polar cap during the summer season have been recognized in a single spectrum of the morning terminator (V. Kunde, personal communication, 1973). If the atmospheric temperature profiles in these two cases were comparable, this would imply no great change in diurnal water content. Complete analysis of this particular spectrum is extremely important, and work on the vertical distribution should also lead to an improved understanding of diurnal variation.

The source of water for the recurring white clouds seen in the Amazonis, Tharsis, and Nix Olympica regions is unknown. These clouds that appear, or at least intensify, during the afternoon may be caused by desorption of water from the upper few centimeters of surface material

by the diurnal thermal wave (Ref. IX-26). If this is the case, then there must either be a continuous supply of juvenile water from below or alternatively diurnal or seasonal replenishment of the water from the atmosphere. It seems unlikely that a supply of juvenile water could be sustained at the high levels required for the remarkable repetition of the cloud phenomena. It is also difficult to understand how a mechanism of diurnal replenishment could be so efficient, although conceivably seasonal replenishment could occur. Local degassing may not be required to explain the clouds. Orographic uplift coupled with active convection may be sufficient to induce condensation of ambient concentrations of atmospheric water vapor in these elevated regions (Ref. IX-4).

The global dust storm that obscured the surface of Mars during the early phases of the *Mariner 9* mission also may have affected atmospheric water abundances. Earth-based and *Mariner 9* observations indicate that the water vapor concentration in the equatorial regions was lower than that observed from Earth at the same season in previous years. One interpretation is that the dust storm influenced either the abundance or the detectability of water. The adsorption of water vapor on dust particles (Ref. IX-15) is a possible mechanism.

Through further analysis of the *Mariner 9* data and with important data gathered from the Viking mission, it should be possible to determine sites of diurnal and seasonal condensation or adsorption of water and to develop a better understanding of rates of horizontal and vertical transport. This may help to identify possible locales of liquid water formation. It also may help us to understand the long-term water budget for Mars. If there is a permanent carbon dioxide polar cap, then this should result in depletion of atmospheric water on a much shorter time scale than that appropriate to atmospheric escape (Ref. IX-22). Presumably internal sources of water including volcanism and ground ice decay (Ref. IX-27) maintain the observed atmospheric concentration. Estimates of the time scale for depletion at a polar cold trap, which could be made on the basis of improved knowledge of water transport properties, could lead, therefore, to revised estimates of the release rate of volatiles into the Martian atmosphere.

## **D. Chemical and Physical Properties of Surface Materials**

Analysis of *Mariner 9* data has led to an improved knowledge of the properties of Martian surface materials;

some of this knowledge is pertinent to the history and behavior of volatiles on the planet. One of the most significant observations in this respect was made by the IRIS and is that of an infrared absorption feature near  $10.2 \mu\text{m}$ . This absorption is attributed to silicate dust derived from the surface, but suspended in the atmosphere. The wavenumber at which the absorption is most intense indicates that the silica content of the dust is about 60%; such a high value suggests significant chemical differentiation of the planet (Ref. IX-15). If significant differentiation of silicate minerals has occurred, the redistribution of any water and carbon dioxide trapped in liquid or solid form within the bulk of the planet is implied. This could explain an hypothesized concentration of ices in the crustal layer (Ref. IX-26) and pertains to the general question of the history of the release of volatiles into the Martian atmosphere.

The possibility that the Martian regolith acts as a source or reservoir of volatiles has already been discussed. Physical observations of surface properties are relevant to whether or not volatiles are trapped in the regolith and what its capacity for volatiles might be. From his analysis of *Mariner 9* IRIS spectra, G. Hunt et al. (Ref. IX-28) concluded that suspended dust particles contain the clay mineral montmorillonite. F. Fanale pointed out that this mineralogy could have developed by the degradation of basalt in the Martian surface environment even in the absence of liquid water. He also demonstrated in the laboratory that the distinctive near-infrared spectral features of this substance, which do not appear in Earth-based spectra of the Martian surface, would be suppressed if the substance is mixed with even small quantities of finely divided dark minerals. Although a montmorillonite composition is not essential if the regolith is to act as a buffer for volatiles, since even crushed basalt has a high adsorption capacity, the large number of adsorption sites in the clay mineral crystal structure would reduce the depth of material required for equilibration with a given volume of either carbon dioxide or water. Evidence that water actually is present in the Martian regolith was presented by J. Pollack on the basis of airplane observations of reflected light from Mars (see Ref. IX-29). Adsorption features near  $3 \mu\text{m}$  indicate that water is present in the surface, but do not discriminate between chemically combined and physically adsorbed water.

Observations of heterogeneity in surface properties have been made which may be related to volcanic activity or fluvial processes. Areas with anomalous thermal properties have been identified (Ref. IX-30), and a thermal high

coincident with one of the major channel features was reported by H. Kieffer and E. Miner in the final Working Group meeting. IRIS spectra for the 9- to  $13\text{-}\mu\text{m}$  region are being analyzed for geographic variations indicative of compositional, particle size, or textural differences. The composition of one of the most distinctive features in the *Mariner 9* pictures, a bright triangular feature in the region Sinus Sabaeus, has been studied using data from the infrared radiometer and ultraviolet spectrometer (see Ref. IX-31).

## E. Layered Deposits and Climatic Cycles

The discovery of layered deposits, or laminated terrain, which are apparently unique to the polar regions, has been interpreted to mean that they are either largely composed of frozen carbon dioxide and water or that the condensation of these materials is important to their formation (Ref. IX-1). The possibility that layering is associated with oscillations of a carbon dioxide equilibrium surface was considered in meetings of the Volatiles Working Group, but has now been discarded. Similarly, the conception that layers represent melt horizons of carbon dioxide also was considered, but seems physically unlikely and inconsistent with many observations. Liquid carbon dioxide, however, may be buried deep within the layers (Ref. IX-32).

A possible connection between the layering and astronomical perturbations of Martian orbit parameters was recognized soon after the layers were first seen and has stimulated a successful search for previously unrecognized perturbations (Refs. IX-33 and IX-34). The conjecture that modulation of dust storm activity, rather than modulation of a carbon dioxide equilibrium surface, leads to layering also has been developed (Ref. IX-35). Further inferences have been made (Ref. IX-36) about the nature of the processes producing the layered deposits, emphasizing the role of the annual caps in trapping and retaining dust in the perennial caps; and the age and erosional history have been discussed.

The origin of the circular escarpments that underlie the perennial frosts has been debated. The idea that these features result from polar wandering and represent fossil latitudinal circles is an appealing one (Ref. IX-6). An alternative idea that wind erosion and deposition by circulating atmospheric motions is responsible also has some observational support (Ref. IX-37).

## F. Role of Volatiles in Martian Landscape Formation

There is considerable interest in the possibility that certain landscape features have been formed either by sublimation of segregated bodies of ground ice or by fluvial processes. Evidence for the latter includes major channels with braided segments and minor channels with dendritic tributaries (Ref. IX-38).

Significant observations include:

- (1) Channels seem to be confined to an equatorial belt.
- (2) All major channels "flow" in the direction of the steepest slope.
- (3) Channels, large and small, are at least hundreds of millions of years old judging from crater impact ages.
- (4) One major channel exhibits an incised braided section.
- (5) Possible fluvial modification of the wall of a crater in the floor of one large channel may indicate a process of formation involving many fluvial episodes spread over many millions of years.

The favored explanation for the largest channels, particularly those radiating from the Chryse basin, is the catastrophic flood hypothesis involving melted ground ice or possible clathrates (Ref. IX-39) originating in regions of chaotic terrain. However, no satisfactory explanation has been advanced regarding large channels for which no obvious source can be seen. The fine channels or furrows are even more difficult to explain. Compelling evidence for fluvial processes in the Martian furrows, if it ever existed, has been erased by subsequent impact cratering and other surface processes. As noted by S. Schumm, diverse ground patterns including dendritic patterns can be obtained by structural deformation. However, fluvial processes still can be considered one possible mode of formation of the Martian furrows.

If major channels and the small furrows have resulted from either flash floods or actual rainfall, then vastly

different thermal and pressure environments are needed. O. Toon and J. Pollack have examined possible models for achieving these conditions.

## G. Planetology

The striking discoveries of volcanism, fluvial features, and an episodic erosional and depositional history have stimulated discussions of the evolution of the planet Mars. Current ideas from comparative planetology presented by F. Fanale suggest that Mars was rich in volatiles at the time of accretion and that a substantial primordial atmosphere then existed (see Ref. IX-40). *Mariner 9* observations have been used to deduce the time history of the Martian atmosphere, resulting in some conflict with theoretical notions. Many observations, notably the youthfulness of Martian volcanoes, may indicate that the Martian atmosphere formed very recently (Ref. IX-41). However, contrary evidence has been discussed (Ref. IX-42) suggesting that erosion and deposition in the equatorial and mid-latitudes of Mars also may be attributable to climatic changes, perhaps involving a reduction in the total content of atmospheric volatiles (Ref. IX-36). Climatic change models for the variation of total planetary volatiles are discussed in Section IX-B and may help to reconcile some of these apparently contradictory results. Work in progress relating to the original size and time history of the Martian atmosphere includes the determination of minor constituents and the age relationships of fluvial and eolian surface features.

## H. Conclusions

The concept of a Working Group has provided a useful mechanism for exchanging ideas and information, which was facilitated by formal and informal presentations, discussions, and exchanges of preliminary and final manuscripts referring to work in process. There has been significant progress during the last year in understanding volatiles on Mars, which is at least in part due to the Working Group interaction. Additional progress can be expected in the future if reduction and interpretation of the *Mariner 9* data can be sustained. Many unresolved problems of the history of Martian volatiles, which are being actively explored, require precise quantitative analysis of the *Mariner 9* data. The variety of hypotheses presented in the Working Group has served to stimulate this kind of careful work. A continuing mechanism of communication and interaction is very desirable in the post mission period.

## I. Participants in the Working Group

The following members participated in the Volatiles Working Group:

J. M. Ajello	C. B. Farmer	A. L. Lane	D. J. Milton	R. S. Saunders	T. Vrebalovich
C. A. Barth	S. Z. Gunter	J. Lederberg	E. D. Miner	S. A. Schumm	W. R. Ward
G. A. Briggs	R. A. Hanel	R. B. Leighton	B. C. Murray	R. P. Sharp	J. Welker
T. E. Burke	W. K. Hartmann	C. B. Leovy	T. Owen	B. A. Smith	R. Wessel
M. H. Carr	H. Hipsher	E. Levinthal	K. Pang	R. S. U. Smith	A. B. Whitehead
E. Christensen	C. W. Hord	J. Lorell	J. Pearl	B. Snythe	P. M. Woiceshyn
J. Conel	N. Horowitz	R. J. Mackin	J. Pirraglia	L. A. Soderblom	G. Wood
B. Conrath	T. V. Johnson	M. C. Malin	J. B. Pollack	G. Soffen	S. C. Yeung
R. J. Curran	J. F. Jordan	H. Masursky	E. Pounder	A. I. Stewart	
J. A. Cutts	H. H. Kieffer	D. Matson	O. Raper	R. H. Steinbacher	
F. P. Fanale	V. G. Kunde	W. Maguire	C. Sagan	O. B. Toon	

## References

- IX-1. Murray, B. C., Soderblom, L. A., Cutts, J. A., Sharp, R. P., Milton, D. J., and Leighton, R. B., "Geological Framework of the South Polar Region of Mars," *Icarus*, Vol. 17, pp. 328-345, 1972.
- IX-2. Pang, K. D., and Hord, C. W., "Mariner 9 Ultraviolet Spectrometer Experiment: Elevation Map of Mars South Polar Region" (to be submitted to *Icarus*).
- IX-3. Soderblom, L. A., Malin, M. C., Murray, B. C., and Cutts, J. A., "Mariner 9 Observations of the Surface of Mars in the North Polar Region," *J. Geophys. Res.*, Vol. 78, 1973.
- IX-4. Leovy, C. B., Briggs, G. A., and Smith, B. A., "Mars Atmosphere during the Mariner 9 Extended Mission: Television Results," *J. Geophys. Res.*, Vol. 78, 1973.
- IX-5. Murray, B. C., and Malin, M. C., "Volatiles on Mars: Theory vs Observation" (submitted to *Science*).
- IX-6. Murray, B. C., and Malin, M. C., "Polar Wandering on Mars," *Science*, Vol. 179, p. 997, 1973.
- IX-7. Briggs, G., *Mariner 9 Observations of the North Polar Region*, paper presented at DPS meeting, Tucson, March 1973.
- IX-8. Leighton, R. B., and Murray, B. C., "Behavior of Carbon Dioxide and Other Volatiles on Mars," *Science*, Vol. 153, p. 136, 1966.
- IX-9. Cross, C. A., "The Heat Balance of the Martian Polar Caps," *Icarus*, Vol. 15, p. 100, 1971.
- IX-10. Leovy, C. B., "Mars Ice Caps," *Science*, Vol. 154, p. 1178, 1966.

## References (contd)

- IX-11. Kliore, A. J., Fjeldbo, G., Seidel, B. L., Sykes, M. J., and Woiceshyn, P. M., "S-Band Radio Occultation Measurements of the Atmosphere and Polar Regions of Mars with Mariner 9: Extended Mission Coverage of Polar and Intermediate Latitudes," *J. Geophys. Res.*, Vol. 78, 1973.
- IX-12. Gierasch, P. J., and Toon, O. B., "Atmospheric Pressure Variation and the Climate of Mars" (in preparation).
- IX-13. Ward, W. R., Murray, B. C., and Malin, M. C., "Climatic Variation on Mars" (in preparation).
- IX-14. Leovy, C. B., Briggs, G. A., Young, A. T., Smith, B. A., Pollack, J. B., Shipley, E. N., and Wildey, R. L., "The Martian Atmosphere: Mariner 9 Television Experiment Progress Report," *Icarus*, Vol. 17, pp. 373-393, 1972.
- IX-15. Hanel, R., Conrath, B., Hovis, W., Kunde, V., Lowman, P., Maguire, W., Pearl, J., Pirraglia, J., Prabhakara, C., Schlachman, B., Levin, G., Straat, P., and Burke, T., "Investigation of the Martian Atmosphere by Infrared Spectroscopy on Mariner 9," *Icarus*, Vol. 17, pp. 423-442, 1973.
- IX-16. Conrath, B., Curran, R., Hanel, R., Kunde, V., Maguire, W., Pearl, J., Pirraglia, J., Welker, J., and Burke, T., "Atmospheric and Surface Properties of Mars Obtained by Infrared Spectroscopy on Mariner 9," *J. Geophys. Res.*, Vol. 78, 1973.
- IX-17. Herr, K. C., and Pimentel, G. C., "Evidence for Solid Carbon Dioxide in the Upper Atmosphere of Mars," *Science*, Vol. 167, p. 147, 1970.
- IX-18. Ajello, J. M., Hord, C. W., Barth, C. A., Stewart, A. I., and Lane, A. L., "Mariner 9 Ultraviolet Spectrometer Experiment: Afternoon Terminator Observations of Mars," *J. Geophys. Res.*, Vol. 78, 1973.
- IX-19. Lane, A. L., Barth, C. A., Hord, C. W., and Stewart, A. I., "Mariner 9 Ultraviolet Spectrometer Experiment: Observations of Ozone on Mars," *Icarus*, Vol. 18, pp. 102-108, 1973.
- IX-20. Hord, C. W., Barth, C. A., and Pearce, J. B., "Ultraviolet Spectroscopy Experiment for Mariner Mars 1971," *Icarus*, Vol. 12, pp. 63-77, 1970.
- IX-21. Barth, C. A., and Hord, C. W., "Mariner Ultraviolet Spectrometer: Topography and Polar Cap," *Science*, Vol. 173, p. 197, 1971.
- IX-22. Broida, H. P., Lundell, O. R., Schiff, H. I., Ketcheson, R. D., "Is Ozone Trapped in the Solid Carbon Dioxide Polar Cap of Mars?", *Science*, Vol. 170, p. 1402, 1970.
- IX-23. McElroy, M. B., "Mars: an Evolving Atmosphere," *Science*, Vol. 175, p. 443, 1972.
- IX-24. Leovy, C. B., "Exchange of Water Vapor Between the Atmosphere and Surface of Mars," *Icarus*, Vol. 18, pp. 120-125, 1973.
- IX-25. Farmer, B. C., "Liquid Water on Mars" (submitted to *Icarus*).
- IX-26. Fanale, F. P., and Cannon, W. A., "Adsorption on the Martian Regolith," *Nature*, Vol. 230, p. 502, 1971.

## References (contd)

- IX-27. Sharp, R. P., Soderblom, L. A., Murray, B. C., and Cutts, J. A., "The Surface of Mars: 2. Un cratered Terrains," *J. Geophys. Res.*, Vol. 76, p. 331, 1971.
- IX-28. Hunt, G., Logan, L., and Salisbury, J., "Mars: Components of Infrared Spectra and the Composition of the Dust Cloud," *Icarus*, Vol. 18, p. 459, 1973.
- IX-29. Houck, J., Pollack, J. B., Sagan, C., Schaack, D., and Decker, J., "High Altitude Infrared Spectroscopic Evidence for Bound Water on Mars," *Icarus*, Vol. 18, p. 470, 1973.
- IX-30. Kieffer, H. H., Chase, S. C., Miner, E., Münch, G., and Neugebauer, G., "Preliminary Report on Infrared Radiometric Measurements from the Mariner 9 Spacecraft," *J. Geophys. Res.*, Vol. 78, 1973.
- IX-31. Cutts, J. A., Malin, M. C., Kieffer, H., and Lane, A. L., "An Unusual Martian Feature" (in preparation).
- IX-32. Sagan, C., "Liquid Carbon Dioxide and the Martian Polar Laminae," *J. Geophys. Res.*, Vol. 78, 1973.
- IX-33. Murray, B. C., Ward, W. R., and Yeung, S. C., "Periodic Insolation Variations on Mars," *Science*, Vol. 180, p. 638, 1973.
- IX-34. Ward, W. R., "Obliquity Variations on Mars" (in press).
- IX-35. Briggs, G. A., "Periodic Variations in Martian Dust Storm Activity and the Layered Deposits of the Polar Regions" (submitted to *Science*).
- IX-36. Cutts, J. A., "The Nature and Origin of Layered Deposits of the Martian Polar Regions," *J. Geophys. Res.*, Vol. 78, 1973.
- IX-37. Cutts, J. A., "Wind Erosion in the Martian Polar Regions," *J. Geophys. Res.*, Vol. 78, 1973.
- IX-38. Milton, D. J., "Water and Processes of Degradation in the Martian Landscape," *J. Geophys. Res.*, Vol. 78, 1973.
- IX-39. Milton, D. J., "Catastrophic Floods and Martian Clathrates" (in preparation).
- IX-40. Fanale, F. P., "History of Martian Volatiles: Implications for Organic Synthesis," *Icarus*, Vol. 15, pp. 279-303, 1971.
- IX-41. Murray, B. C., and Malin, M. C., "Mars Atmosphere: A Late Arrival" (in preparation).
- IX-42. Hartmann, W. K., "Martian Cratering IV: Mariner 9 Initial Analysis of Cratering Chronology," *J. Geophys. Res.*, Vol. 78, 1973.

## X. Atmospheric Phenomena Working Group

Conway B. Leovy  
Atmospheric Sciences Department  
University of Washington, Seattle, Washington 98195

The Atmospheric Phenomena Working Group was formed to provide a mechanism for facilitating the exchange of data and ideas relevant to atmospheric processes. It was believed that such an interaction was needed if the atmospheric observations, which frequently involved data from several *Mariner 9* experiments, were to be understood adequately in a reasonable period of time. Moreover, since several different disciplines and points of view are required to understand some of the atmospheric problems, participation of interested non-*Mariner* scientists was invited at an early stage. This outside participation proved to be highly stimulating to the Working Group.

Many of the problems considered by this Group overlap with problems explored by the Volatiles Working Group, and these have been described in Section IX of this Report. Some of the specific problems considered by the Atmospheric Phenomena Working Group, which were not discussed in Section IX, are presented in the subsequent paragraphs.

### A. Atmospheric Temperature and Wind

It was recognized that the availability of temperature distributions from the infrared interferometer spectrometer (IRIS) and S-band occultation experiments might make it possible to deduce sufficient information about

the distribution of pressure that certain components of the wind systems could be defined. For this purpose, extensive global coverage, day-to-day coverage, and diurnal coverage are needed. Neither experiment provided ideal coverage, nor did the combination of the two experiments. The coverage by IRIS was more extensive early in the mission, especially before revolution 220, during the subsiding phase of the dust storm, and in the late southern summer season. Useful IRIS coverage also was obtained between revolutions 102 and 220 in the northern winter hood region. On the other hand, occultation data were more extensive during the extended mission, and also complement IRIS coverage during the standard mission period. One of the first questions was: Are the IRIS and occultation results compatible? A. Kliore investigated this question, and found that there was generally satisfactory agreement (usually within about 10%) on surface pressure. Temperature comparisons were difficult because of the absence of coincident observations; because of orbital constraints, IRIS observations in a given region for a particular local time usually lagged the occultation measurements by 15 to 45 days. Nevertheless, allowing for the known secular variation of temperature during the dust storm, the comparison was encouraging, and it was felt that the two data sets could be combined usefully to increase total coverage. The two sets of temperature results also are complementary in another respect. IRIS gives reliable results over deep layers, but cannot detect variations in temperature that have small vertical

scales. The occultation data are noisier, but they also may be able to reveal real features at better vertical resolution. Additional statistical analysis of occultation profiles, now in progress, may be able to distinguish between real features in the profiles and noise.

IRIS temperature data have been used in calculations of zonally symmetric wind systems and diurnal and semi-diurnal thermal tide wind systems by Pirraglia and Conrath, and by Leovy, Zurek, and Pollack for conditions during the waning phase of the dust storm. The most difficult aspect of these calculations is the zonally symmetric wind system, since its amplitude is sensitive to the dissipative mechanisms. Two possible ways of resolving uncertainties in this wind system have been proposed: (1) Circulation must be such as to satisfy the meridional heat transport requirements as well as to be consistent with the observed temperature field. (2) Associated meridional variations of surface pressure must be consistent with variations of surface pressure on a geopotential surface, as inferred from occultation data and from orbital determinations of the gravity field. This is especially true in the southern subtropics, where both of the latter types of measurements are reliable. At the time of writing, neither the question of the distributions and intensities of the zonally symmetric wind system nor the thermally driven tides has been resolved completely, but it appears that such a resolution is within reach.

Circulation in the winter northern hemisphere probably is dominated by irregular cyclonic disturbances that cannot be characterized in detail with the limited coverage of *Mariner 9* data. However, the zonal component of the thermal wind can be deduced from IRIS data, and an estimate of the intensity of the westerly surface winds has been obtained by combining these data with television observations of wave clouds. Typically, westerly surface winds on the order of 10 to 20 m/sec increasing to more than 100 m/sec at 20 km appear to prevail in approximately the  $+45^\circ$  to  $+55^\circ$  zone. Investigations of day-to-day variations in these winds have started. The possibility of estimating zonal geostrophic winds during both the standard mission and the extended mission is being explored by Woiceshyn.

Another aspect of the wind systems is the role of topography. The thermal variations associated with topography have been investigated by Conrath. During the dust storm, these effects are much smaller than those predicted for non-dust storm models. The dynamic implications of these temperature variations have not yet been explored.

The most appropriate way to investigate the interaction of all known factors influencing the wind systems is by means of general circulation models. Stimulated by *Mariner 9* results three groups are undertaking such studies: Blumsack and Wessell at Florida State are developing a spectral model; Pirraglia and Conrath at Goddard are extending their model to include nonlinear effects and topography; and Pollack, Leovy, and Mintz are reapplying the Mintz-Arakawa general circulation model to the problem. Some results of these efforts should be available within the next year.

## B. Cloud Processes

Clouds in the areas of the Tharsis ridge and Nix Olympica were observed by the television cameras and by IRIS. The television data showed that some of these clouds are convective in origin and that they form repeatedly over the west slopes of the volcanoes during the afternoon. The IRIS spectra showed that the clouds are composed of water ice, and a preliminary estimate of the optical depth was made, based on matching a model of the infrared radiative transfer by ice clouds to the observed spectra. Refinements of the model may be possible if estimates of optical depth in the visible can be obtained from television data.

The most extensive cloud systems were observed in the north polar hood region during late winter. Temperature distributions inferred from IRIS spectra show that the clouds in the  $+45^\circ$  to  $+60^\circ$  zone were probably water ice; those north of  $+60^\circ$  may have been composed largely of carbon dioxide ice. More information on cloud-forming processes, and on day-to-day changes in circulation in this region can be expected from comparisons among television, infrared and ultraviolet spectrometers, and infrared radiometer data on an orbit-by-orbit basis. These comparisons have begun, but much work still remains.

One cloud system identified in television pictures as a regional dust storm in the Euxinus Lacus area has been investigated by the infrared radiometer. These data show only a very small temperature drop over the cloud, too small to be explained by an optically thick water ice cloud, and therefore adding support to the dust cloud interpretation. More data intercomparisons are needed to verify the nature of this and other clouds that are suspected of being dust storms.

### C. Limb and Terminator Profiles

An intercomparison by A. I. Stewart between television pictures, ultraviolet spectrometer (UVS) limb profiles, and occultation data revealed early in the mission that the dust raised by the global storm extended to the extraordinary height of 55 km. It also showed that the high haze layer viewed in most television limb pictures during the storm was 70 to 80 km above the surface. The high layer was shown to be a condensate layer by its color in the visible and by its identification with a layer of high single-scattering albedo in UVS terminator data analyzed by J. Ajello. G. Briggs has begun to examine the time and space variations in this layer by assembling television pictures of the limb. Both television and UVS data show that the high scattering layer is denser near the morning terminator than elsewhere. Further study of this phenomenon may give clues to the diurnal variations in temperature and circulation in Mars' upper atmosphere. A useful tool in future analyses of these limb phenomena is a complete set of limb profiles from television frames, which is being placed on microfiche.

### D. Minor Constituents

V. Kunde has been investigating minor features in the IRIS spectra. No features other than those of carbon dioxide and water have been identified, and ultimately this investigation is expected to provide more stringent upper limits on some minor constituents. Water vapor concentrations also have been estimated from IRIS spectra. The rather uniform column abundance of about 1 mg/cm<sup>2</sup> obtained during the dust storm is in agreement with Earth-based estimates of water during this period; it is at variance with Earth-based estimates for the same Mars seasonal dates but in other years. One interpretation is that the dust storm influenced either the abundance or the detectability of water.

UVS data showed that ozone, which had been seen over the south polar cap by *Mariner 7*, varies widely in abundance with season and latitude. These variations have a strong inverse correlation with atmospheric temperature, and the interpretation is that the ozone is controlled by reactions with the products of water vapor photolysis, as the concentration of the latter is sharply limited by temperature. Ozone observations may be particularly significant because a similar reaction chain is suspected of limiting the ozone concentration in parts of Earth's stratosphere. To explore the behavior of ozone in more detail, C. Hord compared ozone observations on a particular

orbit with temperature and cloudiness distributions inferred by IRIS data and observed by the television cameras. The ozone was only weakly correlated with cloudiness, but it was highly correlated with temperature. More studies of this type can be expected to lead to improved understanding of the processes controlling ozone abundance.

### E. Global Dust Storm

All experiments provided complementary information on the dust storm. Some of the more significant findings were:

- (1) Depth of the dust cloud was enormous ( $\sim 50$  km).
- (2) Particles were highly absorbing and had a high silicate content.
- (3) Particles probably were largely in the size range of 5 to 10  $\mu\text{m}$ .
- (4) Heating effect of the particles completely altered the circulation and stability of the atmosphere.

The clearing phase of the storm was closely monitored by all of the instruments, and took place predominantly in early January 1972, but some dust was observed by IRIS even during the extended mission.

These observations have generated several interesting working hypotheses on the mechanisms for generating and maintaining such a storm. Further analyses of time and space variations in dustiness, and additional theoretical modeling can be expected to improve our understanding of these mechanisms.

### F. Special Problems

In addition to these rather broad areas, two special topics were considered. Members of the Working Group were asked to comment on the atmospheric structure portion of the Mars engineering model being used by the Viking Program. The Group agreed that the model appeared to be basically sound. The members also were asked to consider the expected variations in atmospheric pressure along geopotential surfaces. This variation could be inferred by relating the surface pressures measured by IRIS at known geometrical heights with the geopotential surfaces obtained from the *Mariner 9* orbit determinations.

By comparing these distributions of surface pressure, corrected to constant geopotential, with the theoretical estimates of pressure variations, the reliability of both the meteorological theory, and the geopotential determinations from orbit data can be assessed. In the tropical regions, the pressure distributions obtained from the occultation and orbit determinations were in qualitative agreement with theory, for the dust storm period, with minimum pressure near  $-30^\circ$ . The amplitude of the latitude variation of pressure provides information on the intensity of the meridional circulation, which is difficult to determine otherwise because of its sensitivity to dissipation. The pressure on the geopotential surface appears to increase north of  $+40^\circ$  latitude, in disagreement with theory and the evidence for westerly surface winds provided by the persistent wave clouds. The orbit determination of the geopotential surface is comparatively weak in this region, and the discrepancy may be due to an unexpectedly large "lump" in the geopotential height north of  $+40^\circ$ . Two km could account for the apparent discrepancy. This problem will be refined over the next year or so as improved theoretical estimates of surface pressure are obtained from the circulation models.

An additional problem under study is the determination of seasonal variations in atmospheric mass. Such variations are predicted on the basis of models of seasonal storage of carbon dioxide in the polar caps. Thus, measurements of the seasonal variation of pressure will provide a strong constraint on these models and on models of long-term storage of carbon dioxide in the caps. Both IRIS and occultation data are being analyzed to search for these effects.

## G. Conclusions

The Working Group provided a very useful mechanism for exchanging information, and for attacking a variety of atmospheric problems on a broad scale. Many of the atmospheric problems have depended on late stages in the data processing; partly for this reason, many of these problems are still unresolved and are being actively explored. It is hoped that equally effective means of communication and interaction can be maintained in the post-mission period.

## H. Participants in the Working Group

The following members participated in the Atmospheric Phenomena Working Group activities:

J. M. Ajello	C. W. Hord	J. Pirraglia
C. A. Barth	J. F. Jordan	J. B. Pollack
S. Blumsack	H. H. Kieffer	S. I. Rasool
G. A. Briggs	A. J. Kliore	E. N. Shipley
T. E. Burke	V. G. Kunde	A. I. Stewart
B. J. Conrath	A. L. Lane	R. Wessell
R. Curran	C. B. Leovy	A. B. Whitehead
J. A. Cutts	J. Lorell	P. M. Woiceshyn
R. Dickinson	M. Malin	R. Zurek
F. P. Fanale	G. Münch	
R. A. Hanel	J. Pearl	

## Bibliography

Following is a selected list of publications dealing with topics that have been discussed at meetings of the *Mariner 9* Atmospheric Working Group:

- Ajello, J. M., C. W. Hord, C. A. Barth, A. I. Stewart, and A. L. Lane, "Mariner 9 Ultraviolet Spectrometer Experiment: Afternoon Terminator Observations of Mars," *J. Geophys. Res.*, Vol. 78, 1973.
- Barth, C. A., A. I. Stewart, C. W. Hord, and A. L. Lane, "Mariner 9 Ultraviolet Spectrometer Experiment: Mars Airglow Spectroscopy and Variations in Lyman Alpha," *Icarus*, Vol. 17, p. 457, 1972.
- Barth, C. A., *Ozone and the Polar Hood of Mars*, paper presented at the AAS-DPS Meeting, Tucson, Arizona, March 1973.
- Barth, C. A., C. W. Hord, A. I. Stewart, A. L. Lane, M. L. Dick, and G. P. Anderson, "Mariner 9 Ultraviolet Spectrometer Experiment: Seasonal Variations of Ozone on Mars," *Science*, Vol. 179, p. 795, 1973.
- Briggs, G. A., *Periodic Variations in Martian Dust Storm Activity and the Layered Deposits of the Polar Regions*, paper presented at the AAS-DPS Meeting, Tucson, Arizona, March 1973.
- Briggs, G. A., *Mariner 9 Observations of the North Polar Hood*, paper presented at the AAS-DPS Meeting, Tucson, Arizona, March 1973.
- Conrath, B. J., *Martian Atmospheric Temperature Fields From the Mariner 9 Infrared Spectroscopy Experiment*, paper presented at the AAS-DPS Meeting, Tucson, Arizona, March 1973.
- Conrath, B., R. Curran, R. Hanel, V. Kunde, W. Maguire, J. Pearl, J. Pirraglia, J. Welker, and T. Burke, "Atmospheric and Surface Properties of Mars Obtained by Infrared Spectroscopy on Mariner 9," *J. Geophys. Res.*, Vol. 78, 1973.
- Curran, R. J., B. J. Conrath, V. G. Kunde, and R. A. Hanel, *Mariner 9 IRIS Observations of Martian Ice Clouds*, paper presented at the AAS-DPS Meeting, Tucson, Arizona, March 1973.
- Hanel, R. A., B. J. Conrath, W. A. Hovis, V. G. Kunde, P. D. Lowman, J. C. Pearl, and B. Schlachman, "Infrared Spectroscopy Experiment on the Mariner 9 Mission: Preliminary Results," *Science*, Vol. 175, p. 306, 1972.
- Hanel, R. A., B. Conrath, W. Hovis, V. Kunde, P. Lowman, W. Maguire, J. Pearl, J. Pirraglia, C. Prabhakara, B. Schlachman, G. Levin, P. Straat, and T. Burke, "Investigation of the Martian Environment by Infrared Spectroscopy on Mariner 9," *Icarus*, Vol. 17, p. 423, 1973.
- Hord, C. W., C. A. Barth, A. I. Stewart, and A. L. Lane, "Mariner 9 Ultraviolet Spectrometer Experiment: Photometry and Topography of Mars," *Icarus*, Vol. 17, p. 443, 1972.
- Kliore, A. J., D. L. Cain, G. Fjeldbo, B. L. Seidel, and S. I. Rasool, "Mariner 9 S-Band Martian Occultation Experiment: Initial Results on the Atmosphere and Topography of Mars," *Science*, Vol. 175, p. 315, 1972.

## Bibliography (contd)

- Kliore, A. J., D. L. Cain, G. Fjeldbo, B. L. Seidel, M. J. Sykes, and P. M. Woiceshyn, *Some Recent Results of Mariner 9 Occultations of Mars*, paper presented at the AAS-DPS Meeting, Tucson, Arizona, March 1973.
- Kliore, A. J., G. Fjeldbo, B. L. Seidel, M. J. Sykes, and P. M. Woiceshyn, "S-Band Radio Occultation Measurements of the Atmosphere and Topography of Mars With Mariner 9: Extended Mission Coverage of Polar and Intermediate Latitudes," *J. Geophys. Res.*, Vol. 78, 1973.
- Kunde, V. G., *Water Vapor Variations in the Atmosphere of Mars From Mariner 9 IRIS*, paper presented at the AAS-DPS Meeting, Tucson, Arizona, March 1973.
- Lane, A. L., C. A. Barth, C. W. Hord, and A. I. Stewart, "Mariner 9 Ultraviolet Spectrometer Experiment: Observations of Ozone on Mars," *Icarus*, Vol. 18, p. 102, 1973.
- Leovy, C. B., G. A. Briggs, A. T. Young, B. A. Smith, J. B. Pollack, E. N. Shipley, and R. L. Wildey, "The Martian Atmosphere: Mariner 9 Television Experiment Progress Report," *Icarus*, Vol. 17, p. 373, 1972.
- Leovy, C. B., G. A. Briggs, and B. A. Smith, "Mars Atmosphere During the Extended Mission: Television Results," *J. Geophys. Res.*, Vol. 78, 1973.
- Leovy, C. B., J. B. Pollack, and R. W. Zurek, "Mechanisms for Mars Dust Storms," *J. Atmos. Sci.*, July 1973.
- Pang, K. D., and C. W. Hord, "Mariner 9 Ultraviolet Spectrometer Experiment: 1971 Mars Dust Storm," *Icarus*, Vol. 18, 1973.
- Pirraglia, J. A., *Martian Thermally Driven Symmetric Winds With an Ekman Layer and Surface Drag*, paper presented at the AAS-DPS Meeting, Tucson, Arizona, March 1973.